Institutional Repository - Research Portal
Dépôt Institutionnel - Portail de la Recherche
researchportal.unamur.be
University of Namur

THESIS / THÈSE

DOCTOR OF SCIENCES

Structural study of HIV-1 integrase inhibition by quinolones: contribution to the rational design of new inhibitors

Vandurm, Pierre

Award date:
2011

Awarding institution:
University of Namur

Link to publication

General rights
Copyright and moral rights for the publications made accessible in the public portal are retained by the authors and/or other copyright owners and it is a condition of accessing publications that users recognise and abide by the legal requirements associated with these rights.

- Users may download and print one copy of any publication from the public portal for the purpose of private study or research.
- You may not further distribute the material or use it for any profit-making activity or commercial gain
- You may freely distribute the URL identifying the publication in the public portal ?

Take down policy
If you believe that this document breaches copyright please contact us providing details, and we will remove access to the work immediately and investigate your claim.

Download date: 05. May. 2023

Facultés
Universitaires
Notre-Dame
de la Paix

Structural study of HIV-1 integrase inhibition by quinolones: contribution to the rational design of new inhibitors

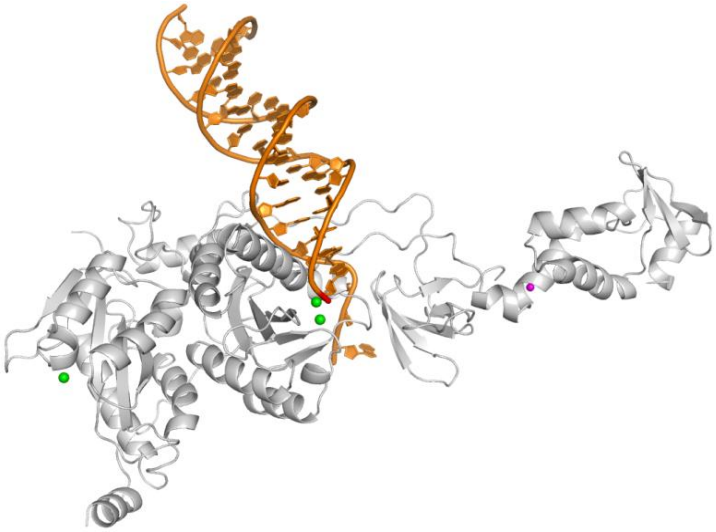

Faculté des Sciences

DEPARTEMENT DE CHIMIE

Dissertation présentée par
Pierre Van Durm
en vue de l'obtention du grade
de Docteur en Sciences

Octobre 2011

FUNDP
Faculté des Sciences
Département de Chimie

Structural study of HIV-1 integrase inhibition by quinolones: contribution to the rational design of new inhibitors

Dissertation présentée par
Pierre Van Durm
en vue de l'obtention du grade
de Docteur en Sciences

Composition du Jury :

Prof. J. Wouters (Promoteur)
Prof. X. De Bolle (FUNDP, Namur)
Prof. B. Masereel (FUNDP, Namur)
Prof. D. Bonifazi (FUNDP, Namur)
Dr. J.-F. Mouscadet (ENS Cachan)

2011

© Presses universitaires de Namur & Pierre Van Durm
Rempart de la Vierge, 13
B - 5000 Namur (Belgique)

Toute reproduction d'un extrait quelconque de ce livre,
hors des limites restrictives prévues par la loi,
par quelque procédé que ce soit, et notamment par photocopie ou scanner,
est strictement interdite pour tous pays.
Imprimé en Belgique
ISBN : 978-2-87037 -735-2
Dépôt légal: D / 2011 / 1881 / 40

Facultés Universitaires Notre-Dame de la Paix
Faculté des Sciences
Rue de Bruxelles 61, B-5000 Namur, Belgique

Etude structurale du mode d'inhibition de l'intégrase du VIH-1 par des dérivés de type quinolone: support à la conception rationnelle de nouveaux inhibiteurs

par Pierre Van Durm

Résumé

Dans le cadre de la conception de nouveaux agents antiviraux contre le SIDA, l'intégrase du VIH-1 constitue une cible de choix car cette enzyme joue un rôle essentiel dans le cycle de réplication du virus en intégrant l'ADN viral dans le génome de la cellule hôte. Parmi les nombreux inhibiteurs de l'intégrase décrits jusqu'à présent, les dérivés β-dicéto-acide représentent une famille importante. Ces composés ont la particularité de posséder un groupement capable de chélater le cofacteur métallique Mg^{2+} présent au sein du site actif de l'enzyme et essentiel à son activité catalytique. Dans ce travail de thèse, nous avons entrepris l'étude du mécanisme d'inhibition de l'intégrase du VIH-1 par des dérivés de type quinolone sur base d'une approche expérimentale et théorique.

Une série de quinolones présentant en position 3 un groupement β-dicéto-acide/ester capable de chélater le cofacteur métallique Mg^{2+} et en position 6 divers groupements (groupements halogène, hydrophile ou hydrophobe) a été synthétisée comme inhibiteurs potentiels de l'intégrase du VIH-1. L'activité anti-intégrase de ces composés a été mesurée par des tests *in vitro* en utilisant de l'intégrase surexprimée dans *E. coli* et purifiée par chromatographie d'affinité. L'activité antivirale de ces composés a également été évaluée dans des tests *ex vivo*.

Dans le but d'obtenir la structure tridimensionnelle d'un complexe enzyme-ligand, le domaine catalytique de l'intégrase du VIH-1 a été surexprimé dans *E. coli* et purifiée par chromatographie d'affinité. Afin d'améliorer la purété de la protéine active obtenue, d'autres techniques de purification ont été testées.

Les études expérimentales (DRX, UV-visible, FT-IR, ATR) et les calculs théoriques réalisés sur les composés dicéto-acide sélectionnés ont permis d'identifier les conformations les plus stables de la chaîne dicétoacide ainsi que son mode de complexation en solution avec le cofacteur Mg^{2+}. Afin de déterminer le mode de liaison des composés quinolone au sein du site actif de l'enzyme lié à son substrat ADN, un modèle intégrase/ADN a été construit. Les études de docking ont mis en évidence un mode de liaison en accord avec les relations structure-activité observées. Ces études de modélisation moléculaire nous ont permis de proposer un mécanisme d'inhibition de l'intégrase du VIH-1 par des composés quinolone.

Dissertation doctorale en Sciences
3 Octobre 2011
Laboratoire de Chimie Biologique Structurale (Prof. J. Wouters)
Promoteur: Prof. J. Wouters

Facultés Universitaires Notre-Dame de la Paix
Faculté des Sciences
Rue de Bruxelles 61, B-5000 Namur, Belgium

Structural study of HIV-1 integrase inhibition by quinolones: contribution to the rational design of new inhibitors

by Pierre Van Durm

Abstract

In the design of new antiviral agents against AIDS, HIV-1 integrase is an attractive target because this enzyme plays an essential role in the virus replication cycle by integrating the viral DNA into the host cell genome. Among all integrase inhibitors described to date, the β-diketo acid derivatives represent an important family. These compounds have the particularity to posess a chemical group able to chelate the Mg^{2+} metal cofactor present in the enzyme active site and essential to its catalytic activity. In this thesis, we have undertaken the study of the mechanism of inhibition of HIV-1 integrase by substituted quinolone based on experimental and theoretical approach.

A series of quinolone substituted at position 3 by a β-diketo-acide/ester motif able to chelate the Mg^{2+} metal cofactor and at position 6 by various groups (halogen, hydrophilic or hydrophobic groups) has been synthesized as potential HIV-1 integrase inhibitors. These compounds were evaluated for their anti-integrase activity in *in vitro* assays using integrase overexpressed in *E. coli* and purified by affinity chromatography. The antiviral activity of compounds was also tested in *ex vivo* assays.

To obtain the three-dimensional structure of an enzyme-ligand complex, the catalytic core domain of HIV-1 integrase was overexpressed in *E. coli* and purified by affinity chromatography. To improve the level of purity of the active protein obtained, other purification techniques were tested.

Experimental studies (XRD, UV-visible, FT-IR, ATR) and theoretical calculations on the diketo acid compounds allowed to identify the most stable conformations of the diketoacid moiety and its complexation mode in solution with the Mg^{2+} cofactor. To determine the binding mode of developed quinolone within the DNA-bound enzyme, integrase/DNA model was built. Docking studies highlighted a binding mode in agreement with the observed structure-activity relationships. These molecular modeling studies allowed us to propose a mechanism of inhibition of HIV-1 integrase by quinolone compounds.

Ph.D. thesis in Sciences
3 Octobre 2011
Laboratoire de Chimie Biologique Structurale (Prof. J. Wouters)
Advisor: Prof. J. Wouters

Au terme de ces quatre années de recherche, je tiens à exprimer toute ma gratitude aux personnes qui m'ont toujours soutenu et ont contribué à l'élaboration de ce travail.

Mes premiers mots vont sans aucun doute au professeur Johan Wouters qui m'a accueilli au sein de son laboratoire durant mon mémoire ainsi que tout au long de ces quatre années de thèse durant lesquelles il m'a porté une grande disponibilité et une pleine attention. Je le remercie pour m'avoir initié à la chimie biologique structurale et m'avoir confié un sujet aussi passionant.

Je tiens également à remercier tous les membres du laboratoire CBS pour leur aide, leur soutien ainsi que leur bonne humeur et leur dynamisme qui m'ont permis de vivre une expérience enrichisssante tout au long de ces cinq dernières années tant au point de vue scientifique que humain. Merci à Bernadette pour tous ses nombreux conseils en matière de cristallographie. Toute ma gratitude va vers Christine (KIKI) pour sa grande disponibilité, sa gentillesse, sa patience et pour m'avoir inculqué une partie de son savoir dans la rédaction de manuscrit. Merci aussi pour tous les bons moments passés. Je remercie également les autres membres du laboratoire CBS, Jenny, Jérémy, Julie, Caroline, Laurence, Annaelle, Kossay et Jérôme.

Ce travail multidisciplinaire alliant biologie moléculaire, biochimie et chimie physique n'aurait pu être réalisé sans l'aide précieuse de différents collaborateurs qui ont chacun apporté une pierre à l'édifice et m'ont permis d'élargir mes horizons ainsi que mes compétences scientifiques.

Merci à Denis Jacquemin et Eric Perpète pour leur aide dans les calculs théoriques. Je remercie également Catherine pour tout son soutien, sa bonne humeur ainsi que pour toutes ses discussions scientifiques qui m'ont permis d'exploiter au mieux tous mes résultats.

Je remercie le laboratoire de virologie moléculaire (ULB) (laboratoire du Professeur Carine Van Lint) pour leur accueil chaleureux au sein de leur établissement ainsi que pour le matériel. Je remercie plus particulièrement Allan pour m'avoir encadré, formé et donné de son temps pour la mise au point des tests enzymatiques. Je le remercie pour tous les bons moments passés aussi bien au sein du laboratoire que dans les différents congrès suivis. Merci aussi à Christelle et Valérie pour leur aide.

Je tiens à remercier vivement le Dr. Jean-François Mouscadet pour m'avoir accueilli durant ma deuxième année de doctorat au sein du laboratoire de Biotechnologie et de Pharmacologie génétique Appliquée de l'Ecole Normale Supérieure de Cachan. J'y ai découvert les joies ainsi que les difficultés de l'expression et de la purification de l'intégrase. Je le remercie également pour tous ses conseils judicieux dans la rédaction des publications. Merci aussi à Gladys pour m'avoir encadré durant toute la durée de mon séjour.

Je remercie également l'unité de chimie organique (UCO) pour son accueil et l'accès à l'équipement RMN. Je tiens aussi à remercier Kiet, Ben, Innès et Vincent pour m'avoir fait profiter de leur expérience et de leurs connaissances en chimie organique. Merci à eux de leur disponibilité et des bons moments passés à leur côté. Je remercie également les Professeurs Vincent et Hevesi pour leurs conseils en chimie organique.

Je ne peux que remercier le Fonds pour la formation à la Recherche dans l'Industrie et dans l'Agriculture (FRIA) pour m'avoir donné la chance de pouvoir réaliser cette thèse et d'avoir financé ces travaux de recherche.

Finalement, je remercie de tout mon cœur mes proches qui m'ont soutenu tout au long de ce périple. Tout d'abord ma maman sans qui je ne serais pas là où je suis aujourd'hui. Merci pour avoir toujours été là et m'avoir aiguillé vers le bon chemin même dans les moments les plus difficiles et les périodes de doute. Je remercie mon frère et ma sœur qui m'ont également soutenu tout au long de ce cursus. Finalement, un dernier merci mais non des moindres à ma tendre moitié pour me supporter depuis maintenant huit ans, de m'avoir toujours soutenu et de s'être autant interessé à mon travail.

Merci à tous

LIST OF ABREVIATIONS

AIDS	Acquire Immunodeficiency Syndrome
APOBEC3G	Apolipoprotein B mRNA-editing enzyme-catalytic polypeptide-like 3G
ATP	Adenosine triphosphate
AZT	Azidothymidine
CA	Capsid protein
CCD	Catalytic core domain
CDK	Cyclin dependent kinase
CTD	C-terminal domain
DKA	Diketoacid
DNA	Deoxyribonucleic acid
env	envelope gene
FDA	Food and Drug Administration
gag	group-specific antigen gene
gp	Glycoprotein
GDP	Guanosine diphosphate
GTP	Guanosine triphosphate
HAART	Highly Active Antiretroviral Therapy
HCV	Hepatitis C virus
HIV	Human Immunodeficiency Virus
HMGI	High-mobility group 1 protein
HT-IN$^{50-212}$ (F185K)	His-tagged HIV-1 integrase catalytic core domain
HT-wt-IN$^{1-288}$	His-tagged wild-type HIV-1 integrase
IBD	Integrase-binding domain
IN	Integrase
INBI	Integrase DNA-binding inhibitor
INSTI	Integrase strand sransfer inhibitor
IPTG	Isopropyl-β-D-galactoside
LEDGF	Lens Epithelium Derived Growth Factor
LEDGIN	Inhibitors of LEDGF/p75-integrase interaction
LTR	Long terminal repeat
MA	Matrix protein
MAb	Monoclonal antibody
Nef	Negative regulatory factor
NC	Nucleocapsid protein
NLS	Nuclear localization signal

NMR	Nuclear magnetic resonance
NNRTI	Non-nucleoside reverse transcriptase inhibitor
NPC	Nuclear pore complexe
NRTI	Nucleoside reverse transcriptase inhibitor
NTA	Nitrilotriacetic acid
NTD	N-terminal domain
NtRTI	Nucleotide reverse transcriptase inhibitor
NUP	Nucleoporin
3'-P	3'-processing
PDB	Protein Data Bank
PFV	Prototype Foamy Virus
PIC	Pre-integration complex
pol	polymerase gene
PR	Protease
RAN	Ras-related nuclear protein
Rev	Regulator of virion protein
RNA	Ribonucleic acid
RT	Reverse Transcriptase
RTC	Reverse-transcription complex
SAR	Structure-activity relationship
SEC	Size-exclusion chromatography
SIV	Simian Immunodeficiency Virus
SN_2	Nucleophilic substitution type 2
ST	Strand transfer
SU	Envelope glycoprotein (gp120)
TAK	Tat-associated kinase
Tar	Trans-activating response
Tat	Transactivating regulatory protein
TDF	Tenofovir disoproxil fumarate
TM	Transmembranar glycoprotein (gp41)
TRIM5α	Tripartite motif protein 5alpha
tRNA	Transfer ribonucleic acid
Vif	Viral infectivity factor
Vpr	Viral protein R
Vpu	Viral protein U

TABLE OF CONTENTS

Part I
Introduction

1 HIV/AIDS: epidemic overview and biological properties

Human Immunodeficiency Virus Type 1 (HIV-1) is the causal agent of acquired immunodeficiency syndrome (AIDS), a widespread disease firstly identified 30 years ago. In this first introductive chapter, an overview of the global HIV/AIDS epidemic as well as a description of the biological aspects of HIV infection are presented. After a brief historic of the discovery of AIDS and the worlwide epidemic situation in section 1.1, a full description of the virus and its mechanism of action are given in section 1.2.

1.1. More than 30 years of AIDS

In 2011, the AIDS epidemic is going down in its fourth decade. Indeed, it's in the early 1981's that the first cases of some extremely rare diseases such as Kaposi's sarcoma or Pneumocystis carinii pneumonia were reported among homosexual men.[1,2] This new set of symptoms, a syndrome in medical terms, which were consistent with damage to the immune system, was called Acquired Immunodeficiency Syndrome or AIDS. In 1983, both the Gallo and Montagnier groups identified at the same time in the blood of patients the etiological agent of AIDS: the Human Immunodeficiency Virus or HIV-1.[3,4] No sooner had HIV-1 been discovered than another human immunodeficiency virus emerged, appearing to be less pathogenic, taking longer to damage the immune system after infection and affecting mainly population in West Africa.[5,6] Identified in 1985, this virus was designated HIV-2. Despite its origin remains steeped in controversy, most of scientists accept that HIV evolved at some point from the closely related Simian Immunodeficiency Virus (SIV), which was transferred from wild-living chimpanzees (Pan troglodytes troglodytes) and gorillas (Gorilla gorilla gorilla) to humans in West central Africa.[7]

Confronted with a growing worldwide epidemic, a lot of research programs were investigated, leading to the approval in 1987 of the first antiretroviral agents, the Azidothymidine (AZT), able to block the HIV reverse transcriptase (RT) which constitutes one of the key enzymes for the viral replication.[8] This discovery opened the way for the design of new anti-HIV therapies, with the beginning in 1995 of bitherapies associating two RT inhibitors in order to have an higher efficiency against the virus.[9,10] In 1996, the commercialization of the anti-HIV protease (PR) drugs led to the clinical use of a tritherapy (Highly Active Antiretroviral Therapy, or HAART) based on the synergic effect of two anti-HIV RT and one anti-HIV PR inhibitors.[11]

This treatment marked by undetectable viral load in treated HIV-seropositive patients was quickly considered as a solution to cure AIDS. Currently, this great enthusiasm is falling due to the appearance of resistant viral strains and strong side effects associate with this treatment. Even though HAART extend and improve the lives of people living with HIV, it does not allow to eradicate HIV in the human body.

Nearly thirty years after its first appearance, the AIDS epidemic is still nowadays the leading case of mortality and morbidity in the world.[12] In 2009, there were 33.3 million people living with HIV and 1.8 million of AIDS-related deaths. Nevertheless, since few years, the spread of AIDS epidemic seems to be halted and begun to reverse. In 2009, there were an estimated 2.6 million people who became newly infected. This is 19 % fewer than the 3.1 million people newly infected in 1997, the year in which annual new infections peaked (Figure 1.1a). The number of annual worldwide AIDS-related deaths is steadily decreasing from the peak of 2.1 million in 2004 to an estimated 1.8 million in 2009 (Figure 1.1b).

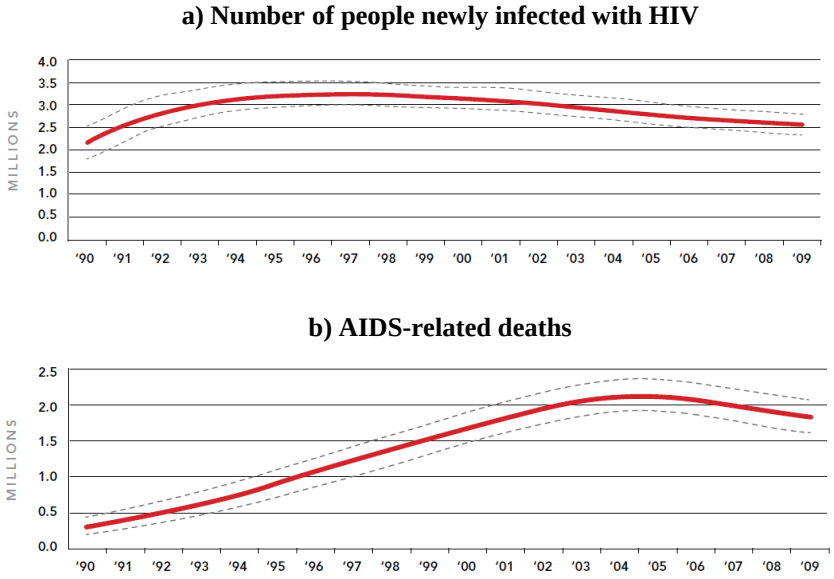

Figure 1.1. Global HIV trends from 1990 to 2009.[12]

Sub-Saharan Africa remains the epicenter of epidemic with 22.5 million people living with HIV, 68 % of the global total. Moreover, the estimated 1.3 million people who died of HIV comprised 72% of the global total of 1.8 million deaths attributable to the epidemic.

Despite the declining of the HIV spread, the number of new infections and AIDS-related deaths are still high. Consequently, the research of new and improved antiretroviral treatments remains today essential.

1.2. Biological aspects of HIV-1 infection

HIV-1 belongs to the retrovirus family, a group of viruses that contains positive single-stranded RNA as genetic material which is retro-transcribed into proviral DNA by a reverse transcriptase. Because a long latency period occurs between the infection (during sexual relations, blood-borne or maternal-fetal transmission) and the first symptoms of the disease, HIV-1 is classified as a lentivirus.

1.2.1. HIV pathogenesis[13]

Once in the human body, HIV targets cells that express CD4 receptors at the surface of the plasmic membrane such as T lymphocytes, dendritic cells or macrophages. HIV infection can be divided into three basic stages based on the $CD4^+$ T cell counts and the level of virus in the blood stream of patients: the acute infection, the latency stage and AIDS (Figure 1.2). In the first stage of infection, or acute infection, a fast viral replication occurs leading to an abundance of viruses in the peripheral blood and a marked drop in the numbers of circulating $CD4^+$ T cells (HIV budding from the plasma membrane causing cells damage, attacks of cytotoxic T lymphocytes, appearance of syncytia, apoptosis). During this period (usually 2-4 weeks post-exposure) most individuals develop some symptoms such as influenza or mononucleosis-like illness. These ones disappear within two weeks, when a strong immune defense reduces the number of viral particles in the blood stream, marking the start of a latent period (which can last until 20 years) during which no clinical symptoms are observed. Nevertheless, the concentration of $CD4^+$ T cells progressively decreases over time. When the cells count is below 200 cells/mm^3, AIDS is associated to opportunistic infections such as Kaposi's sarcoma, Pneumocystis carinii pneumonia or toxoplasma.

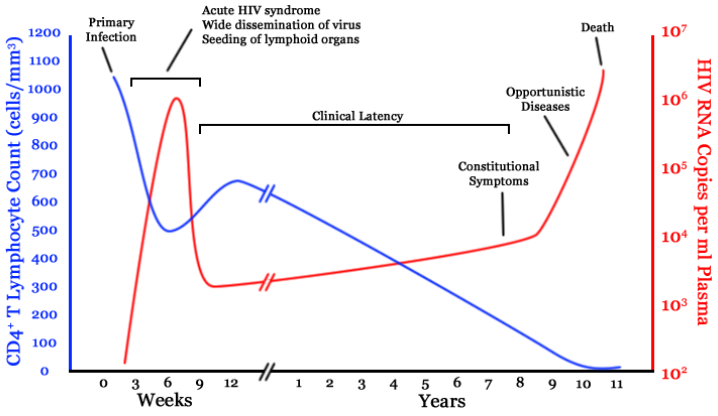

Figure 1.2. Evolution of the viral load (red curve) and CD4 cells counts (blue curve) over the average course of untreated HIV infection.[13]

1.2.2. Structure and genome of HIV-1[14]

Mature HIV-1 virions (Figure 1.3) are roughly spherical particles varying in diameter from 1000 to 3000 Å. The outer envelope consists of a lipid bilayer studded with two glycoproteins: the envelope glycoprotein (gp120 or SU) and a transmembranar glycoprotein (gp41 or TM). The matrix protein (p17 or MA) forms a layer under the viral membrane and is essential for the viral stability. The genetic material of the virus is enclosed by a coating of capsid proteins (p24 or CA). This core contains two copies of single-stranded RNA tightly bound to nucleocapsid proteins (p7 or NC), viral proteins (p6, Tat, Rev, Vif, Nef, Vpr and Vpu) as well as three key enzymes for viral replication: HIV-1 RT, HIV-1 PR and HIV-1 integrase (IN).

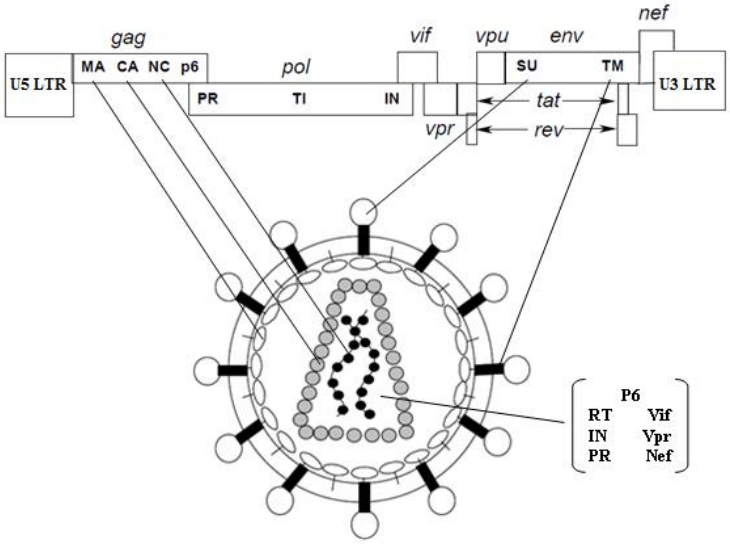

Figure 1.3. Structure and organization of the HIV-1 genome and virion.[14]

The HIV-1 genome encodes nine open reading frames flanked by two Long Terminal Repeat sequence (U5 and U3 LTR) which regulate viral gene expression via their interaction with multiple viral and host factors. Among these nine genes, the gag, pol and env genes are common to all retroviruses:

- The gag (group-specific antigen) gene provides the basic physical infrastructure of the virus by encoding the matrix, capsid, nucleocapsid and p6 proteins.
- The pol (polymerase) gene encodes three enzymes essential for the virus replication: RT, PR and IN.
- The env (envelope) gene encodes for viral envelope glycoproteins gp120 and gp41.

The six additional genes of HIV-1 genome (tat, rev, vif, nef, vpr and vpu) encode for accessory and regulatory proteins.

1.2.3. HIV-1 life cycle

Like all other retroviruses, HIV-1 uses the CD4+ T cell's machinery to replicate itself. The replication cycle can be divided into 5 major steps (Figure 1.4): the virus entry into host cell, the uncoating of the capsid core and reverse transcription of viral RNA, the nuclear entry and the integration of viral DNA into the host cell DNA, the transcription and translation of viral polyproteins, the budding and maturation of the new retroviral particle.

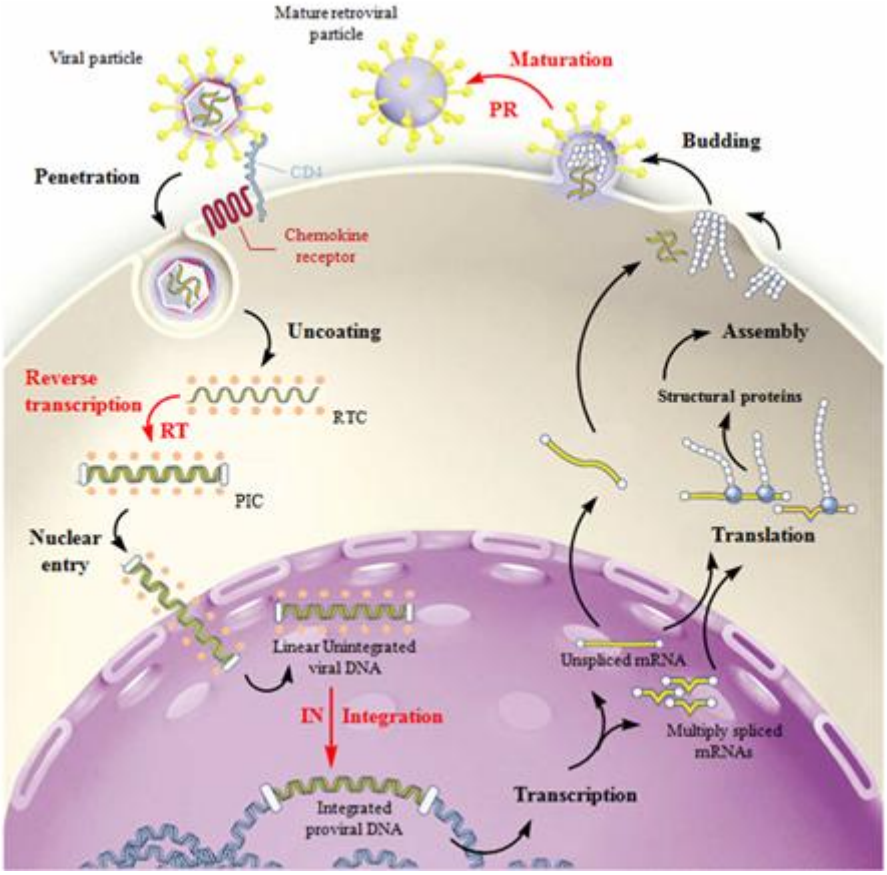

Figure 1.4. HIV-1 replication cycle.[15]

I. Entry

The early phase of the replication cycle begins with the attachment of the envelope glycoprotein gp120 present at the surface of viral particles to the CD4 T-cell receptor. This interaction triggers a conformational change in gp120 leading to its binding to a chemokine coreceptor such as CXCR4 and CCR5.[16] This second interaction induces new conformational shifts in the envelope glycoprotein gp120 and lead to the dissociation of gp120 from gp41. Finally, the insertion of gp41 fusion peptide into the membrane results in the fusion of viral and cell membrane and the release of the viral core into the cytoplasm.[17]

II. Uncoating and reverse transcription[18]

Although early work suggested that the viral core undergoes a disassembly immediately after its release into the cytoplasm[19], recent studies proposed that capsids remain intact until HIV-1 incoming complexes reach the nuclear membrane and that uncoating occurs at the nuclear pore upon completion of reverse transcription. The retrotranscription of the viral RNA in viral DNA is initiated by a cellular tRNA(Lys) and catalyzed by HIV-1 RT within reverse-transcription complexes (RTCs) surrounded by the intact capsid core. HIV-1 RT requires the RNA-dependent DNA polymerase activity to synthesize DNA from an RNA template and the Rnase H activity to degrade the RNA after the first strand DNA has been synthesized. Vif would protect, in cells producing viruses, the newly formed double-strand DNA by preventing the deamination reaction of deoxycytidine to deoxyuridine in viral DNA catalyzed by the host APOBEC3G protein.[20,21] During reverse transcription, HIV-1 RTCs move rapidly toward the nuclear compartment, using microtubules and actin filaments to reach the nuclear pore.[22] There, the completion of reverse transcription and the formation of the central DNA Flap facilitate uncoating.[23] Recent work indicates that the host protein TRIM5α promotes the rapid and premature disassembly of viral capsids thus abrogating productive reverse transcription.[24,25] Nevertheless, TRIM5α-mediated restriction is modulated by the host protein Cyclophilin A (Cyp A) which could also interact with the capsid of HIV-1.[26]

III. Nuclear entry and integration

In order to form the provirus, the viral genome must cross the cell's nuclear membrane to integrate the host cell DNA. Upon uncoating of the viral core, the viral complex becomes a pre-integration complex (PIC) competent for import into the nucleus. Although the complete identification of PIC components remains uncertain, viral proteins such as IN, MA, Vpr, RT and the cellular protein HMGI(Y) have been identified as PIC components.[27] The HIV-1 active nuclear import model proposed is a process by which the nuclear localization signal (NLS) identified into IN and MA proteins is recognized and bound by a member of the importin family of nuclear import receptors (importin-α and -β).[28] Among its many roles play in HIV-1 infection, Vpr mediates the targeting of the PIC to the nucleus via its interaction with importin-α, ultimately promoting binding to nuclear pore proteins.[29] The RAN-GDP/RAN-GTP gradient that exists between the cytoplasm and nucleus serves to drive the direction of the import complex whereas the movement into the nucleus occurs through nuclear pore complexes (NPCs) containing nucleoporins (NUPs) that assemble to form the larger pore complexes.

It has been shown that NUP153 plays a central role in PIC nuclear import by interacting via its C-terminal domain with HIV-1 IN. The dynamic distribution of the C-terminal domain of NUP153 throughout the channel as well as its exposure to the cytoplasm under active transcription offers the PIC a direct link from the cytoplasm to the chromosomal DNA environment best suited to support integration catalyzed by HIV-1 IN (This will be detailed in chapter 3).[28,30] Cellular DNA binding proteins have been described to interact with IN and seem therefore critical for the integration process. Lens epithelium-derived growth factor (LEDGF/p75), a protein implicated in the regulation of gene expression and in the cellular stress response, was found to interact with IN and seems to be required to dock the PIC to the host chromatin.[31]

IV. Transcription and translation of viral proteins

Once integrated, the HIV proviral genome is transcribed by the host RNA polymerase II. Activation of transcriptional elongation occurs following the recruitment of HIV-1 Tat protein to the transcription machinery via a specific interaction with an RNA regulatory element called TAR (Transactivation Response Element). After binding to TAR RNA, Tat stimulates a kinase called TAK (Tat-associated kinase) which hyperphosphorylates RNA polymerase and stimulates its activity.[32] The interaction of HIV-1 Nef protein with Tat may also enhance the HIV-1 gene expression.[33] After transcription, a set of spliced mRNAs are free to move away from the nucleus and are translated into viral polyproteins in the cytoplasm using host ribosomes. The unspliced mRNA, which constitutes the genetic material of the new virions, is efficiently transported by the HIV-1 Rev protein through its binding to the Rev-responsive element (RRE) sequence.[34]

V. Budding and maturation[35]

Viral particle formation is a multi-step process driven by the viral polyprotein Gag. Gag contains three conserved regions (MA, CA, NC) that perform distinct functions during viral assembly: the N-myristoylated MA domain targets the protein to cellular membrane, the CA domain makes important protein-protein interactions during particle assembly, and the NC domain captures the viral RNA genome and couples RNA binding and assembly. The viral protease activated during assembly cleaves Gag to generate a set of new proteins which then reassemble to form the distinct layers of the mature virion. Finally, the budding of the new retroviral particle is mediated by the recruitment of cellular proteins.

Vpu, a membrane-associated accessory protein that is unique to HIV-1, enhances the release of progeny virions from infected cells by antagonizing tetherin, an interferon-regulated host restriction factor that directly cross-links virions on host cell-surface.[36]

2 HIV antiretroviral therapy

For over 30 years, AIDS research focused on both the development of vaccines and the discovery of antiretroviral drugs able to block the HIV-1 replication cycle. Despite no vaccines have been shown effective, a success has been achieved in anti-HIV drug discovery. In the first section of this chapter, the different classes of anti-HIV-1 drugs and their mechanism of action are presented. Current status and future prospects of antiretroviral therapies are finally discussed in section 2 and 3, respectively.

2.1. Twenty-five antiretroviral drugs licensed

The currently 25 FDA- and EMEA-approved anti-HIV-1 drugs can be divided into four groups based on the step blocked in the HIV-1 life cycle: entry inhibitors, RT inhibitors, IN inhibitors and PR inhibitors.

2.1.1. Entry inhibitors

One of the key steps in the infection of the host cells by HIV-1 is the interaction of the envelope glycoprotein gp120 with CD4 and CXCR4/CCR5 chemokine receptors. These associations lead to the insertion of the gp41 fusion peptide into the host cell membrane. Entry inhibitors hold considerable potential for the treatment of HIV infection, particularly in patients harboring viruses resistant to RT and PR inhibitors. Currently, only antagonists that block fusion and CCR5 binding have been approved by the FDA for treatment of HIV-infected patients.

Pharmacological agents that disrupt gp41-mediated membrane fusion, also called fusion inhibitors, were the first entry inhibitors to be approved for the treatment of HIV infection. **Enfuvirtide**[37] (Figure 2.1) is a polypeptide of 36 amino acids that mimics the C-terminal region of gp41. Due to its poor oral bioavailability, this drug has to be administered twice daily by subcutaneous injection, inevitably leading to injection site reactions including erythema, induration, nodules and cysts. Moreover, mutations within gp41 seem to emerge promptly in patients upon monotherapy with enfuvirtide.[38] A number of other next-generation peptidic fusion inhibitors active against some enfuvirtide-resistant strains are under investigation.[39,40]

However, since peptidic fusion inhibitors are not orally bioavailable and must be administered via injection, another approach based on the development of small molecule inhibitors of gp41-mediated fusion was developed.[41]

Maraviroc[42] (Figure 2.1) is the only CCR5 co-receptor antagonist used in the treatment of HIV-1 infection. Orally administered twice daily, it appeared to be well tolerated and is indicated for use in combination with other antiretroviral agents in treatment-experienced adult patients infected with multidrug-resistant, CCR5 tropic HIV-1.[43] Another CCR5 antagonist, **vicriviroc**[44] (Figure 2.1), is currently in phase III clinical trials. In addition, others inhibitors seem to be promising candidates for further development.[45,46] However, there are some concerns regarding the use of this class of anti-HIV-1 drugs as treatment because blocking the CCR5 co-receptor could drive the virus to use the other CXCR4 co-receptor, leading to the emergence of resistant HIV strains and a more aggressive disease.[47] Therefore, there is also a need to develop effective drugs able to block CXCR4 co-receptor. Thus far, none of the CXCR4 antagonists in development have shown promise in HIV clinical trials.

Ac-Tyr-Thr-Ser-Leu-Ile-His-Ser-Leu-Ile-Glu-Glu-Ser-Gln-Asn-Gln-Gln-Glu-Lys-Asn-Glu-Gln-Glu-Leu-Leu-Glu-Leu-Asp-Lys-Trp-Ala-Ser-Leu-Trp-Asn-Trp-Phe-NH2

enfuvirtide (Fuzeon®)

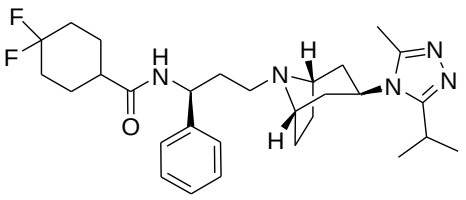

maraviroc (Celsentri®)

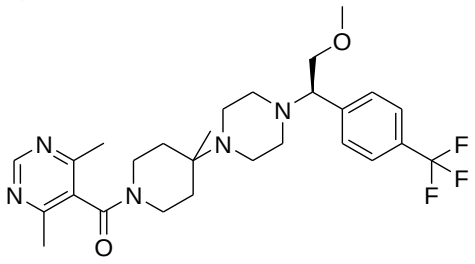

vicriviroc

Figure 2.1. Structure of HIV-1 entry inhibitors.

2.1.2. RT inhibitors

The first anti-HIV-1 drug approved for the treatment of AIDS was AZT, also known as **zidovudine**[8]**,** a nucleoside RT inhibitor (**NRTI**). Since there, extensive research has led to the design of new nucleoside-based analogs as well as non-nucleoside RT inhibitors (**NNRTIs**).

Once phosphorylated by cellular kinases to their triphosphate derivatives, **NRTIs** interact with the DNA polymerase active site of RT and are incorporated into the growing DNA. Due to the lack of 3'-hydroxyl group, these compounds prevent the incorporation of the incoming nucleotide that results in terminating the elongation of the growing DNA double strand.

In addition to the 7 currently approved NRTIs, multiple compounds are in phase II or III clinical trials (Figure 2.2).[48]

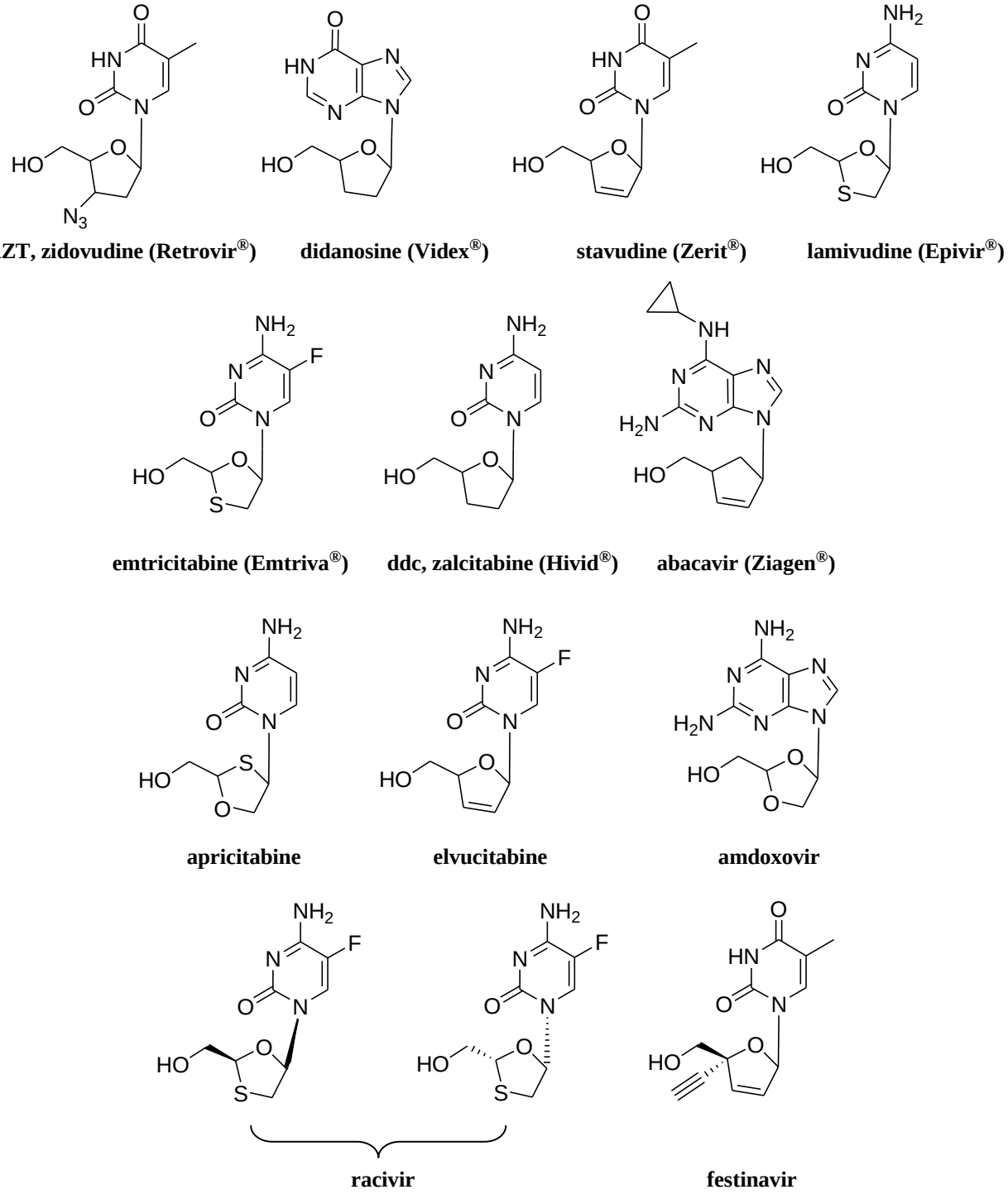

Figure 2.2. Structures of NRTIs currently approved by the FDA (top 2 lines) and undergoing phase II or III clinical trials.

Despite these are extensively used in HAART, their effectiveness can be limited by the emergence of drug resistance and adverse events.

Due to their poor selectivity, these compounds exhibited acute toxicity. The inhibition of mitochondrial DNA polymerase gamma (mtDNA pol γ) is one of the major causes of all NRTIs-related adverse effects.[49] Besides RT mutations, NRTIs resistance might arise through a repair reaction called pyrophosphorolysis whereby the nucleoside inhibitor is removed from the growing viral DNA chain, allowing reverse transcription to resume.[50] Metabolic activation of NRTIs also represent a relevant problem for this class of compounds with the first phosphorylation being generally assumed as the rate-limiting step.[51]

To overcome the problem of NRTIs activation process, nucleotide analog prodrugs (NtRTIs) have been developed with the aim to deliver nucleoside analogs monophosphates. FDA-approved **tenofovir disoproxil fumarate**[52] (**TDF**) (Figure 2.3) is widely used in antiretroviral regimens for both treatment-naive and -experienced patients and is active against some nucleoside-resistant strains of HIV-1. Nevertheless, cross resistance with other NRTIs as well as side effects such as acute renal failure are associated to the clinical use of this drug. Recently, **GS-9131**[53] (Figure 2.3) characterized by improved resistance profile, safety and long term tolerability has been identified. This compound is considered as a promising drug candidate for the treatment of HIV-1-infected individuals.

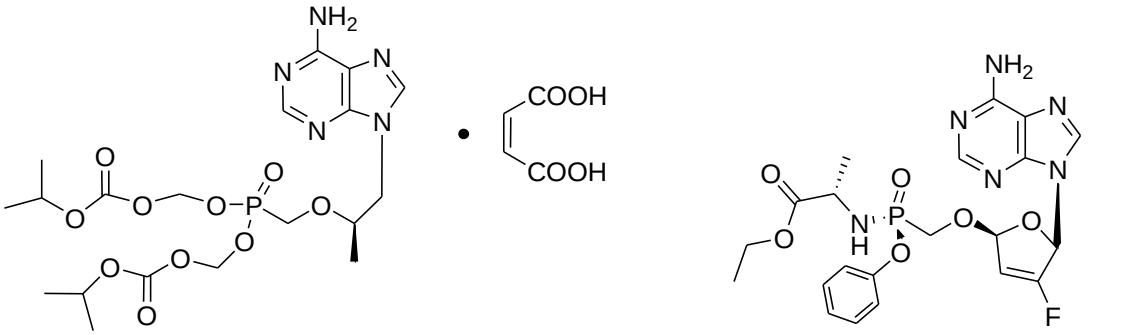

TDF, tenofovir disoproxil fumarate (Viread®) **GS-9131**

Figure 2.3. Structures of NtRTIs.

NNRTIs inhibit RT activity by binding noncompetitively to an allosteric site located about 15 Å from the catalytic site. This interaction induces a conformational change within the enzyme that blocks the RT polymerase activity. Contrary to NRTIs, these drugs are relatively specific, that confers on them low side effects. A major limitation to the success of the first generation of NNRTIs (Figure 2.4, first line) is the rapid emergence of HIV-1 variants resistant to these drugs which contain one or more mutations in the non-nucleoside inhibitor binding pocket of RT.[54,55]

In this context, a second generation of NNRTIs with a better resistance profile and an increased genetic barrier to the development of resistance was developed. Among these next generation NNRTIs, **etravirine**[56] was approved by the FDA whereas four more are currently under clinical development (Figure 2.4, second and third line).[55]

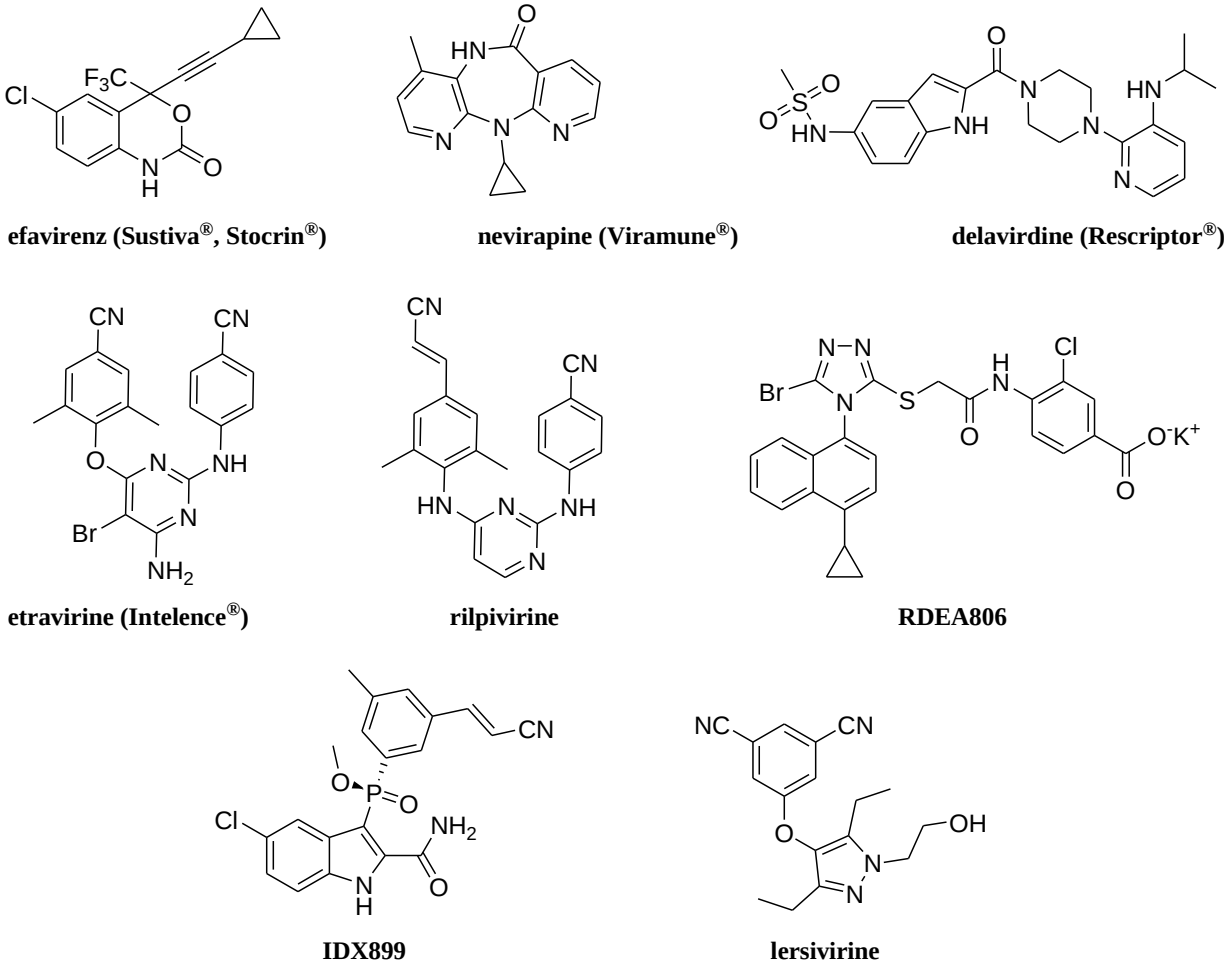

Figure 2.4. Structures of first generation FDA-approved (first line) and second generation NNRTIs.

2.1.3. IN inhibitors

The integration of the viral DNA into the host cell genome is an essential step in the viral replication cycle. This process is catalyzed by HIV-1 IN which is considered as one of the most promising antiviral drug targets. HIV-1 IN inhibitors currently approved or in clinical development were identified as **strand transfer inhibitors** (**INSTIs**). They block the DNA strand transfer reaction of the enzyme by interacting with the magnesium cofactor (Mg^{2+}) at the enzyme catalytic site. Their mechanism of action will be described in more details in chapter 3.

At the moment, **raltegravir**[57] (Figure 2.5) is the only FDA- and EMEA-approved HIV-1 IN. This one is an orally, well tolerated active compound dosed 400 mg twice daily and metabolized by glucuronidation.[58] Raltegravir is only licensed in combination with other antiretroviral agents for the treatment of HIV-1 infection in treatment-experienced adult patients who have evidence of viral replication and HIV-1 strains resistant to multiple antiretroviral agents.[59,60] On the basis of its metabolic profile and preclinical data, raltegravir has a low propensity to be involved in clinically meaningful drug interactions.[61] Similar to all antiretroviral drugs, raltegravir is associated with treatment failure, i.e., partial or complete loss of viral suppression. HIV resistance to raltegravir is the consequence of mutations located close to the IN active site, which can be divided into three main evolutionary pathways: the N155H, the Q148R/H/K and the Y143R/C pathways.[62] Each of these primary mutations can be accompanied by a variety of secondary mutations that both increase resistance and compensate for the variable loss of viral replicative capacity that is often associated with primary resistance mutations.[63] **Elvitegravir**[64,65] (Figure 2.5) is the next most advanced INSTI currently in phase III clinical development. Like raltegravir, it has also shown potent antiviral activity *in vivo* against HIV-1 carrying resistance mutations to multiple antiretroviral drug classes when it is administered with active background therapy.[66] Nevertheless, resistance mutations (Q148R/H/K, N155H, E92Q and T66I as major mutations) and cross-resistance to raltegravir have been identified in phase II clinical studies.[67] Recently, a second generation once daily unboosted INSTI, S/**GSK-1349572**[68] (GSK-572), that retains antiviral activity in clinical isolates resistant to raltegravir and elvitegravir has been developed (Figure 2.5). This compound was recently started phase III clinical trial.

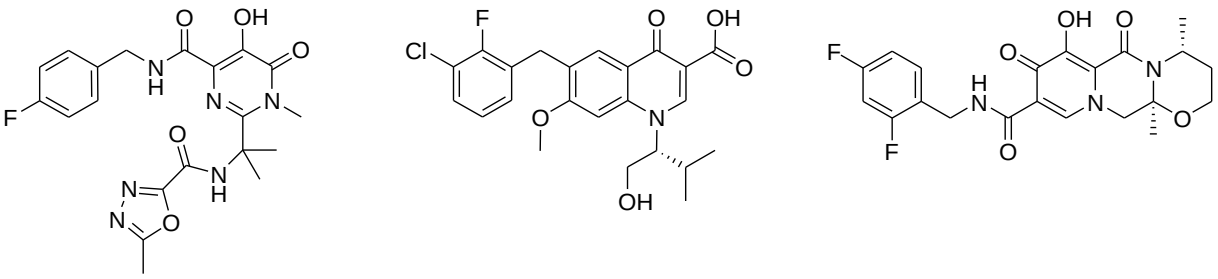

Figure 2.5. Structures of raltegravir, elvitegravir and S/GSK1349572.

2.1.4. PR inhibitors

HIV-1 PR is responsible for the cleavage of polyproteins to the structural proteins, thereby providing the new mature virion.

PR inhibitors interfere with this late stage of the viral replication cycle and prevent the formation of infectious virus. Currently, there are 10 FDA-approved PR inhibitors which can be divided into two major classes: the **peptidomimetic** and **non-peptidic** inhibitors (Figure 2.6).[69]

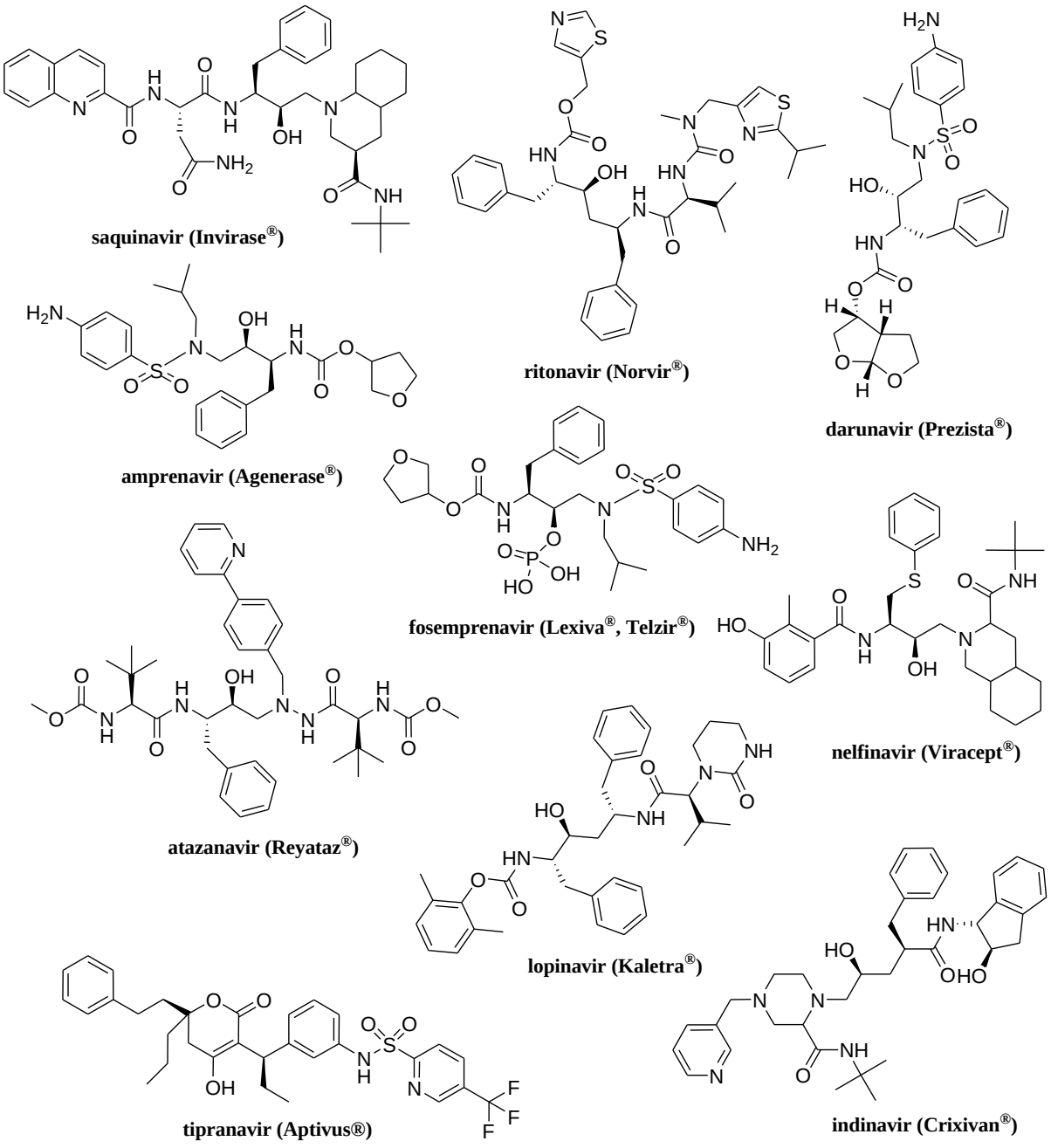

Figure 2.6. Structures of the 10 FDA-approved peptidomimetic and non-peptidic PR inhibitors.

Peptidomimetic inhibitors contain a hydroxyethylene core mimicking the transition-state formed during the HIV-1 PR-catalyzed proteolysis of viral polyproteins.

Most of PR inhibitors are prescribed with a lowdose of **ritonavir** as boosting agent because it was recognized that this drug reduces the metabolism of administered compounds through hepatic and intestinal cytochrome P450 3A4 inhibition, leading to the dramatical improvement of bioavailability and half-life.[70] Like other drug molecules with peptidic character, the efficiency of these agents is limited by their poor bioavailability. Furthermore, this class of drugs suffers from the ever-present problem of resistance and cross-resistance as well as a specific toxicity profile (e.g., gastrointestinal disturbances and lipodistrophies).

This has prompted the search for **non peptidic** inhibitors, with **tipranavir**[71] which contains a dihydropyrone ring as a central scaffold instead of the peptidomimetic hydroxyethylene. It was approved by the FDA in 2005 for the treatment of highly experienced patients with resistance to multiple PR inhibitors. Tipranavir is a potent inducer of its own metabolism through induction of the cytochrome P450 expression, which results in a need for dose ritonavir boosting.[70] Despite its virological benefits, this antiretroviral agent presents diverse side effects such as diarrhea, nausea and vomiting.

2.2. Current status of antiretroviral therapy[72]

Since the introduction of combination therapy in 1990s, termed Highly Active Antiretroviral Therapy (HAART), the number of people dying from AIDS has significantly decreased.[11] Current HAART regimens combine two or three drugs that target more than one step of the virus life cycle: NRTIs, NNRTIs and PR inhibitors. The clinical benefits of using multi-therapies are the synergic effects of the different drugs, side effects decrease as well as the improvement of drug resistance profile. The decision to begin antiretroviral therapy for any patient must balance the burden and toxicity of the drug regimen against the benefits of decreased HIV-related morbidities and increased life expectancy. For all patients, the goal of the therapy is the reduction of plasma viral load to below detectable levels (50 copies/ml). Several factors need to be considered when choosing an initial regimen such as comorbidities (e.g., cardiovascular, renal, or psychiatric disease), potential adverse drug effects, interactions with other medications the patient may be receiving and patient adherence. Based on the results of genotypic-resistance testing, a regimen should be constructed to maximize the probability of virologic suppression while minimizing adverse effects, toxicities, and pill burden.

Most preferred regimens for initiating therapy include a **dual-NRTI backbone** in combination with an **NNRTI**, a **ritonavir-boosted PR inhibitor** or an **INSTI**.

A combination of **TDF** and **emtricitabine** has become the most commonly used dual-NRTI backbone in first-line therapy because of superior virologic efficacy, reduced drug resistance and less toxicity than other NRTI regimens.[73-75] The choice of whether to use an NNRTI, a boosted PI, or an INSTI needs to be individualized. The combination of **TDF**, **emtricitabine** and **efavirenz**, co-formulated into a once daily Atripla[76] tablet has markedly simplified the drug regimen for HIV-1 infected patients. Clinical assessment, together with measurement of HIV RNA levels and CD4 cell counts, should be used to assess the need to change therapy. Single drug substitutions of individual antiretroviral, usually within the same class, is recommended for toxicity, drug-drug interaction or intolerance. If the patient experiences resistance, the switch of the entire regimen from first to second line is required. At least two, and preferably three, fully active drugs should be included in the new regimen, ideally using agents from at least one new class.

There is no doubt that HAART has substantially reduced the death rate from AIDS and improved the quality of life for HIV-1-infected patients. Nevertheless, the issues of the currently used drugs such as resistance and the formation of HIV-1 latent reservoirs in patients undergoing HAART show need to design new antiretroviral agents.

2.3. New and emerging targets for HIV therapy

As discussed above, a number of significant problems associated to the clinical use of the currently anti-HIV drug are observed. Although the discovery of anti-HIV drugs that belong to the already existing classes are still needed to deliver new drugs that benefit AIDS patient, the design of new agents with novel mechanism of action could be of greater benefit, as they could overcome the current resistance mechanism or prevent HIV-1 infection. New agents in preclinical and clinical development are presented below.

2.3.1. Pharmacological cycline dependent kinase inhibitors

Cyclin dependent kinases (CDKs) are cellular enzymes which bind to a protein called cyclin to form cyclin/CDK complexes involved in HIV-1 Tat transactivation. Upon cellular stress, natural CDK inhibitor p21/waf1 is normally induced and regulates cell cycle progress. Recent studies have shown that HIV-1 latently infected T cells do not induce expression of p21/waf1 after injury to the host cell.[77] Consequently, CDKs could be targeted for both inhibition of HIV-1 replication and HIV-1 latent reservoirs using drugs that mimic the natural CDK inhibitors.

R-roscovitine (Figure 2.7), currently in phase I cancer clinical trials, reversibly competes for ATP binding site in CDKs.[78] It has been shown in preclinical studies to inhibit HIV-1 production and induce apoptosis in latent and activated HIV-1-infected cells without the release of infectious virions.[79]

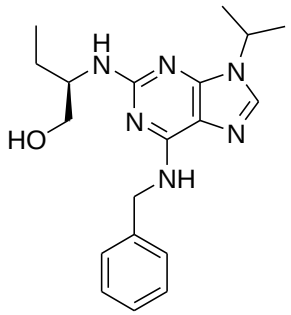

Figure 2.7. Structure of R-roscovitine.

2.3.2. Modified anti-sense oligonucleotides

Modified anti-sense oligonucleotides are short single strands RNAs designed to have a high affinity for their target sequence and inhibit gene expression. The inhibitory effect is largely based on strong binding of antisense oligonucleotides to the target mRNA, which can block splicing events or the elongating ribosome through steric hindrance.[80] Moreover, cleavage of the viral RNA could also mediated by recruitment of RNase H.[81] One antisense drug, **HGTV43**[82] is starting Phase II trials.

2.3.3. Immune-based therapies

As described in chapter 1 (section 1.2.3), virus entry is mediated by the binding of the envelope glycoprotein gp120 to the Human T cell receptor CD4. The monoclonal antibody (MAb) **ibalizumab**[83] (TNX-355) is a humanized IgG4 MAb which interferes with viral entry by interacting with the antibody binding site of the CD4 receptor distinct from the site required for the binding of gp120 and major histocompatibility complex proteins which play an important role in the immune system. Ibalizumab does not inhibit gp120 binding to CD4 but appears to exert its antiviral effect by post-binding conformational effects that prevent CD4-bound gp120 from interacting with CCR5 or CXCR4. Administered by intravenous infusion once every other week, TNX-355 was found in phase II clinical trial to produce dose dependent reduction in HIV-1 viral load and increase in CD4 cell count.[84] Moreover, synergistic effect with the fusion inhibitor enfurvirtide was observed.[85]

The development of an effective HIV-1 vaccine remains nowadays one of the major goals of AIDS research to end the epidemic. Traditional methods of vaccine design including live attenuated virus, whole killed virus or subunit proteins are thought to be too dangerous or ineffective in protecting against HIV. Current most advanced HIV-1 vaccine trials are based on the use of viral vectors which are rendered replication-defective by mutations and by deletion of adenovirus genes. These are replaced by HIV genes to form replication-incompetent viruses able to insert their genomes into the host cell DNA and expressed HIV proteins-mediated immunity response.[86] One of the most advanced vaccine regimen combines the Alvac-HIV and Aidsvax vaccines. Alvac-HIV uses the canarypox virus vector containing the three env, gag and pol HIV-1 genes whereas Aidsvax vaccine contains recombinant surface glycoprotein gp120. The co-administration of the two vaccines could both stimulate the HIV specific T lymphocytes and activate neutralizing anti-HIV antibodies. An induction of prespecified cellular and humoral immune responses as well as no serious adverse events and HIV-1 infections associated to Alvac-HIV/Aidsvax vaccine regimen has been reported in phase III clinical trial. Although this treatment has low-level efficacy in reducing HIV-1 acquisition, it offers insight for future research.[87]

3 Focus on HIV-1 IN

HIV-1 IN is an attractive target for new AIDS chemotherapeutics. This enzyme which belongs to the family of proteins with DDE motif, also called polynucleotidyl transferase family, is essential to the virus replication cycle by integrating viral DNA into the host cell genome. Moreover, it has no human counterparts, suggesting that low side effects could be associated with the enzyme inhibition. This third part of the introduction focuses on HIV-1 IN. In the first section, key role played by the enzyme in the integration process is described. The second section reports the HIV-1 IN structure whereas the different classes of HIV-1 IN inhibitors and their mechanism of action are presented in the third section.

3.1. Catalytic activities

Integration of viral DNA into the host-cell chromosome is catalyzed by HIV-1 IN through a two general sequential reactions (Figure 3.1) that are also observed for polynucleotidyl transferase family enzymes.[88,89] The first one, named **3'-processing** (3'-P), occurs in the cytoplasm and more specifically in a preintegration complex (PIC) including viral DNA, viral proteins (RT, IN, …) and host cellular proteins (HMG-A1, LEDGF/p75, …).[27] This process corresponds to an endonucleolytic cleavage at each 3' ends of double stranded viral DNA extremities. IN specifically recognizes two inverted DNA sequence (U3 and U5 LTR) and cleaves GT dinucleotides immediately 3' to a conserved CA dinucleotides to produce two reactive 3'OH ends. Following 3'-P reaction, PIC is actively transported across the nuclear membrane into the nucleus and targeted to the host genomic DNA to perform the second catalytic reaction catalyzed by IN, called **strand transfer** (ST). The two 3'-OH ends generated during 3'-P attacks two phosphodiester bonds (spaced 5 base pairs apart) of cellular DNA to inserts the viral DNA into the host cell genome. Finally, the integration process ends by the cleavage of the two nucleotides at the 5'-end and gap filling from the 3'-end of the host genomic DNA probably by cellular DNA repair enzymes.[90]

IN may catalyze a third reaction, named **disintegration**, which corresponds to the apparent inverse reaction of ST.[91] Contrary to 3'-P and ST reactions which require full-length protein, disintegration can be catalyzed by the catalytic domain alone ($IN^{50–212}$) or by truncated proteins ($IN^{1–212}$ or $IN^{55–288}$).[92]

Although it is not clear whether it may occur *in vivo*, this process is observed *in vitro* and was widely used for testing the competitive mechanism of some inhibitors.

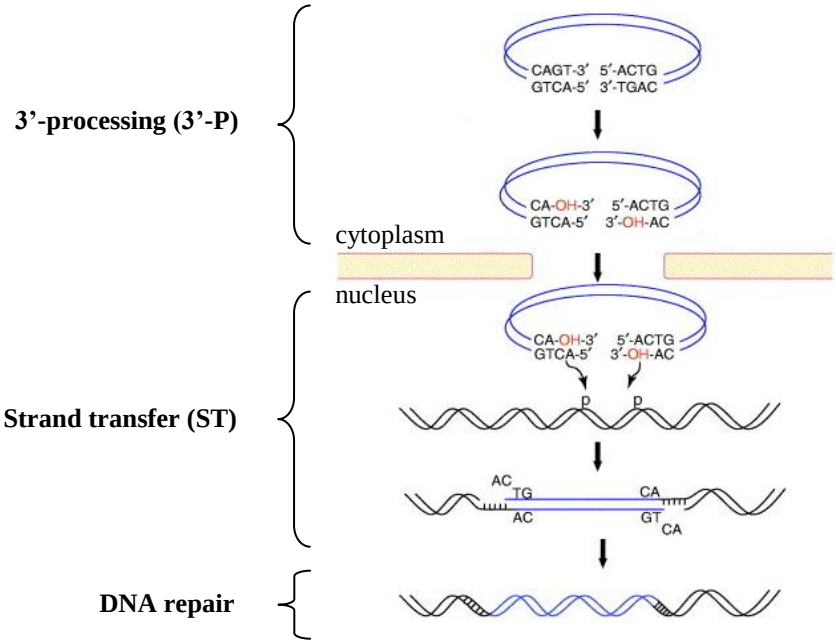

Figure 3.1: Mechanism of viral DNA integration catalyzed by HIV-1 IN.[93]

All three processes require a metallic cofactor such as Mn^{2+} or Mg^{2+}. Some experimental evidence suggest that Mg^{2+} is more physiologically relevant: (i) IN displays strong non-specific nuclease activity in the presence of Mn^{2+}.[94] (ii) The sequence variation at both viral DNA ends is much greater in the presence of Mn^{2+} than in the presence of Mg^{2+}.[95]

Crystallographic studies of proteins belonging to the polynucleotidyl transferase family and catalyzing 3'-P and ST have shown that these reactions occured by a one-step SN_2-like mechanism.[96-98] Crystal structures of *B. halodurans* RNase H1/RNa-DNa complexes allowed the reconstruction of the course of 3'-P reaction and point to the involvement of a general two-metal ion catalysis implicating water molecules (Figure 3.2).[99,100] In this mechanism, metal ions are located on two sides of the scissile phosphate and form stable octahedral complex: the B-site Mg^{2+} coordinates, positions and activates the nucleophile (water molecule) to attack the phosphorus atom of the scissile phosphate (Figure 3.2a) whereas the A-site Mg^{2+} stabilizes the transition state and the leaving group. This step is associated to the move of the two metal ions close together to promote the formation of the transition state. Interestingly, the 5'-phosphate is displaced from the active site after the completion of the hydrolysis to form a stable complex in which the two Mg^{2+} are octahedrally coordinated by a conserved DDE motif, water molecules and 3'-OH extremity of the processed strand.

Recently, Maertens et al. reported an SN_2 mechanism for ST reaction based on the superimposition of crystal structures of PFV IN/DNA complexes.[101] In this mechanism, the 3'-hydroxyl group of viral DNA coordinated to B-site Mg^{2+} is positioned to perform an in-line SN_2 nucleophilic substitution at the phosphorous atom of the scissile phosphodiester in target DNA (Figure 3.2 b). As a result, the viral DNA-target DNA phosphodiester shifts from its pre-strand transfer position (~ 110° rotation) and is thereby ejected from the active site.

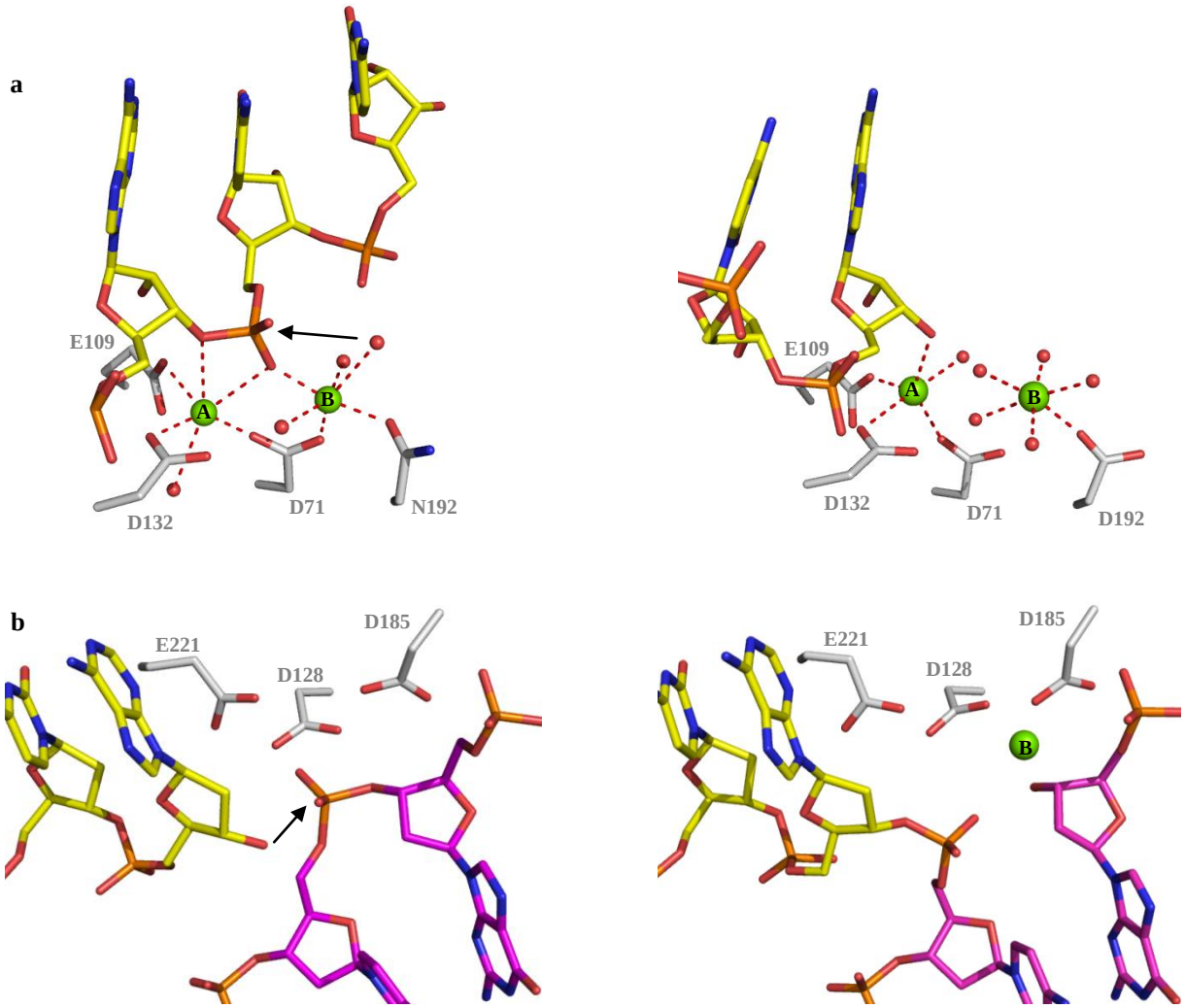

Figure 3.2. Proposed catalytic mechanism of 3'-P and ST reactions. Mg^{2+} ions and water molecules are shown as green and red spheres, respectively. DDE acidic residues are shown as grey sticks, RNA/DNA and viral DNA substrate are shown as yellow sticks whereas target DNA is shown as purple sticks. a) Endonucleolytic cleavage catalysed by RNase H1 enzymes. Left: Pre-reactive state obtained with RNA/DNA hybrid substrate (PDB code 1ZBL).[99] Right: Product complex obtained with 5'-phosphorylated RNA/DNA hybrid (PDB code 2G8V).[100] b) ST reaction catalyzed by PFV IN. Left: Pre-catalytic target capture complex obtained with 3'-processed viral DNA and target DNA in the absence of Mg^{2+} ions (PDB code 3OS2).[101] Right: Post-catalytic strand transfer complex obtained with 3'-processed viral DNA and target DNA in the presence of Mg^{2+} ions (PDB code 3OS0).[101]

3.2. Structure

HIV-1 IN is a metalloenzyme of 32 kDa (288 amino acids) which belongs to the polynucleotidyl transferase family. It is composed of three functional domains each required for catalytic reactions (Figure 3.3).

- The **N-terminal domain** (amino acids 1-49) contains a HHCC zinc-finger motif that promotes protein multimerization.
- The **catalytic core domain** (CCD) (amino acids 50-212) contains a DDE triad conserved among the polynucleotidyl transferase family. These residues are involved in the complexation of metallic cofactor(s) (Mg^{2+}) essential for the catalytic activity.
- The **C-terminal domain** (amino acids 213-288) binds non-specifically to viral DNA and stabilizes the IN/DNA complex.

To date, crystal structure of full-length IN alone or in complex with its cognate DNA substrate has not yet been resolved. Nevertheless, the structures of the isolated N-terminal (IN^{1-49}) and C-terminal ($IN^{219-270}$) domains have been determined by NMR (Figure 3.3).[102,103] IN^{1-49} has a structure consisting of four α helices stabilized by a Zn^{2+} cation tetrahedrally coordinated by a HHCC motif. $IN^{219-270}$ structure consists of five antiparallel β-strands forming a β-barrel and adopting a SH3-like fold. The structure of the catalytic core domain (CCD) has been determined by crystallographic studies and is built around a mixed α/β structure, with five β-sheets and six α-helices.[104-106] The active site residues D64, D116 and E152 are presented by the middle of β1-sheet, coil and α4-helix, respectively. Crystal structures of the isolated CCDs available to date show a single Mg^{2+} ion coordinated by the two aspartate residues D64 and D116. Nevertheless, similar to other polynucleotidyl transferases, a second metal can be most likely coordinated by E152 (with D64) once HIV-1 IN binds to its DNA substrate.[89] CCD also encompasses a flexible loop comprising residues 140-149 known to be essential for 3'-P and ST reactions.[107] Crystal structures of two domains constructs of HIV-1 IN that contain either the NTD-CCD (IN^{1-212}) or CCD-CTD (IN^{50-288}) have also been obtained.[108,109]

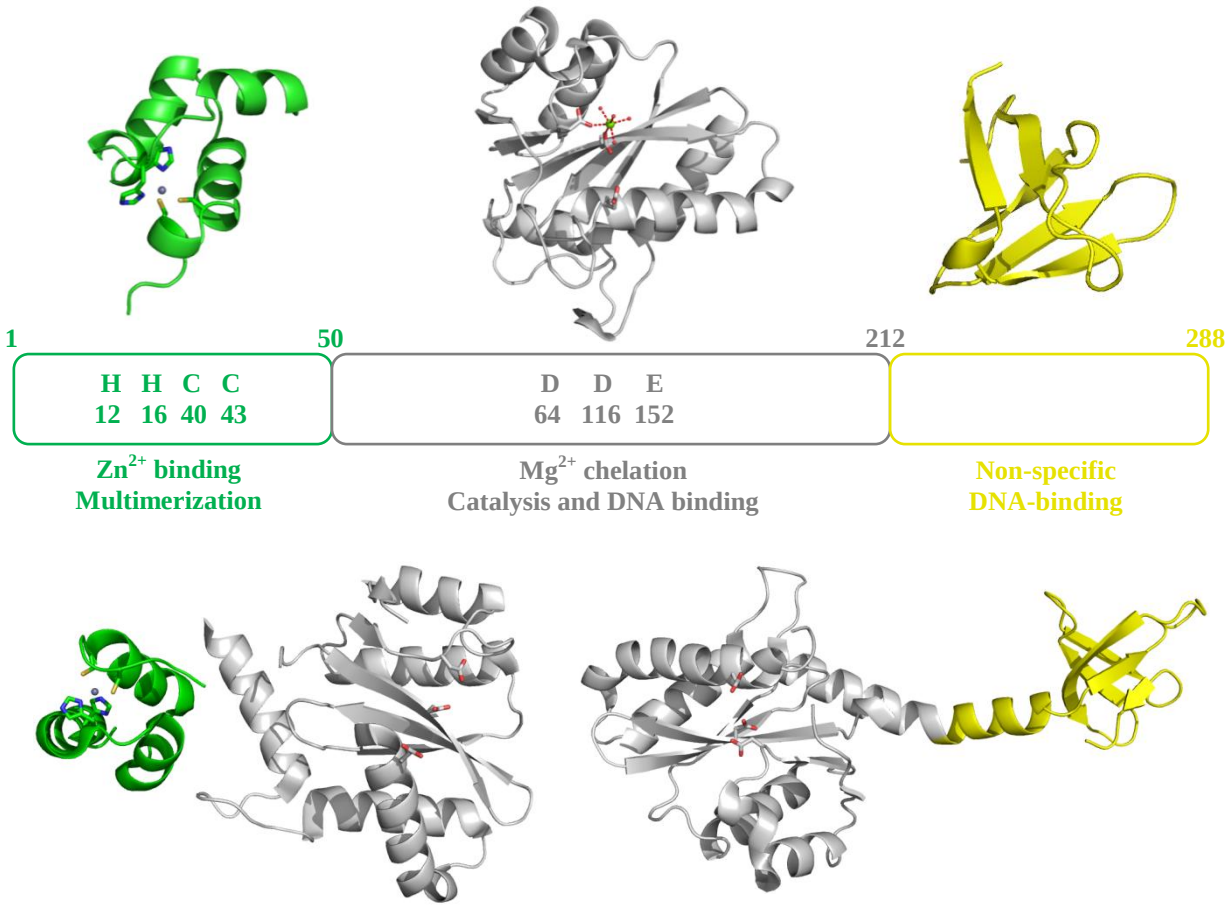

Figure 3.3. Structural domains of HIV-1 IN. (Top) N-terminal ($IN^{1–49}$, left)[102] (PDB code 1WJA), catalytic-core ($IN^{50–212}$, middle)[106] (PDB code 1BL3) and C-terminal ($IN^{219–270}$, right)[103] (PDB code 1IHW) domains; (Bottom) left, N-terminal/catalytic-core domain ($IN^{1–212}$)[108] (PDB code 1K6Y) and right, catalytic core/C-terminal fragment ($IN^{52–288}$)[109] (PDB code 1EX4).

Despite the lack of detailed structural information of full-length IN, experimental studies are in agreement with an active multimeric protein. Time-resolved fluorescence anisotropy studies showed that a single IN dimer at each extremity of viral DNA molecules is required for 3'-P.[110] Cross-linking studies suggested that a tetrameric IN bound to the viral DNA ends is the complex involved in ST reaction.[111] The recent X-ray crystal structure of IN from the prototype foamy virus (PFV-1 IN) in complex with its cognate viral DNA consists of an IN tetramer tightly associated with a pair of viral DNA ends.[101,112] This complex is consistent with a low-resolution structure obtained by electron microscopy and single-particle reconstruction for HIV-1 IN in complex with its cellular cofactor, the lens epithelium-derived growth factor.[113]

3.3. HIV-1 IN inhibitors

Over the past decade of research, two strategies have been considered for the development of HIV-1 IN inhibitors (Figure 3.4). The first targets the free, unbound protein (**IN DNA-binding inhibitors** or **INBIs**) whereas the second targets the complex resulting from the association of integrase with viral DNA (**IN strand transfer inhibitors** or **INSTIs**). More recently, another approach based on the inhibition of the interaction between HIV-1 IN and its cofactor LEDGF/p75 allowed to identify new leads in anti-IN drug design (**LEDGINs**). These three families of HIV-1 IN inhibitors are presented in this section.

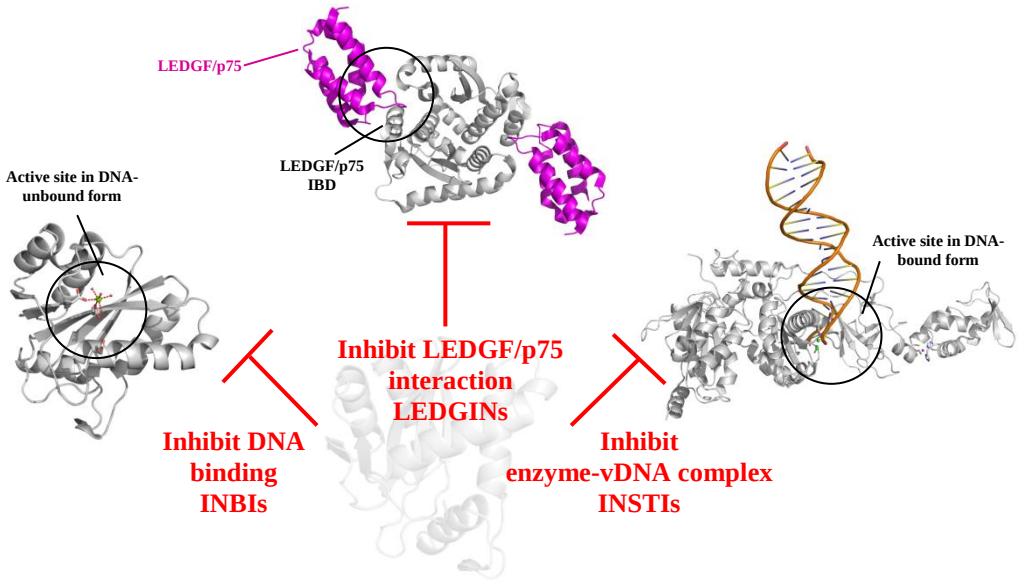

Figure 3.4. Strategies used for the design of HIV-1 IN inhibitors. (Top) Crystal structure of HIV-1 CCD dimer (grey cartoon) (PDB code 2B4J)[114] in complex with LEDGF/p75 (magenta cartoon) depicting the LEDGF/p75 IN binding domain (LEDGF/p75 IBD). (Left) Crystal structure of HIV-1 IN CCD (PDB code 1BL3)[106] depicting the DNA-unbound form of the active site. (Right) Crystal structure of PFV-1 IN in complex with its cognate DNA substrate depicting the active site in DNA-bound form (PDB code 3OY9)[112].

3.3.1. IN DNA-binding inhibitors (INBIs)

Styrylquinoline (Figure 3.5, compound a) and **pyranodipyrimidine** (Figure 3.5, compound b) derivatives represent two of the most important INBI series. They act on the 3'-P reaction *in vitro* by competing with viral DNA for binding to IN within the active site.[115,116] Further studies carried out with these compounds have revealed a multimodal mechanism of action. Indeed, it has been showed that styrylquinolines efficiently inhibit *in vitro* nuclear import of IN whereas pyranodipyrimidine block the viral entry.[117,118] Random screening led to the discovery of a novel series of **1-pyrrolidineacetamides** (Figure 3.5, compound c) which bind to specific residues in the HIV-1 IN CCD (K103, K173, and T174).[119]

Based on fluorescent stains (for labeling DNA) known to bind non-covalently and site-specifically to the minor groove of DNA, other promising INBIs were developed. Specifically, the replacement of N-methylpiperazine rings by more hydrophilic N,N-dimethylaminopropyl carboxamide groups, combined with dimerization have led to identify an interesting **bis-benzimidazole** derivative (Figure 3.5, compound d).[120]

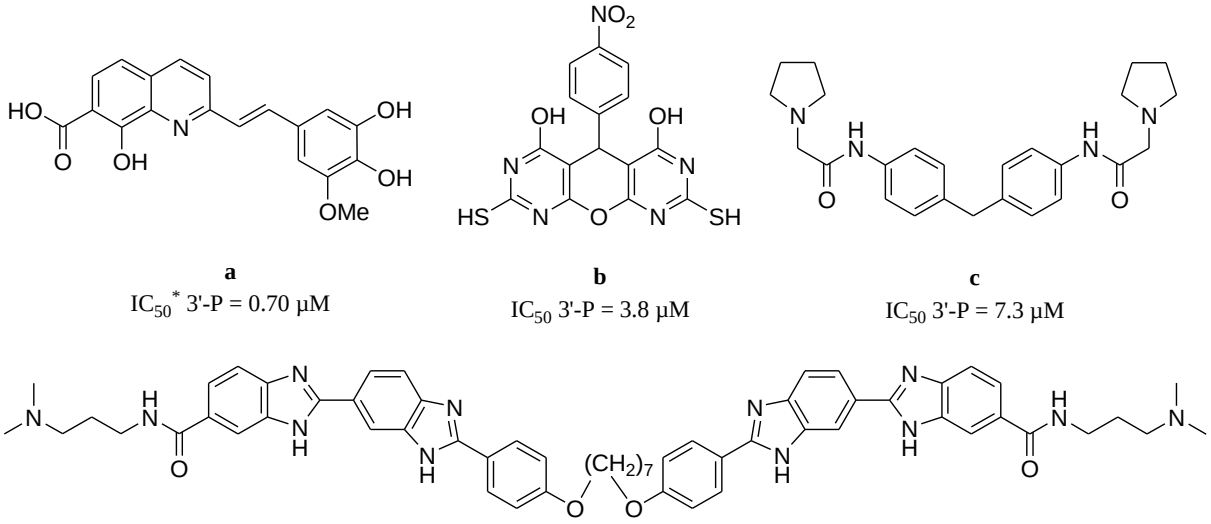

Figure 3.5. Structures of most representative INBIs.

3.3.2. IN strand transfer inhibitors (INSTIs)

3.3.2.1. Development

During a previous random large-scale screen, compounds with β-diketoacid (DKA) moiety were identified as potent HIV-1 IN inhibitors, presenting a significant preference for ST inhibition over 3'-P *in vitro*.[121] The most active compounds of this study, **L-731,988** and **L-708,906** (Figure 3.6) were the first INSTIs demonstrated to have antiviral activity directly as a consequence of their effect on HIV-1 integration. Simultaneously, other potent DKA containing aromatic indole rings and a tetrazole group in place of the common DKA carboxylic acid moiety were developed, leading to the first inhibitor co-crystallized with IN, **5-CITEP** (Figure 3.6).[122] X-ray crystal structure of the complex showed that 5-CITEP binds in the middle of the active site of the enzyme, lying between the three catalytic acidic residues, D64, D116 and E152, in the vicinity of the active site metal ion.

* IC_{50}: inhibitor concentration required to reduce enzymatic activity to 50 %.

Further pharmacomodulations in the series of indole derivatives led to the inclusion of multiple nitrogen and oxygen-containing heterocycles. **S-1360**[123] (Figure 3.6) was the first clinically tested inhibitor. Nevertheless, it failed clinical phase II due to its reduction in humans at the carbon linked to the triazole heterocycle, yielding an inactive metabolite that was rapidly cleared through glucuronidation in the non-cytochrome P450 pathway.[124]

Structure-activity relationship (SAR) studies revealed the contributions of two common pharmacophoric features for ST inhibition and selectivity [125]: (i) the sequestration of active site divalent metal ions by an aryl DKA chain (marked in bold) is critical for ST inhibition whereas (ii) an aromatic hydrophobic group (marked in dashed box) on a flexible tether at a relatively well-defined distance and angle from the metal binding center is crucial for potency and ST selectivity.

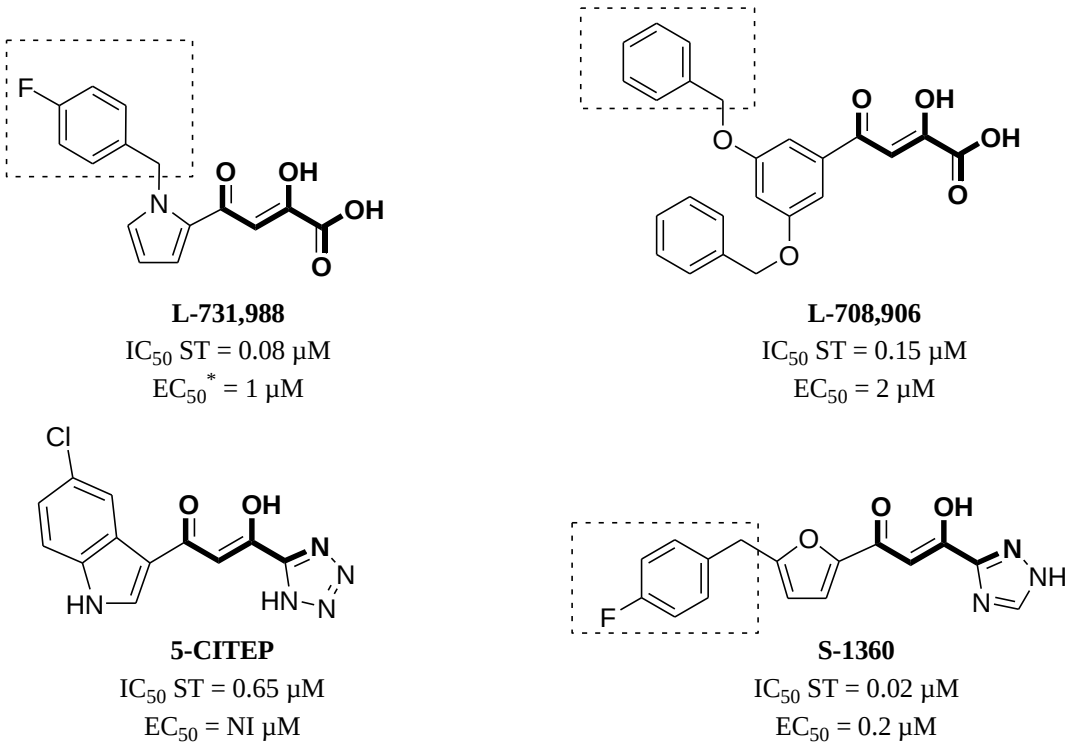

Figure 3.6. Structure of firstly developed β-diketoacid compounds with DKA moiety in bold.

Due to the relevance of Mg-chelating functions for ST inhibition, isosteric replacements for the diketo acid pharmacophore have led to the rational design of new INSTIs classes (Figure 3.7).

* EC_{50}: inhibitor concentration required to inhibit 50 % of HIV-1 replication.

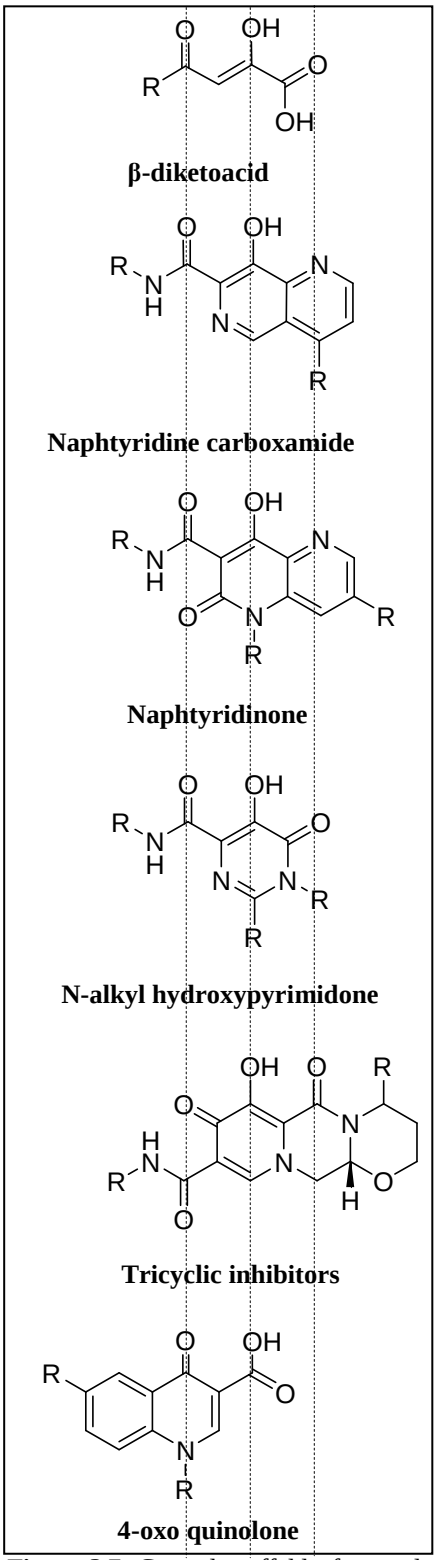

Figure 3.7. General scaffold of several INSTIs classes derived from β-diketoacid pharmacophore**.**

➢ *1,6 Naphtyridine carboxamide*

The substitution of the DKA pharmacophore with a naphthyridine carboxamide core led to the development of **L-870,810**[126] (Figure 3.8), a 8-hydroxy-1,6-naphthyridine-7-carboxamide derivative, showing very promising activity and becaming the second HIV-1 IN inhibitors to enter clinical trials. However, its significant human plasma protein binding brought a premature end to the drug's clinical progress.[127] Various modifications at the 4-Fluorobenzyl group were explored in order to decrease protein binding. 2-Amide analogue (Figure 3.8, compound a) had a lower percentage of protein binding than L-870,810, good pharmacokinetic properties and is undergoing further preclinical development.[128]

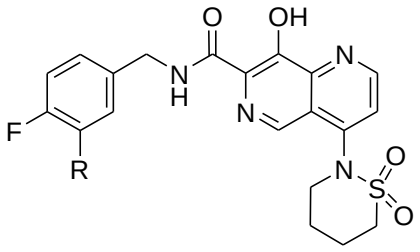

L-870,810	**a**
R = H	R = CONHMe
IC_{50} ST = 0.01 μM	IC_{50} ST = 0.01 μM
CIC_{95}* (NHS) = 0.1 μM	CIC_{95} (NHS) = 0.016 μM

Figure 3.8. Structures of the two most representative naphthyridine carboxamide derivatives.

➢ *Naphtyridinone*

In studies to develop follow-up analogs of S-1360, a joint research effort of scientists from Shionogi and GlaxoSmithKline exploited a new series of naphtyridinone.

* CI_{95} (NHS): concentration of inhibitor that reduce the spread of HIV-1 infection to 90% in the presence of normal human serum.

By combining optimal substituents at three positions (i.e., methyl group at N-1, *N*-(2-hydroxy) ethylcarboxamide at C-3, and 4-fluorobenzyl at C-7), **GSK-364735**[129,130] (Figure 3.9), exhibiting antiviral potency and ST inhibition comparable to raltegravir and elvitegravir was developped. It demonstrated satisfactory results in a phase I clinical trial[131], but its clinical development had been halted.

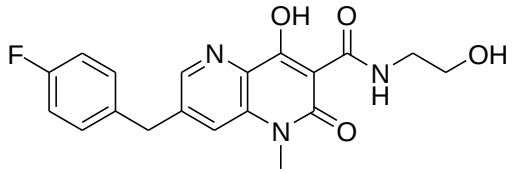

GSK364735
IC_{50} ST = 0.008 µM
EC_{90}* (PBMC) = 0.040 µM

Figure 3.9. Structure of the naphtyridinone derivative GSK364735.

- *N-alkyl hydroxypyrimidone*

A previous screening of HCV polymerase inhibitors led to the identification of a new potent and selective class of INSTIs, the N-alkyl hydroxypyrimidones, having more drug-like properties than DKA compounds.[57,132-134] Extensive SAR studies on the carboxamide moiety resulted to the identification of p-fluorobenzyl group as the optimal amide residue and dimethyl amino gem-dimethyl as the optimal 2-substituent (Figure 3.10, compound a). Further SAR studies were conducted to improve the activity against IN, focusing on the basic amine and the gem-dimethyl moieties. Substitution of the dimethyl amino group by acetamide functionality resulted in compound b (Figure 3.10) showing higher potency in both enzymatic and cell-based assays. The incorporation of aromatic and heteroaromatic amide as capping groups of the amine portion led to the identification of lead compounds with low nanomolar enzymatic and antiviral activities (Figure 3.10, compounds c, d and raltegravir). Further clinical development of **raltegravir** led to the first HIV-1 IN inhibitors approved by the FDA. This compound is included in current HAART regimen.

* EC_{90} (PBMC): inhibitor concentration required to inhibit 90 % of HIV-1 replication in peripheral blood mononuclear cell.

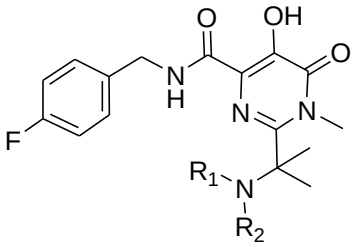

a
$R_1 = R_2 = Me$
IC_{50} ST = 0.230 µM
CI_{95} (NHS) = 1 µM

b
$R_1 = H$
$R_2 = COMe$
IC_{50} ST = 0.007 µM
CI_{95} (NHS) = 0.40 µM

c
$R_1 = H$
R_2 = 1-(3-pyridazinyl)ethanone
IC_{50} ST = 0.015 µM
CI_{95} (NHS) = 0.500 µM

d
$R_1 = H$
R_2 = 1-(2-pyrimidinyl)ethanone
IC_{50} ST = 0.007 µM
CI_{95} (NHS) = 0.050 µM

raltegravir
$R_1 = H$
R_2 = 1-(5-Me-2-(1,3,4-oxadiazolyl))ethanone
IC_{50} ST = 0.015 µM
CI_{95} (NHS) = 0.031 µM

Figure 3.10. Structures of N-alkyl hydroxypyrimidone class of compounds.

- *Tricyclic inhibitors*

In the aim to identify new INSTIs active towards raltegravir resistant mutants, pseudosymmetric tricyclic hydroxyl-pyridone carboxamides inhibitors were designed. The pseudo-symmetry is thought to contribute to multiple binding modes and as a result, escape from IN mutations. Optimization of this series led to the discovery of **S/GSK1349572**[68] (Figure 3.11), starting phase III clinical trials. This compound had a markedly different resistance profile as evidenced by limited cross-resistance to raltegravir resistant HIV strains. Keeping in mind the relevance to design new INSTIs with a high genetic barrier to resistance, new pyrazinopyrrolopyridazines derivatives were developed.[135] The replacement of a pyridinone ring with a pyridazinone in original tricyclic hydroxypyrrole inhibitors resulted in higher oxidative stability of the hydroxypyrrole moiety. As a result, a lead compound, termed **MK-2048**[136] (Figure 3.11), exhibiting favorable pharmacokinetics and potent antiretroviral activity against four IN mutants displaying raltegravir resistance was identified. MK-2048 is still in pre-clinical development. Based on the previously developed L-870,810, conformational constraint on the carboxamide carbonyl by cyclization led to a new class of pyrrolloquinolone inhibitors. Various C-5 substitutions in the pyrrolloquinolone core by amino derivatives resulted in a lead compound, **GS-9160** (Figure 3.11), showing low nanomolar potency.[137,138]

The pharmacokinetic profile of GS-9160 in healthy human volunteers revealed that once-daily dosing was not likely to achieve antiviral efficacy. Consequently, the clinical development of this compound was discontinued.[139]

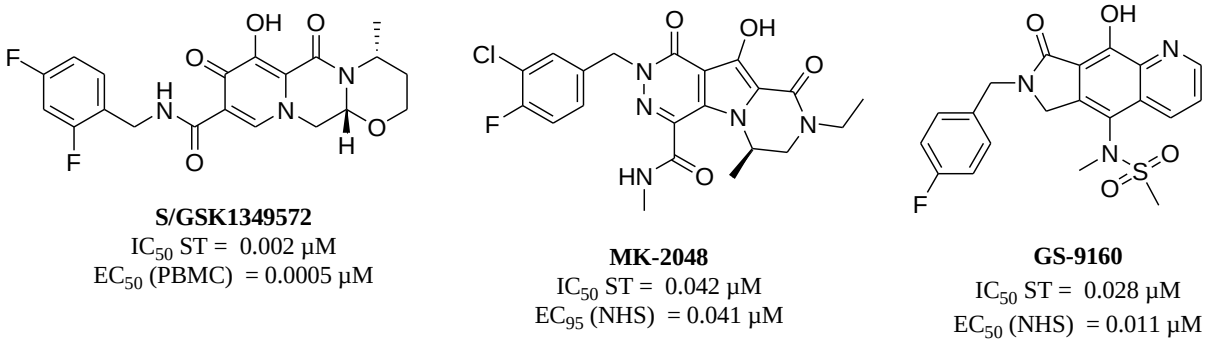

S/GSK1349572
IC_{50} ST = 0.002 µM
EC_{50} (PBMC) = 0.0005 µM

MK-2048
IC_{50} ST = 0.042 µM
EC_{95} (NHS) = 0.041 µM

GS-9160
IC_{50} ST = 0.028 µM
EC_{50} (NHS) = 0.011 µM

Figure 3.11. Structures of the three most representative tricyclic inhibitors.

- *4-oxo quinolone*

Based on the core structure of quinolone antibiotics, a novel class of quinolone 3-carboxylic acids containing a coplanar arrangement of a ketone and a carboxylic acid moiety was developed. In order to understand the SAR, various modifications were introduced at the N-1 and C-6 positions on the 4-quinolone-3-glyoxlic acid scaffold (Figure 3.12, compound a).[64,65] Introduction of 2'-fluoro-3'-chloro substituents into the distal benzene ring and a hydroxyethyl group at the 1-position of the quinolone ring led to a significant improvement of ST inhibition and antiviral activity (Figure 3.12, compound b). Substitution at the 7-position with a methoxy group resulted in the higher potent compound c (Figure 3.12). Finally, introduction of an isopropyl group at the 1S-position of the hydroxyethyl moiety led to **elvitegravir**, the next promising HIV-1 IN inhibitors currently in phase III clinical trials.[140]

Quinolonyl diketo acid derivatives have also been explored for their anti-IN activity.[141,142] These compounds contain the two pharmacophoric features essential for ST, i.e., a diketoacid chain and a p-F-benzyl group at 3- and 1-position of the quinolone scaffold (Figure 3.12, compounds d-k). SAR studies showed that the introduction of halogen atom in the quinolone ring resulted in inhibitory activity similar to that of the unsubstituted compound. The anti-IN activities appear to be influenced by the position of the halogen in the quinolone ring. A 1-pyrrolidinyl substitution at position 7 decreased IN inhibitory potency but improved the antiviral activity.

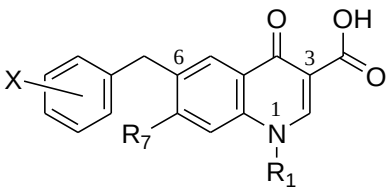

a
$R_1 = R_7 = X = H$
IC_{50} ST = 1.6 µM
EC_{50} = > 30 µM

b
$R_1 = CH_2CH_2OH$
$R_7 = H$
X = 2'-F, 3'-Cl
IC_{50} ST = 0.024 µM
EC_{50} = 0.076 µM

c
$R_1 = CH_2CH_2OH$
R_7 = OMe
X = 2'-F, 3'-Cl
IC_{50} ST = 0.009 µM
EC_{50} = 0.017 µM

elvitegravir
R_1 = (S)-CH(iPr)CH_2OH
R_7 = OMe
X = 2'-F, 3'-Cl
IC_{50} ST = 0.007 µM
EC_{50} = 0.0009 µM

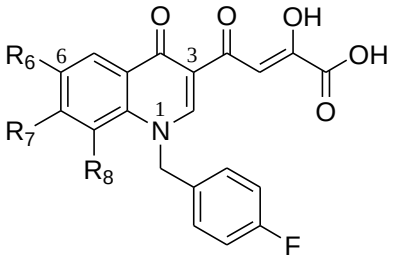

d
$R_6 = R_7 = R_8 = H$
IC_{50} ST = 0.04 µM
EC_{50} = 4.1 µM

e
R_6 =F
$R_7 = R_8 = H$
IC_{50} ST = 0.030 µM
EC_{50} = > 50 µM

f
$R_6 = R_8$ =H
R_7 = F
IC_{50} ST = 0.020 µM
EC_{50} = > 50 µM

g
$R_6 = R_7$ =H
R_8 = F
IC_{50} ST = 0.018 µM
EC_{50} = > 50 µM

h
R_6 = Cl
$R_7 = R_8 = H$
IC_{50} ST = 0.028 µM
EC_{50} = 46.1 µM

i
$R_6 = R_8$ =H
R_7 = Cl
IC_{50} ST = 0.019 µM
EC_{50} = > 50 µM

j
$R_6 = R_7$ =H
R_8 = Cl
IC_{50} ST = 0.023 µM
EC_{50} = > 50 µM

k
$R_6 = R_8$ =H
R_7 = 1-pyrrolidinyl
IC_{50} ST = 0.028 µM
EC_{50} = 0.17 µM

Figure 3.12. Structures of quinolone 3-carboxylic acid (a-c, elvitegravir) and Quinolinonyl diketoacid inhibitors (d-k).

3.3.2.2. Mode of action

Crystallographic structure of inhibitors bound to the HIV IN-viral DNA complex continues to be a significant challenge. Consequently, the mechanism of action of INSTIs remains unclear. Based on biochemical data, it is hypothesized that INSTIs act as "interfacial inhibitors" by binding at the IN/DNA interface and coordinating one or two catalytic magnesium ions in a pocket flanked by the end of the viral LTR.[143-145] This speculative mechanism of action tends to be validated by the recent X-ray crystal structure of PFV-1 IN in complex with its cognate viral DNA and INSTIs (Figure 3.13a-d).[112,146]

These structures revealed a two-metal ion mechanism of action involving the coordination of the two metal cofactors within the active site by the common metal-coordinating pharmacophore of the INSTIs (Figure 3.13c). This interaction with the two Mg^{2+} ions resulted in the displacement of the terminal 3′ adenosine (Figure 3.13b) and the fit of the halobenzene groups into a pocket created by displacement of the terminal 3′ adenosine (Figure 3.13d). In this way, the inhibitor would probably prevent the attack of the viral 3′-end on a target DNA phosphodiester bond.

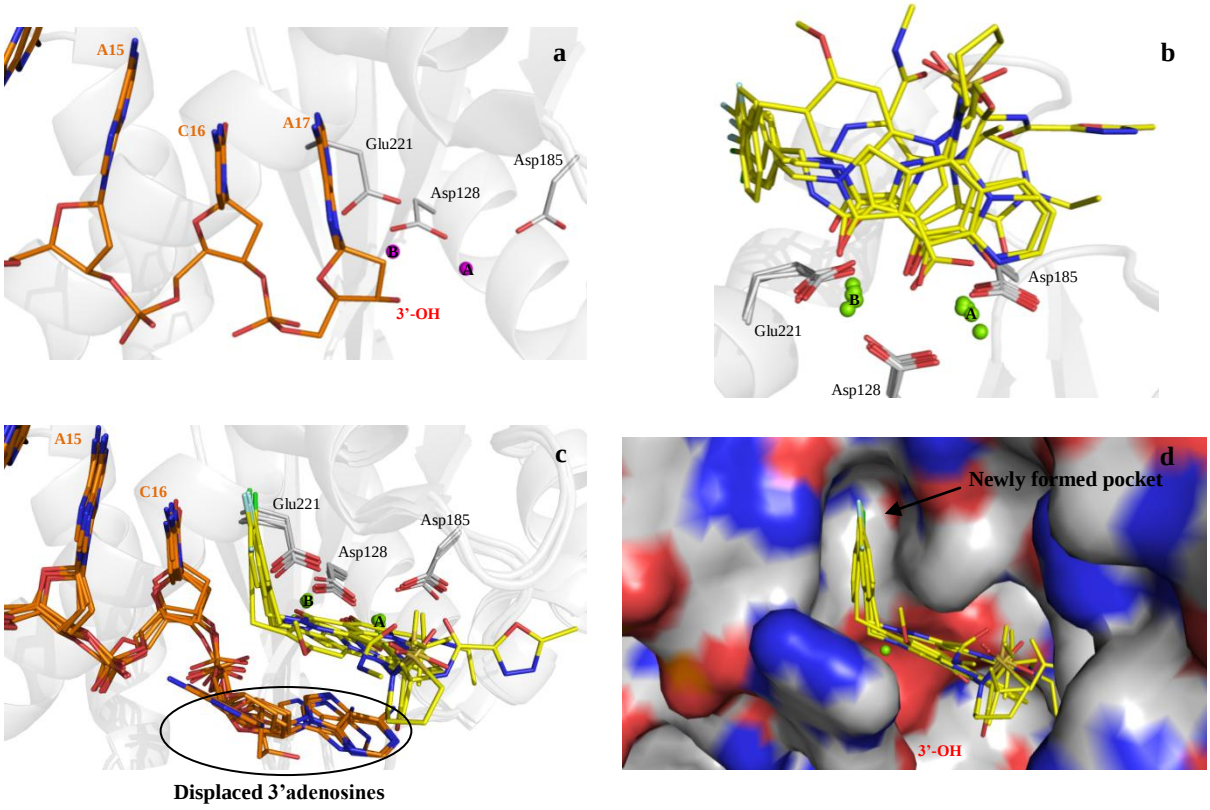

Figure 3.13. Crystal structure of PFV IN/DNA complex in its active and INSTI inhibited form. Mn^{2+} and Mg^{2+} ions are shown as purple and green sphere, respectively. Protein is represented as grey cartoon whereas DNA and INSTIs are shown as orange and yellow sticks, respectively. a) PFV IN/DNA complex in its active Mn^{2+}-bound form (PDB code 3OY9)[112]. b) Superimposition of Mg^{2+}/INSTIs-bound PFV active site (PDB code 3L2U/3OYA/3OYB/3OYD/3OYF)[112,146] highlighting the two-metal ion mechanism of action of INSTIs. c) and d) Alternative views showing the displacement of terminal 3′ adenosine from the active site and the fitting of halobenzyl groups into the newly formed pocket.

3.3.3. Inhibitors of LEDGF/p75-IN interaction (LEDGINs)

LEDGF/p75 is a cellular cofactor of HIV-1 IN that promotes viral integration by shifting IN oligomerization towards tetrameric structures and tethering the preintegration complex to the chromatin.[147] Based on LEDGF/p75 functions, peptide LEDGF/p75 402-411 has been designed to shift IN towards tetrameric structures which do not catalyze 3'-P reaction requiring dimeric structures. This one inhibits both 3'-P and ST reactions with IC_{50} values below 21 µM.

Moreover, it was non-toxic in cell-based assays.[148] Disrupting the interaction between IN and LEDGF/p75 by small molecules has recently been recognized as a potential therapeutic strategy. As revealed by crystal structure of HIV-1 IN CCD-LEDGF/p75 complex, LEDGF/p75 forms a specific interaction into a HIV-IN binding pocket at the interface of two monomers[114]. More specifically, four relevant amino acid residues Ile365, Asp366, Phe406 and Val408 are considered essential for the direct contact with HIV-1 IN CCD residues. On this basis, various small molecules with IC_{50}s in the low micromolar range mimicking Asp366 residues have been designed (Figure 3.14).[149-151] Crystal structure of HIV-1 IN CCD in complex with compound **c** showed that the inhibitor occupied the same space in the binding pocket that LEDGF/p75, confirming an allosteric inhibition of HIV-1 IN.[149]

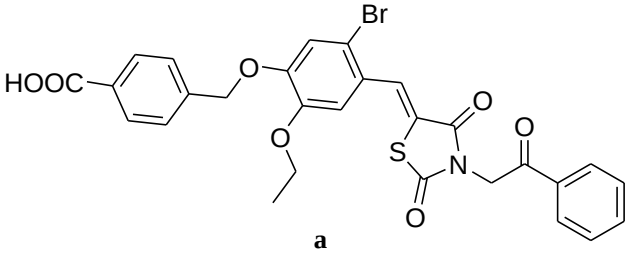

a

K_d* HIV-1 IN CCD = 6.83 µM

EC_{50} =ND

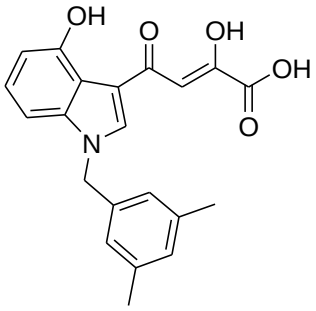

b

IC_{50} LEDGF/p75 interaction = 3.5 µM

EC_{50} = ND

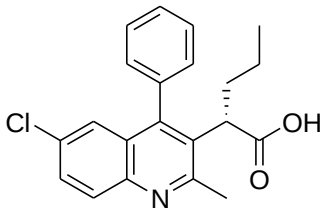

c

IC_{50} LEDGF/p75 interaction = 1.37 µM

EC_{50} = 2.35 µM

Figure 3.14. Chemical structures of IN-LEDGF/p75 interaction inhibitors.

* K_d: equilibrium dissociation constant.

Part II
Objective and strategy

HIV-1 IN is an attractive and validated target for the development of novel therapeutics against AIDS. Over the last past decade, extensive research focusing on the ligand-based drug design approach have led to the identification of a plethora of INSTIs. Due to the lack of detailed structural information concerning HIV-1 IN/DNA-INSTI ternary complex, structure-based inhibitor design selective for IN/DNA complex has not kept pace. A more detailed understanding of INSTIs binding mode could lead to the design of more potent inhibitors with a higher genetic barrier against the emergence of resistant mutants.

This thesis is in line with a project (WALEO 2 Program, ANTISIDA 2 Project, 515995/616295) initiated together with the University of Namur (FUNDP, Chemistry Department) and Brussels (ULB, campus Gosselies, Laboratoire de virologie moleculaire) aiming at the design of HIV-1 IN inhibitors. The major goal of this work was to study the inhibition mechanism of HIV-1 IN by quinolone compounds combining experimental and theoretical approaches with a view to provide new insights into the mechanism of action of INSTIs.

Previously, DKA derivatives containing the quinolinone scaffold have been reported as potential HIV-1 IN inhibitors.[141,142] Based on this series, new compounds substituted at C-6 with various substituents were synthesized in collaboration with Pr. Laszo Hevesi (FUNDP, Chemistry Department) (Figure 1).

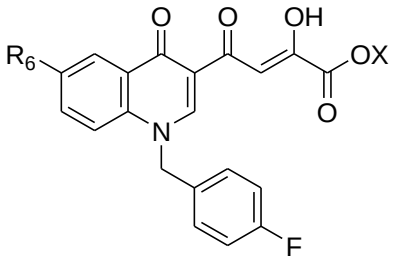

X = Et, H
R_6 = Br, O-CH_2(4'-F-Ph), HC=CHCOOEt(H)

Figure 1. Structure of 6-substituted quinolone compounds synthesized.

All these compounds were evaluated for their anti-integrase and antiviral activity and SARs were established. The enzyme required for the evaluation of anti-integrase activity was expressed, purified and tested for its enzymatic activity. IC_{50} and EC_{50} values of quinolone compounds were then evaluated in *in vitro* and cell-based assays. All biological assays were performed in collaboration with the laboratory of Pr. Carine Van Lint (Laboratoire virologie moléculaire, ULB) and Dr. Jean-François Mouscadet (LBPA, ENS Cachan).

Otherwise, HIV-1 IN CCD expression and purification experiments were performed with a view to obtain a crystal structure of the enzyme in complex with short oligonucleotide substrate and/or quinolone compounds.

In parallel, we studied the interaction between HIV-1 IN and quinolone compounds considering partners (DNA, Mg^{2+}, water molecules) present during ST reaction. Physicochemical studies were performed to identify stable conformations as well as to investigate magnesium-chelating properties of quinolone compounds. Based on the very recent crystal structures of PFV-IN in complex with its cognate DNA substrate and INSTIs, a new HIV-1 IN/DNA theoretical model was also built. This model was used for docking studies to both predict the binding mode of quinolone compounds within HIV-1 IN/DNA complex and rationalize the observed SARs. Based on these results, a detailed mechanism of inhibition for quinolonyl DKA compounds was proposed.

Part III
Results and discussion

1 Biochemical characterization of the inhibition of HIV-1 IN by quinolones

The establishment of SAR is an essential step to identify ligands stereoelectronics requirements essential for the interaction with their target enzyme. In this chapter, we planned to explore the effect of chemical modifications at position 6 of the quinolone scaffold by synthesizing new compounds containing at position C-6 an halogen atom or bulky hydrophilic and hydrophobic substituents (Figure 1.1). These compounds were synthesized in collaboration with the group of Laszlo Hevesi. To evaluate the anti-integrase activity of quinolone compounds, wild-type HIV-1 IN was expressed and purified. The activity of the produced enzyme was evaluated and IC_{50} values of quinolone compounds were determined in *in vitro* inhibition assays. Antiviral activities of these compounds were also evaluated by the laboratory of Pr. Carine Van Lint (Laboratoire virologie moléculaire, ULB).

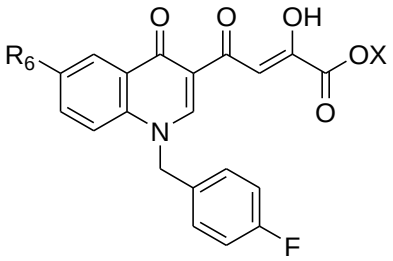

1a: X = Et; R_6 = Br
1b: X = Et; R_6 = O-CH_2(4'-F-Ph)
1c: X = Et; R_6 = HC=CHCOOEt
2a: X = H; R_6 = Br
2b: X = H; R_6 = O-CH_2(4'-F-Ph)
2c: X = H; R_6 = HC=CHCOOH

Figure 1.1. Structure of 6-substituted quinolone compounds synthesized.

1.1. Synthesis of quinolonyl diketo ester and acid compounds

The title compounds **1a-c** and **2a-c** were synthesized according to Di Santo's procedure[141,142] with modifications as presented in Scheme 1. The key intermediates 3-acetyl-4(1*H)*-quinolinones (**4a,b**) were obtained by reaction of the appropriate aniline with ethyl ethoxymethyleneacetoacetate, followed by thermic cyclization in diphenyl ether. Then, **4a,b** were alkylated with 4-fluorobenzylbromide in alkaline medium (K_2CO_3) to give compounds **5a,b**. Acrylate derivative **5c** was obtained by palladium-catalyzed Heck reaction of **5a** with acrylic acid ethyl ester. Compounds **5a-c** was condensed with diethyl oxalate in the presence of sodium ethoxide to afford diketo esters derivatives **1a-c**, which were in turn hydrolyzed by saponification reaction to give DKA derivatives **2a-c**.

Scheme 1[a]**.** General synthetic pathway for the synthesis of quinolonyl diketo ester and acid derivatives (**1a-c**, **2a-c**).

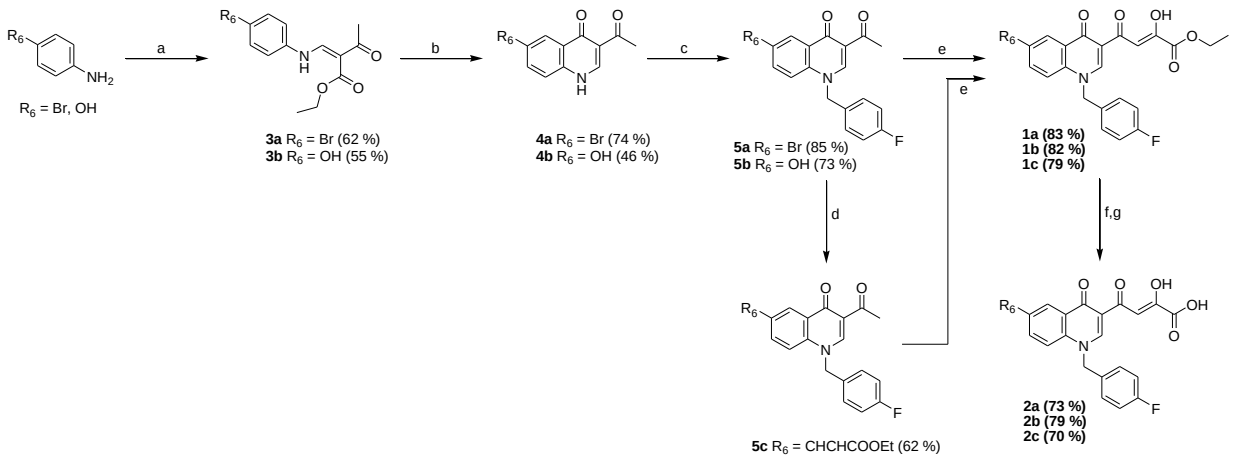

[a] Reagents and conditions: (a) ethyl ethoxymethyleneacetoacetate, 120 °C, 5 min; (b) Ph_2O, reflux 40 min; (c) 4-fluorobenzyl bromide, K_2CO_3, DMF, 100°C, 2 h; (d) $Pd(OAc)_2$ cat., PPh_3, NEt_3, acrylic acid ethyl ester, DMF, 80°C, 48 h; (e) diethyl oxalate, C_2H_5ONa, THF, 20 h, HCl, rt; (f) 1 N NaOH, THF/MeOH (1:1), 1.15 h; (g) HCl 1N, rt.

1.2. His-tagged wild-type HIV-1 IN preparation

Full-length wild-type HIV-1 IN is known to be an insoluble protein with very poor stability at room temperature. Consequently, enzyme preparation required stringent conditions (t°c, pH, ionic strength ...) to purify in its native form. All attempts performed in our laboratory did not allow to produce active IN. For this reason, enzyme preparation was performed within the laboratory of Dr. J.-F. Mouscadet (LBPA, ENS Cachan).[92]

1.2.1. Expression in BL21(DE3)pLysS

pET-15b-IN plasmid encoding for His-tagged wild-type HIV-1 IN (HT-wt-IN$^{1-288}$) was a generous gift of R. Craigie (NIH, AIDS Research and Reference Reagent Program, USA). It contains a T7 promoter just upstream of the protein-coding region, regulating its expression and an ampicillin resistance gene used as a selectable marker (Figure 1.2). In this system, the interest protein is produced when bacterial T7 RNA polymerase binds to T7 promoter. In normal conditions, T7 RNA polymerase is not or very weakly produced. The addition of isopropyl-β-D-galactoside (IPTG) induces the expression of T7 RNA polymerase and consequently, the interest protein.

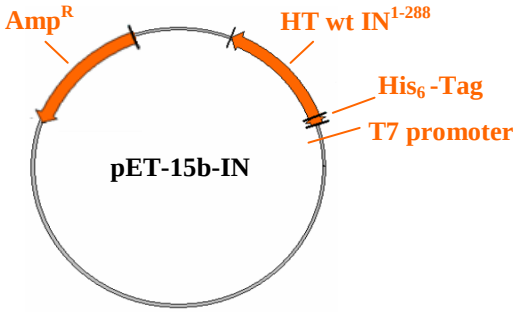

Figure 1.2. pET-15b-IN plasmid encoding for HT-wt-IN$^{1-288}$.

HT-wt-IN$^{1-288}$ was expressed in *E. coli* BL21(DE3)pLysS competent cells. These ones contain the pLysS plasmid expressing T7 lysozyme that suppresses basal expression of T7 RNA polymerase prior induction toxic for cells. After bacterial protein expression by IPTG induction, crude lysate obtained by cells lysis were centrifuged in the aim to obtain the interest protein in the supernatant and other bacterial proteins and cellular debris in pellets. To verify the expression level of IN protein, the crude lysate, supernatant and pellets were analyzed by SDS/PAGE (Figure 1.3). Whole analyzed fractions showed induced IN of the predicted size (32 kDa) that migrated just below the 37 kDa molecular size marker. Although a large part of insoluble enzyme was retained in pellet, HIV-1 IN was recovered as a soluble protein in the supernatant in reasonable quantity.

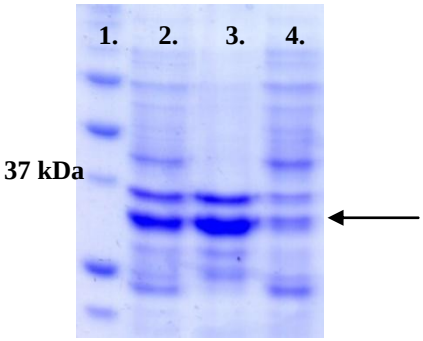

Figure 1.3. Coomassie stained SDS/PAGE analysis of Wild-type HIV-1 IN expression. The arrow indicates the position of His-tagged IN. Lane 1 = molecular size marker, lane 2 = lysate, lane 3 = pellet and lane 4 = supernatant.

1.2.2. Purification by affinity chromatography

The presence of an His-tag at the N-terminus of the protein of interest allowed purification by affinity chromatography (Ni^{2+}) of the supernatant containing HT-wt-IN$^{1-288}$.

His-tagged proteins having an affinity for nickel ions immobilized on nitrilotriacetic acid-agarose (NTA) resin are retained whereas other proteins and contaminants which don't have affinity for nickel ions are directly eliminated. Finally, proteins specifically fixed on Ni-NTA resin are eluted with imidazole.

Due to the poor enzyme stability at room temperature, purification procedure was adapted to keep protein extracts on ice. In this procedure, his-tagged enzyme bounded to Ni-NTA agarose beads was purified and eluted by washing beads with buffer A containing growing imidazole concentrations (from 0 to 1M). At each step of the procedure, protein supernatants were isolated from beads by gravity settling on ice. SDS/PAGE analysis of the different fractions corresponding to beads and proteins supernatants from washes and elution is represented at figure 1.4. A large part of protein contaminants having not or low affinity for Ni-NTA beads were eluted with 0 and 80 mM of imidazole (Figure 1.4, lane 4-7). As a result, the elution of the His-tagged enzyme with 1M imidazole (Figure 1.4, lane 8) gave a band just below the 30 kDa molecular size marker with other contaminants bands. Finally, purified IN was dialyzed in dialysis buffer to obtain a precipitated enzyme which was dosed using the Bradford method. Global yield was about 9 ml of purified enzyme at 0.7 mg/ml from 700 ml of culture medium.

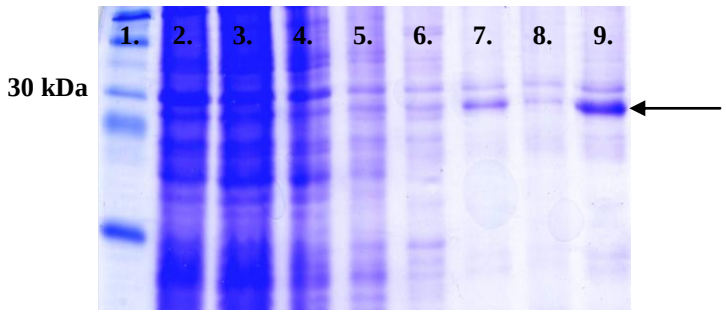

Figure 1.4. Coomassie stained SDS/PAGE analysis of HT-wt-IN$^{1-288}$ purification profile. The arrow indicates the position of His-tagged IN. Lane 1 = molecular size marker, lane 2 = lysate, lane 3 = supernatant of crude *E. coli*, lane 4 and 5 = supernatant and beads after overnight incubation with Ni-NTA agarose, lane 6 and 7 = beads after washing with tampon containing 0 and 80 mM imidazole, lane 8 = elution product with 1 M imidazole, Lane 9 = protein after dialyzis.

1.2.3. Western-blot analysis

Identity of purified IN was validated by Western blot analysis using HIV-1 IN specific antibodies. The precipitated protein obtained after dialysis was first subjected to SDS-PAGE (Figure 1.5 left) and then transferred to nitrocellulose membrane. As shown by antibodies revelation (Figure 1.5 right), the major band just above 30 kDa corresponded to HT-wt-IN$^{1-288}$. The other bands revealed at higher molecular weight could correspond to aggregated proteins.

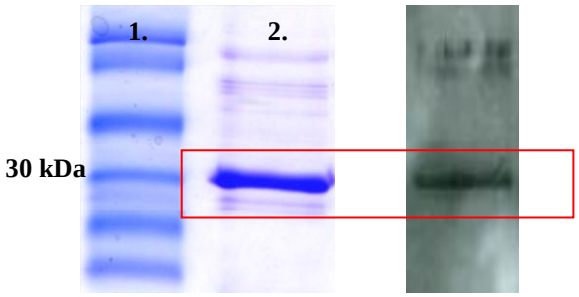

Figure 1.5. (Left) Coomassie stained SDS/PAGE of precipitated wild-type HIV-1 IN. Lane 1 = molecular size marker, lane 2 = dialyzed IN. (Right) Western blot analysis of proteins separated by SDS-PAGE using HIV-1 IN specific antibodies.

1.3. Biological assays

All biological assays were performed within the laboratory of Pr. Carine Van Lint following protocol optimized by the laboratory of Dr. J.-F. Mouscadet (LBPA, ENS Cachan).[92]

1.3.1. Catalytic properties of purified recombinant IN

1.3.1.1. Radioactive gel-based assay

Purified IN was evaluated for its 3'-P and ST activity using a radioactive gel-based assay (Figure 1.6). Oligonucleotides (21 mers) derived from U5LTR extremity of viral DNA were radiomarked at 5'end with ^{32}P. Following 3'-P reaction, HIV-1 IN cleaves a dinucleotide at 3'-end extremity, giving 19-mer oligonucleotide which constitutes the substrate for ST reaction (Figure 1.6a). Indeed, this later is integrated in other strands, leading to 19 + n multimeric oligonucleotides (Figure 1.6b). All these enzymatic reaction products were finally separated on acrylamide/urea gel which was exposed to a PhosphorImager screen absorbing radioactive emission. As a result, specific bands corresponding to 3'-P and ST activity of HIV-1 IN were quantified with ImageQuant software.

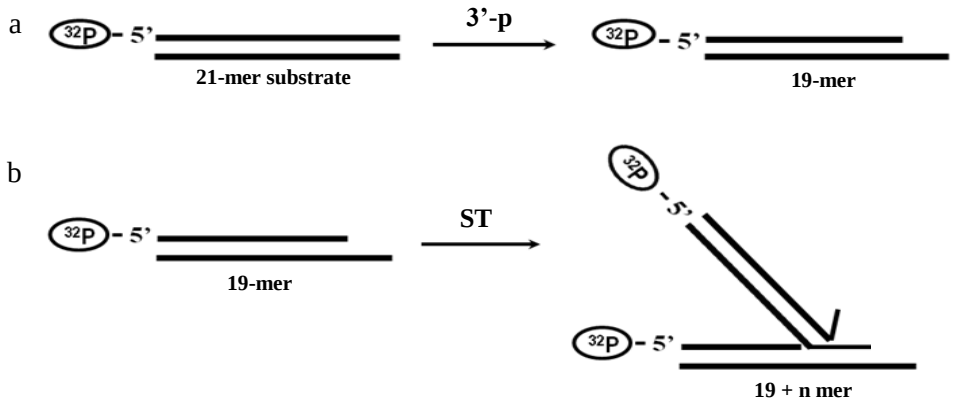

Figure 1.6. Principle of the radioactive gel-based assay used for the evaluation of HIV-1 IN 3'-P and ST activities.

A range of enzyme concentrations (from 50 to 800 nM) was tested to determine the optimum enzyme concentration for *in vitro* inhibition assays (Figure 1.7). The purified enzyme showed optimum 3'-P and ST activity at 400 and 800 nM.

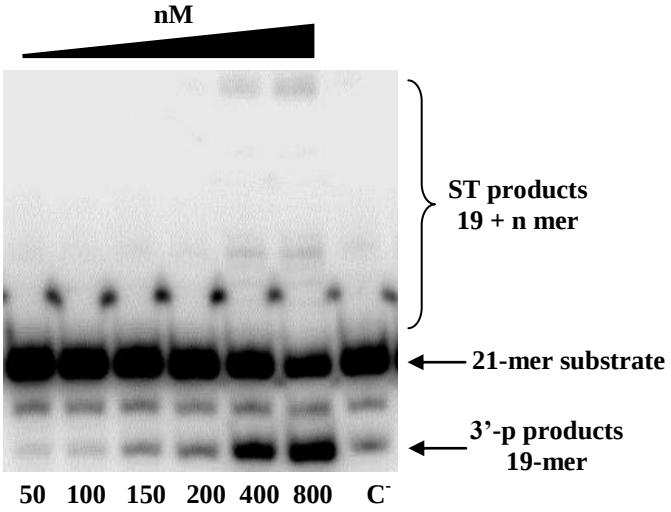

Figure 1.7. Phosphorimager picture showing enzymatic activities for various IN concentrations. C^- corresponds to EDTA-inactivated enzyme.

1.3.1.2. Colorimetric assay

Enzymatic activity of purified IN was also evaluated in a more rapid and easy-to-use colorimetric assay (Figure 1.8).

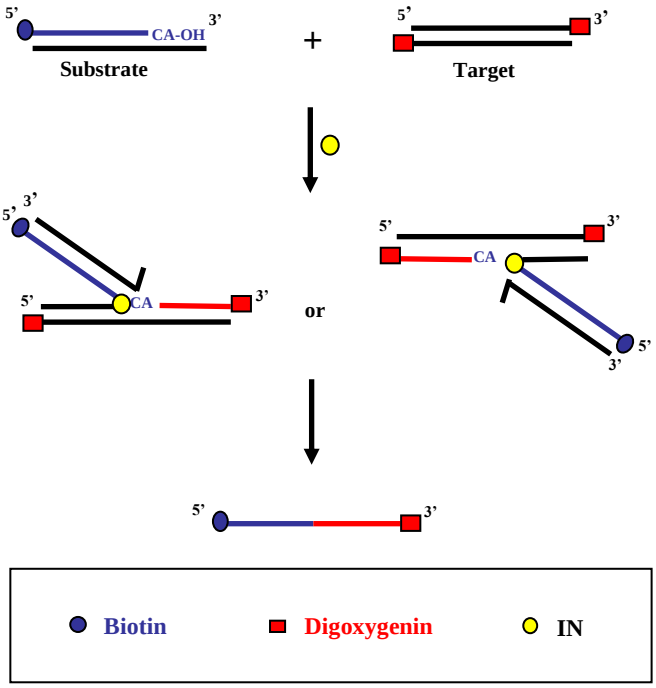

Figure 1.8. Principle of colorimetric assay evaluating ST activity of HIV-1 IN.

In this assay, ST activity of HIV-1 IN is evaluated by using a 5'-biotin labeled pre-processed 19-mer oligonucleotides as substrate and a 3'-digoxygenin labeled oligonucleotides as target. Following ST reaction, biotinylated substrate is inserted into digoxinylated target to form oligonucleotide products marked at the two extremities. These latter are then coated on streptavidine plate due to the specific interaction between biotin and streptavidine. Anti-digoxygenin antibodies (horseradish peroxidase conjugated) are added to the well and revealed with chromogenic substrate (ABTS) at 405 nm.

The two optimal IN concentrations determined by radioactive experiment (400 and 800 nM) were tested (Figure 1.9). Data obtained showed that these two enzyme concentrations showed significant ST activity, with an absorbance at 405 nm 3 and 5 fold higher than that of the negative control (EDTA-inactivated enzyme). Nevertheless, high variability in absorbance measurement was observed, with standard deviation of 0.24 and 0.21. As a consequence, this test was not used in subsequent inhibition assays.

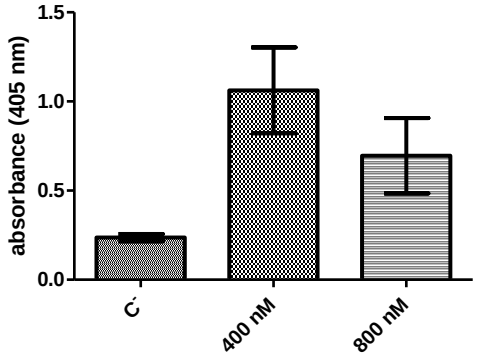

Figure 1.9. ST activity of HT wt IN$^{1-288}$ detected in colorimetric assay by measurement of the absorbance at 405 nm.

1.3.2. Biological evaluation of quinolone compounds

Diketo ester and acid derivatives **1a-c** and **2a-c** were tested for their ability to inhibit 3'-P and ST reactions in radioactive gel-based assay. IN was used at 400 nM because this concentration allowed to have a good level of activity without consuming too much protein. IC_{50} values were calculated using dose response curves (Table 1). As already observed for quinolonyl DKA series[141,142], acidic derivatives were more potent than the corresponding esters, with a high selectivity against ST. The replacement of a bromine atom at C-6 by an anionic (acrylate) or a hydrophobic (4-fluoro-benzyloxy) group did not lead to a significant improvement of HIV-1 IN inhibition.

Indeed, compounds **2b** and **2c** showed IC_{50} values against ST (ST IC_{50}= 0.03-0.05 µM) similar to the one of 6-bromide analogue **2a** (ST IC_{50}= 0.03 µM) with a moderate increase in the selectivity for ST versus 3'-P. These results suggest that the size of substituents at C-6 on the quinolone scaffold affects the ability of the inhibitor to discriminate between the active site of the DNA-bound or -unbound form of HIV-1 IN. Moreover, once the inhibitor is bound to the IN/DNA complex, substituents at C-6 do not make significant interaction.[152,153]

The activity of the title quinolone compounds against wild-type HIV-1 was established by determining their ability to inhibit viral infection using TZM-bl cell lines.[38] These cells are genetically engineered HeLa cell lines that express CD4, CXCR4 and CCR5 and contains β-Gal reporter genes encoding for β-galactosidase enzyme which is only expressed under the control of the HIV-1 LTR sequence. HIV-1 infection in cells is so evaluated by measuring β-galactosidase activity using a colorimetric assay. The cytotoxicity was evaluated based on the cleavage of the tetrazolium salt by mitochondrial dehydrogenases in viable TZM-bl cells. Cytotoxicity (CC_{50}) and antiviral activities (EC_{50}) of compounds **1a-c** and **2a-c** are presented in Table 1. All tested compounds showed antiviral activity at non-cytotoxic concentrations. All derivatives were characterized by low cytotoxicity with CC_{50} values up to 1 mM. The antiviral activities are correlated with the anti-integrase activities. Indeed, acidic derivatives **2a-c** were more potent than the corresponding esters **1a-c** and showed similar EC_{50} values. Ester derivatives **1a** and **1b** were able to inhibit HIV-1 infection in cells with EC_{50} values of 17 and 13 µM. This potential inhibitory activity could be explained by the presence of hydrolases in the cytoplasm of the cells which could partly convert ester compounds into active acidic compounds. Compared to **1a** and **1b**, ester derivative **1c** showed lower inhibitory potency against HIV-1 with EC_{50} value up to 140 µM, suggesting a weaker hydrolyzed fraction of the compound in cells.

Table 1. Cytotoxicity, antiviral and anti-integrase activities of diketo ester and acid derivatives **1a-c** and **2a-c**.

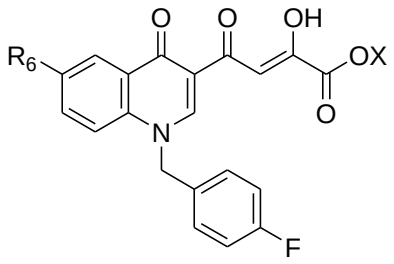

Compd	R	X	anti-IN activity, IC_{50}[a]		antiviral activity	
			3'-P	ST	EC_{50}[b]	CC_{50}[c]
1a	Br	Et	78	0.12	17	> 1000
1b	O-CH_2-4-F-Ph	Et	> 300	> 300	13	> 1000
1c	HC=CHCOOEt	Et	> 300	> 300	> 140	> 1000
2a	Br	H	1.6	0.03	4	> 1000
2b	O-CH_2-4-F-Ph	H	3	0.05	1	> 1000
2c	HC=CHCOOH	H	8	0.03	5	> 1000

[a] Inhibitory concentration 50 % (µM) determined from dose response curves. [b] *Ex vivo* anti-HIV activity (µM) (TZM-bl cells). [c] Cytotoxic concentration 50 % (µM) (TZM-bl cells).

1.4. Conclusion

This first chapter was focused on the biological evaluation of 6-substitued quinolone compounds as potential HIV-1 IN inhibitors. These synthesized compounds showed potent antiviral and anti-integrase activity, with a high selectivity for ST reaction. SAR studies established that acid compounds were more potent than corresponding esters whereas the introduction of both hydrophilic or hydrophobic substituents at C-6 did not have any effect on the activity in comparison with the activity observed with bromine derivative.

In term of these results, it appeared clear that these compounds interacted specifically with the DNA-bound form of HIV-1 IN. The study of the interaction of quinolone compounds within such complex was so essential to predict their binding mode.

2 Expression and purification of HIV-1 IN CCD

Prior efforts to crystallize full-length HIV-1 IN have been hampered by poor enzyme solubility. The mutation F185K markedly improved solubility of the central IN CCD, leading to the resolution of its crystal structure alone or in complex with an INSTI (5-CITEP).[122] Nevertheless, it is doubtful whether this structure represents the true binding mode when DNA substrate is present. The knowledge of a three-dimensional structure of HIV-1 IN CCD in complex with viral DNA and an INSTI would allow determining their binding mode.

In this chapter, we report the production and purification attempts of HIV-1 IN CCD with a view to crystallize the enzyme with short oligonucleotide substrate and quinolone compounds.

2.1. Expression of soluble His-tagged HIV-1 IN CCD in *E. coli*

Plasmid encoding for soluble His-tagged HIV-1 IN CCD (HT-IN$^{50-212}$ (F185K)) was a generous gift of R. Craigie (NIH, AIDS Research and Reference Reagent Program, USA). It contains an IPTG-inducible T7 promoter allowing the expression of the interest protein. HT-IN$^{50-212}$ (F185K) was expressed following protocol described in literature[154] by transforming *E. coli* BL21(DE3)pLysS competent cells with pET-15b-IN plasmid. After IPTG induction, crude lysate obtained by cell lysis was centrifugated to give supernatant and pellet. Whole fractions analyzed by SDS/PAGE (Figure 2.1) showed induced enzyme of the predicted size (20 kDa) that migrated just below the 20 kDa molecular size marker. Although a part of insoluble enzyme was retrieved in pellet, HT-IN$^{50-212}$ (F185K) was recovered as a soluble protein in supernatant.

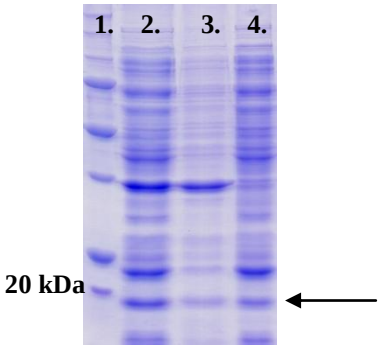

Figure 2.1. Coomassie stained SDS/PAGE analysis of HT-IN$^{50-212}$ (F185K) expression. The arrow indicates the position of the enzyme. Lane 1 = molecular size marker, lane 2 = lysate, lane 3 = pellet and lane 4 = supernatant.

2.2. Purification of HT-IN$^{50-212}$ (F185K)

2.2.1. Nickel affinity chromatography

The presence of an His-tag at the N-terminus of the enzyme allowed first purification of HT-IN$^{50-212}$ (F185K) by nickel affinity chromatography. Due to its higher solubility and stability compared to full-length enzyme, the recombinant truncated enzyme was purified using FPLC system. This automated liquid chromatography allowed to separate proteins through constant flow rate of solvents controlled by pumps and monitorated protein elution by measuring the absorbance at 280 nm. The chromatogram profile obtained and SDS/PAGE analysis of corresponding fractions are represented in figure 2.2.

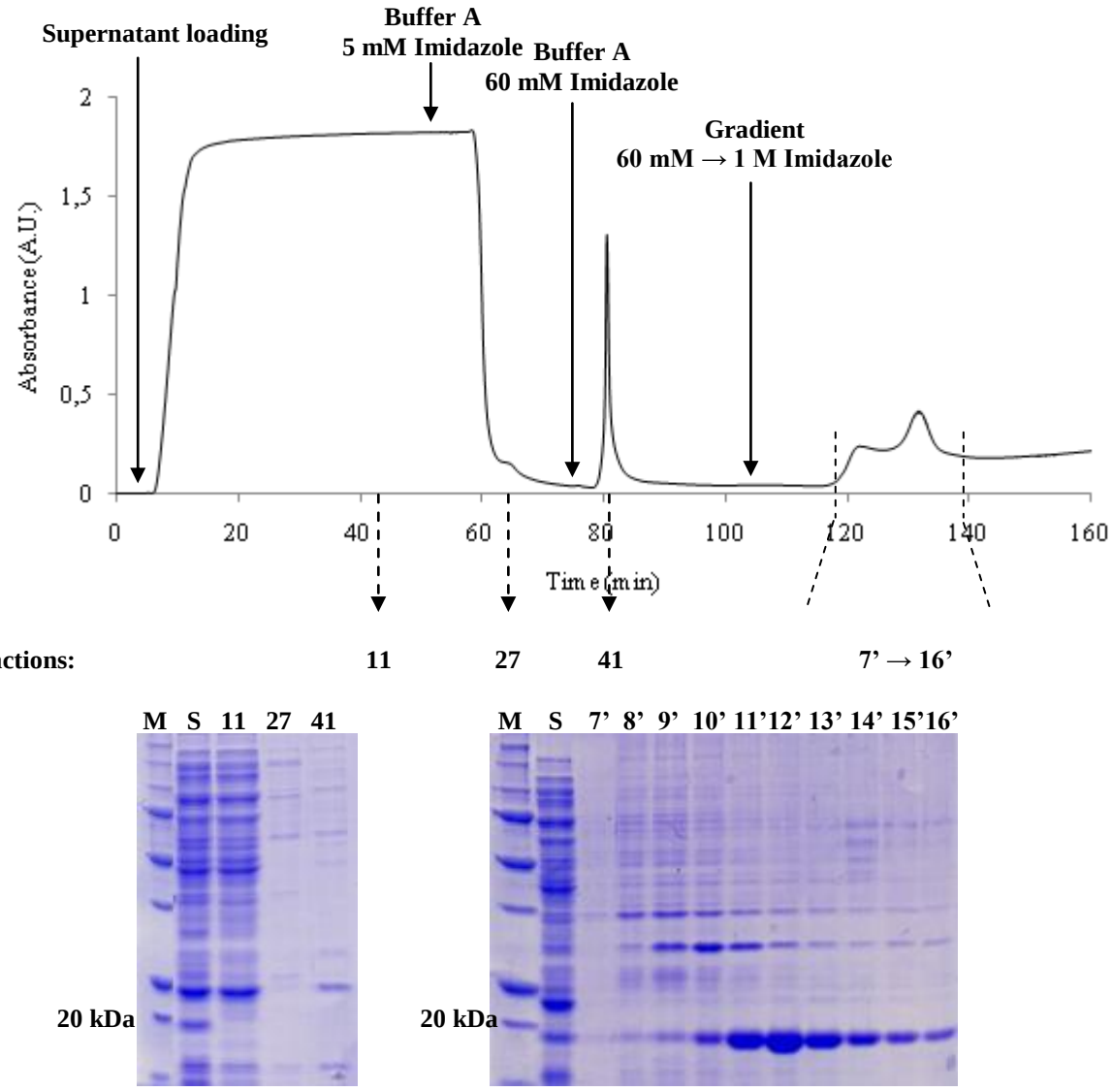

Figure 2.2. Chromatogram profile (top) and SDS/PAGE analysis of corresponding fractions (bottom) obtained from nickel affinity chromatography of HT-IN$^{50-212}$ (F185K). Molecular size marker and initial supernatant are shortened by M and S respectively.

After passing the supernatant through Ni-NTA sepharose column, proteins which had no or low affinity for Ni-NTA matrix were directly eliminated by two washing steps with buffer A containing 5 and 60 mM imidazole (fractions 11, 27 and 41). The application of a linear imidazole gradient (60 mM to 1 M) gave two overlapped peaks corresponding to the elution of the His-tagged enzyme with other contaminants (fractions 7' to 16'). The presence of these latter could be due to nonspecific binding of bacterial proteins to the Ni-NTA matrix.

Fractions 7' to 16' containing purified enzyme were recolted, dialyzed against storage buffer and protein concentration was evaluated by measuring the absorbance at 280 nm (nanodrop). Global yield was about 30 ml of purified HT-IN$^{50-212}$ (F185K) at 0.5 mg/ml for 800 ml of culture medium. Finally, the enzyme was aliquoted and conserved at -80°C.

At this stage, enzyme purity obtained was not sufficient to perform crystallographic assays. Before the investigation of other purification steps, we evaluated the enzymatic activity of purified HT-IN$^{50-212}$ (F185K).

2.2.2. Evaluation of enzymatic activity

Purified HT-IN$^{50-212}$ (F185K) was tested for its disintegration activity using a radioactive gel-based assay (Figure 2.3). Hairpin oligonucleotide substrate containing HIV-1 LTR sequence was radiomarked at 5'end with ^{32}P. Disintegration reaction occurring precisely at the junction between the viral and the target DNA sequence is expected to form two products, i.e., a 14-nucleotide hairpin (14-n) and a 24-nucleotide circular molecule (24-n). After separation on acrylamide/urea gel and exposition to a PhosphorImager screen absorbing radioactive emission, only the radiomarked 14-nucleotide hairpin is observed.

A range of purified HT-IN$^{50-212}$ (F185K) concentrations (from 100 to 1600 nM) were tested (figure 2.3 left) and active full-length IN previously prepared (see chapter 1 of results) was used as positive control (figure 2.3 right). As revealed by the presence of a radiomarked 14-nucleotide hairpin, the purified enzyme was active and possessed like full-length IN optimum catalytic activity at 400 and 800 nM.

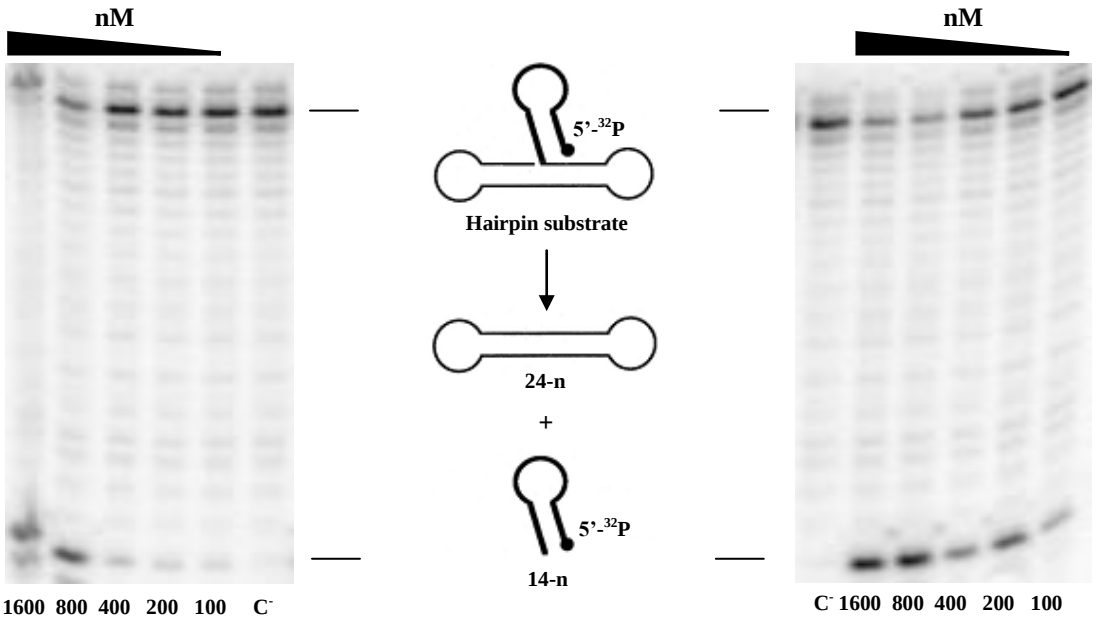

Figure 2.3 Catalytic disintegration of purified HT-IN$^{50-212}$ (F185K) (left) and wild-type HIV-1 IN (right). C$^-$ corresponds to EDTA-inactivated enzyme.

2.2.3. Size-exclusion chromatography

The presence of high molecular weight contaminants led us to purify HT-IN$^{50-212}$ (F185K) by size exclusion chromatography (SEC) using ÄKTA automated liquid chromatography system. The separation of the sample molecules is achieved by the differential exclusion as they pass through a bed of porous particles. Molecules that are smaller than the pore size can enter the particles and therefore have a longer path and longer transit time than larger molecules that cannot enter the particles. This method allows the elution of proteins in reverse order of their molecular size.

The protein was dialyzed against buffer at pH 7.5 and passed through sephadex column. The chromatogram profile obtained (Figure 2.4 top) showed two minor peaks completely overlapped by a major one. This profile could be explained by the presence in solution of different HT-IN$^{50-212}$ (F185K) oligomerization state. Coomassie and silver stained SDS/PAGE (Figure 2.4 bottom) revealed that the major part of HT-IN$^{50-212}$ (F185K) with high molecular weight contaminants were retrieved in fractions 17 corresponding to the major elution peak whereas very small quantities of pure enzyme were retrieved in fractions 24 to 34 corresponding to the third minor peak. In other words, SEC did not allow to obtain sufficient amount of pure enzyme to perform crystallographic assays.

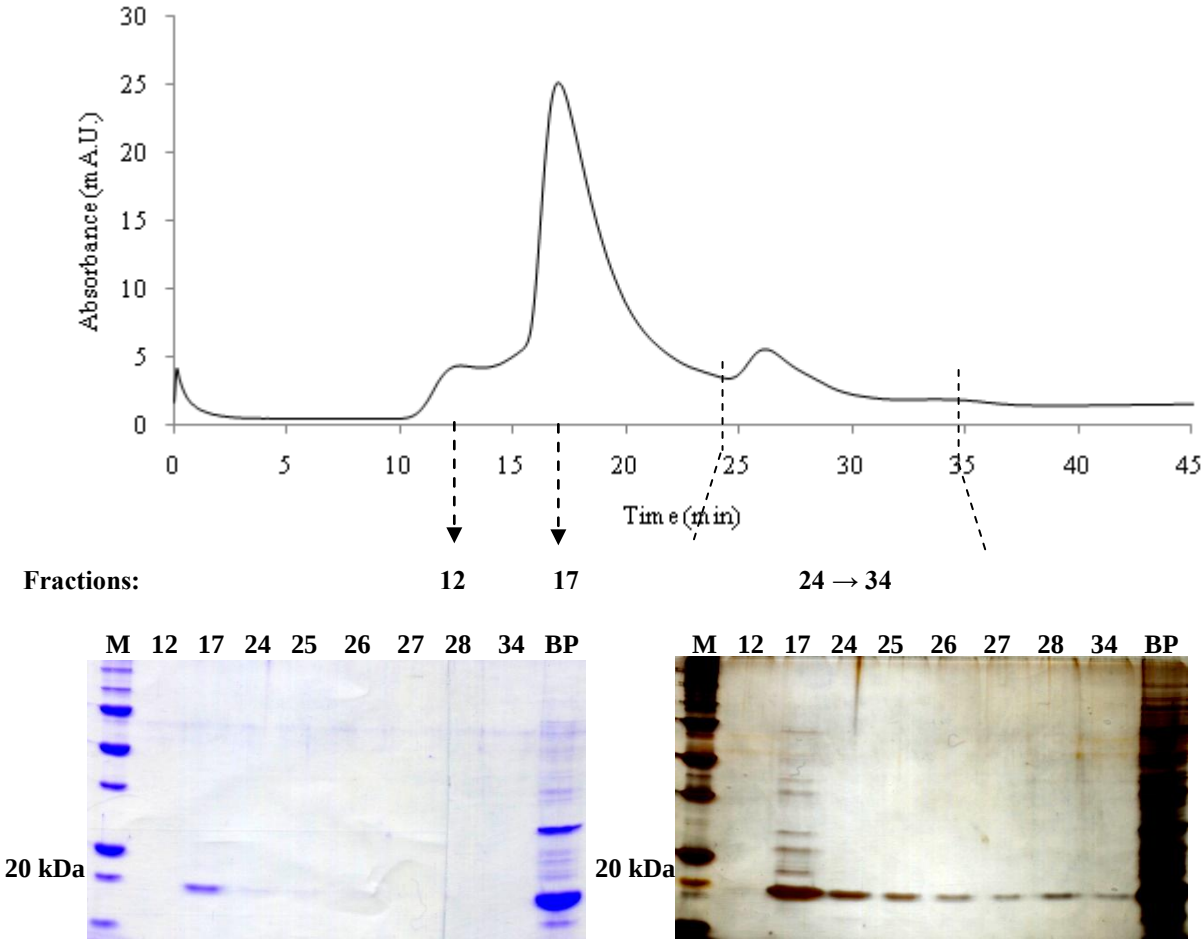

Figure 2.4. (Top) Chromatogram profile obtained from SEC. (Bottom) Coomassie stained (left) and silver stained (right) SDS/PAGE of corresponding fractions. Molecular size marker and protein sample before purification are shortened by M and BP respectively.

2.2.4. Ion-exchange chromatography

Parallel to SEC, other purification attempts were performed by ion exchange chromatography which separated proteins based on their charge. Separation depends upon the reversible adsorption of charged solute molecules to immobilized groups of opposite charge. These ionizable groups are charged positively (anion exchange) or negatively (cation exchange) and reversibly bound to exchangeable conter ions (Na^+ or Cl^-). Given the fact that the isoelectric point of HT-IN^{50-212} (F185K) is comprised between 7 and 8, the protein solution was adjusted at pH 9.5 and 6 for anion and cation exchange chromatography, respectively.

2.2.4.1. Anion-exchange chromatography

In order to charge protein negatively and remove NaCl from the solution, protein sample was dialyzed against a buffer without NaCl at pH 9.5.

After loading the protein sample onto the MonoQ column (GE Healthcare), a first wash buffer containing 0.25 M NaCl was applied to directly elute proteins which were not sufficiently charged to interact with the resin. Then, a linear gradient from 0 to 1 M NaCl was applied to elute proteins fixed to the resin.

The chromatogram profile and SDS/PAGE analysis of corresponding fractions are represented in figure 2.5. The presence of the major part of HT-IN$^{50\text{-}212}$ (F185K) with other protein contaminants in elution peak (fractions 3 to 6) indicated that the enzyme binds very weakly to the resin. Very small quantities of pure enzyme (only detected by silver stain) were eluted with linear gradient (fractions 6' and 7').

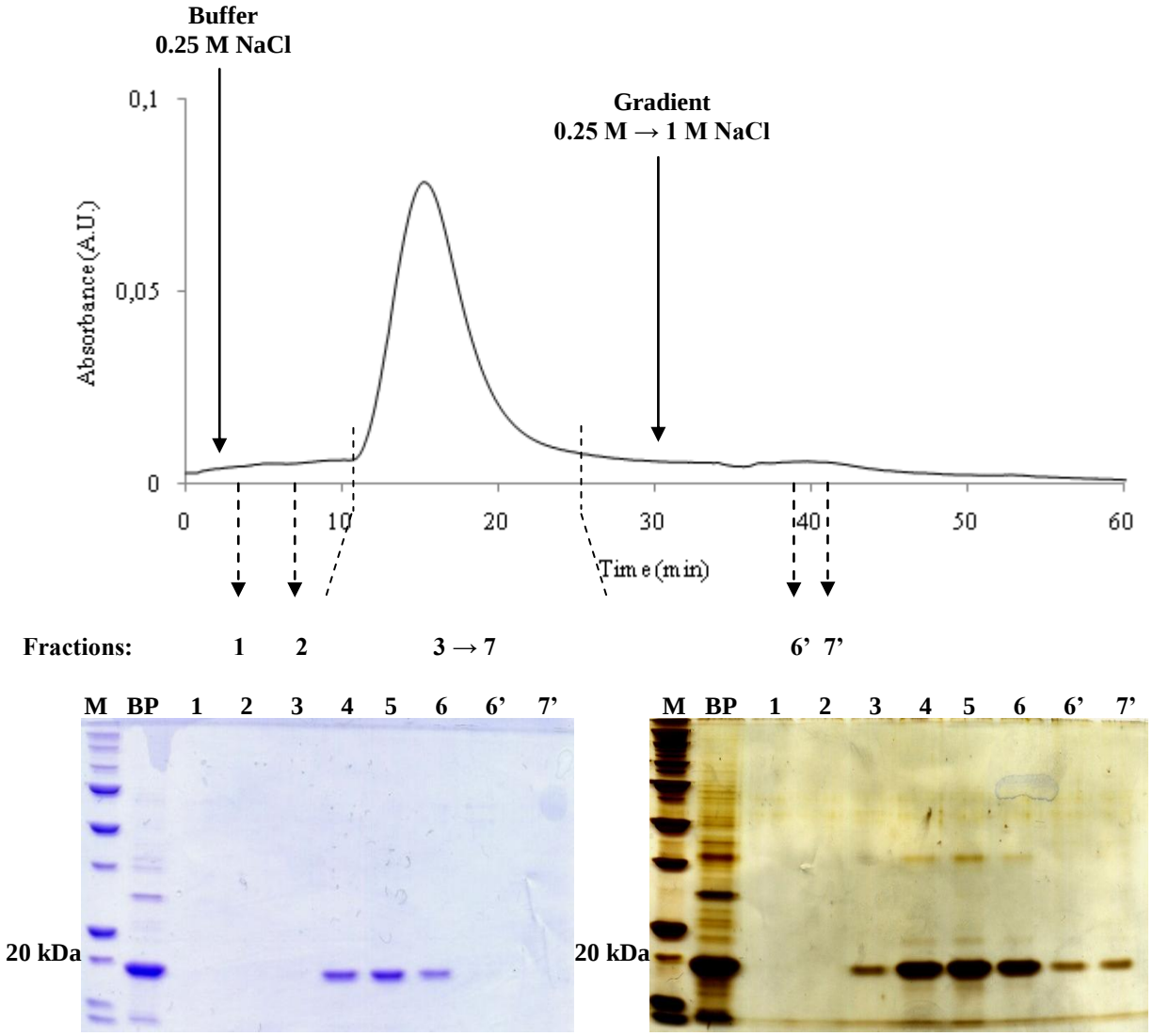

Figure 2.5. (Top) Chromatogram profile obtained from anion-exchange chromatography. (Bottom) Coomassie stained (left) and silver stained SDS/PAGE of corresponding fractions. Molecular size marker and protein sample before purification are shortened by M and BP respectively.

2.2.4.2. Cation-exchange chromatography

Protein sample was dialyzed against buffer at pH 6 to charge protein positively and remove NaCl from the solution. After loading the protein sample onto the SP column (GE Healthcare), buffer containing 0.25 M NaCl was applied to the column to elute weakly positively charged proteins. Then, a linear gradient from 0.25 to 1 M NaCl was applied to elute proteins fixed to the resin. The chromatogram profile and SDS/PAGE analysis of corresponding fractions are represented in figure 2.6.

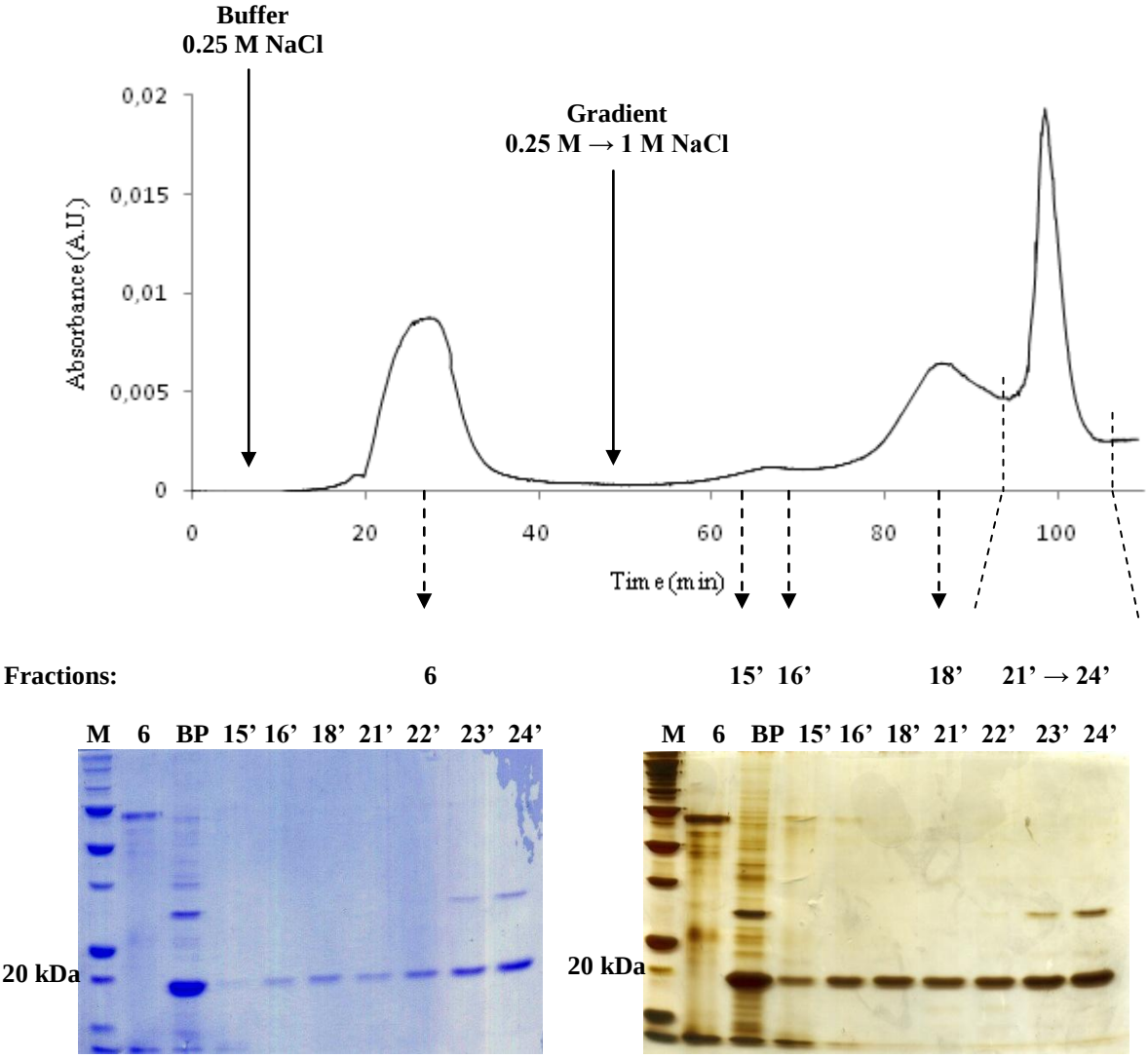

Figure 2.6. (Top) Chromatogram profile obtained from cation-exchange chromatograph. (Bottom) Coomassie stained (left) and silver stained (right) SDS/PAGE of corresponding fractions. Molecular size marker and protein sample before purification are shortened by M and BP respectively.

Interestingly, contaminants proteins are directly eliminated from the column (fraction 6) whereas HT-IN$^{50\text{-}212}$ (F185K) was eluted during NaCl gradient (fractions 15' to 24').

Indeed, fractions 18' to 22' corresponding to the first and second eluted peak contained highly pure enzyme. However, the slow elution of the enzyme resulted in high dilution as well as considerable lack in fractions containing other contaminants (fractions 15', 16' and 23', 24').

2.3. Thrombin cleavage of HT-IN$^{50-212}$ (F185K)

All crystallographic studies of HIV-1 IN CCD described to date report the removal of the hexahistidine tag from the recombinant protein. A thrombin cleavage site (Leu-Val-Pro-Arg-Gly-Ser) was included in linker regions of the recombinant fusion protein construct. Thrombin can be used to selectively cleave between the Arginine and Glycine residues of the cleavage site, effectively removing the purification tag from the protein of interest with a high degree of specificity.

Due to the low amount of pure enzyme obtained by SEC and ion-exchange chromatography, we decided to investigate His-tag cleavage by incubating 1 mg of purified protein after IMAC with thrombin protease. To determine optimum cleavage conditions, fractions corresponding at different incubation times (20 min to 60 min) were analyzed by SDS/PAGE (Figure 2.7). The presence of a smaller molecular size band just below that corresponding to HT-IN$^{50-212}$ (F185K) after thrombin addition highlighted partial cleavage of His-tag. As revealed by the intensity of the band corresponding to non-cleaved protein, maximum cleavage occurred in the first 20 minutes.

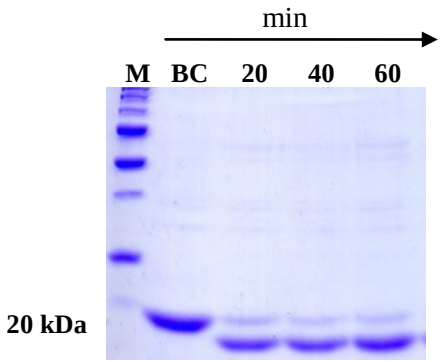

Figure 2.7. Coomassie stained SDS/PAGE analysis of HT-IN$^{50-212}$ (F185K) thrombin cleavage assay. Molecular size marker and protein sample before thrombin cleavage are shortened by M and BC, respectively.

Non-cleaved protein was removed by passing protein sample through a nickel affinity column by following the same procedure than for HT-IN$^{50-212}$ (F185K) purification with minor modifications. The chromatogram profile and silver stained SDS/PAGE analysis of corresponding fractions indicated that purification process allowed to separate cleaved protein from non-cleaved protein (Figure 2.8).

Indeed, an unique band corresponding to cleaved protein was retrieved after washing the column with buffer A containing 20 and 60 mM imidazole (fractions 19, 25, 26), highlighting the non-specific affinity of cleaved enzyme for Ni-NTA resin.

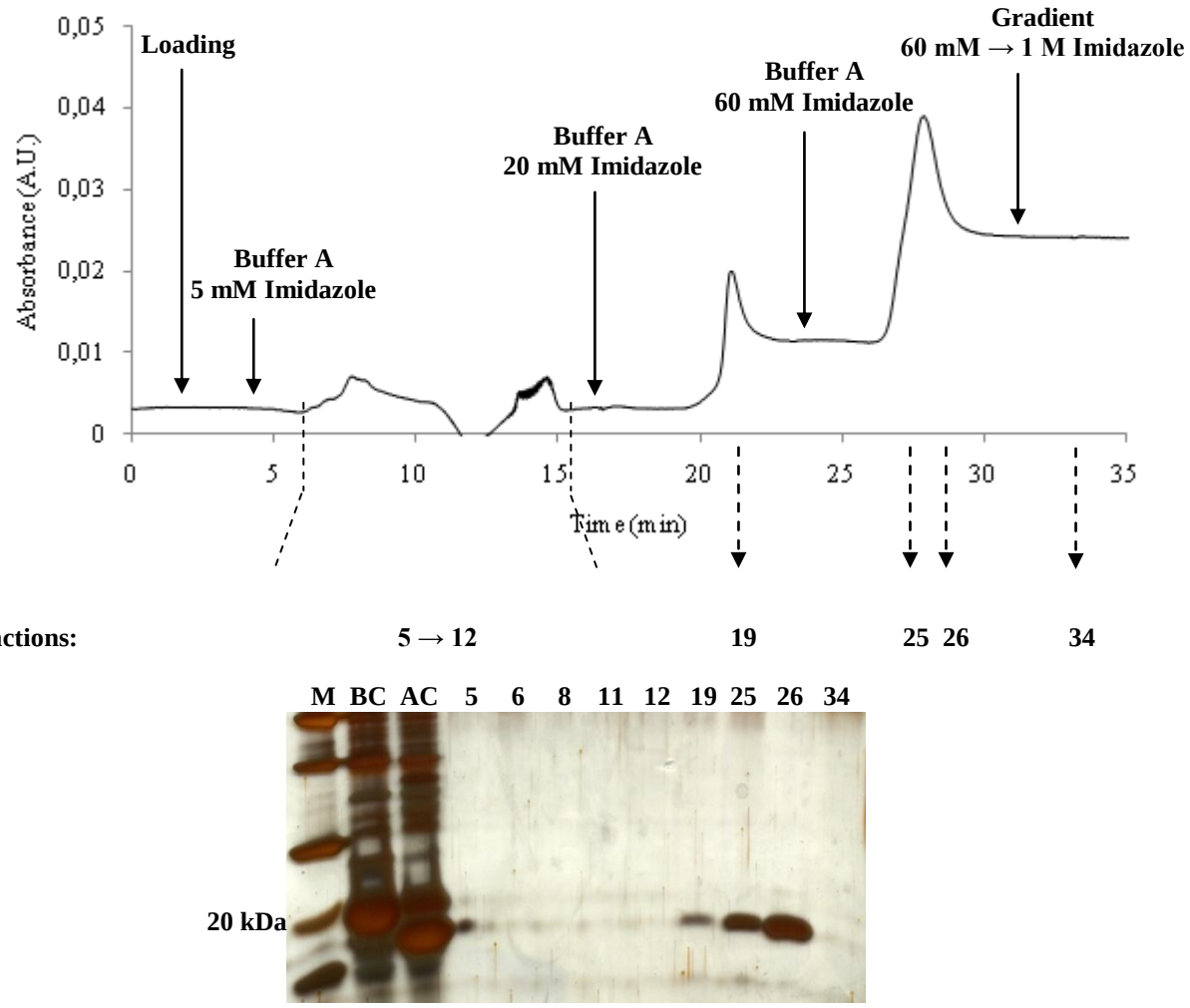

Figure 2.8. (Top) Chromatogram profile obtained from nickel affinity chromatography of protein sample after thrombin cleavage. (Bottom) Silver stained SDS/PAGE analysis of corresponding fractions. Molecular size marker, protein sample before cleavage and after cleavage are shortened by M, BC and AC respectively.

After affinity purification, it should be relevant to check the presence of thrombin protease in protein sample and remove it on benzamidine sepharose. This resin contains a covalently attached synthetic trypsin-like serine protease inhibitor (p-aminobenzamidine) allowing specific interaction with thrombin protease. Then, further protein purification could be performed with a view of its crystallization.

2.4. Conclusion

At the term of this experimental work, different conditions were tested to obtain pure and active HIV-1 IN CCD essential to perform crystallographic assays. Protein expression in BL21(DE3)pLysS followed by a nickel affinity chromatography allowed to obtain a good level of active enzyme. Other purification attempts were investigated to increase enzyme purity. SEC and ion-exchange chromatography did not allow to obtain sufficient amount of pure enzyme. His-tag cleavage with thrombin followed by a nickel affinity chromatography gave cleaved protein which could be purified.

At this stage, it is clear that optimizations should have been done to obtain pure cleaved protein to perform crystallographic assays. The inherent difficulty in protein crystallization as well as the publication of crystal structures of PFV IN in complex with both DNA and INSTIs[112,146] led us to focus our research towards the determination of quinolone compounds binding mode using physicochemical and molecular modeling studies.

3 Study of the interaction between quinolone compounds and HIV-1 IN/DNA complex

As mentioned in chapter 1, the determination of the binding mode of quinolone compounds required to study their interaction with HIV-1 IN considering different partners (DNA substrate, Mg^{2+} ions and water molecules) involved in ST reaction.

In this chapter, physicochemical studies of selected quinolone compounds were performed in order to identify the most stable conformations of those quinolone derivatives as well as the magnesium-chelating properties of their diketoacid moiety. In addition, a new HIV-1 IN/DNA model was built and docking studies were performed to predict the binding mode of synthesized quinolone compounds and to rationalize the observed SARs. Based on these results, a detailed mechanism of inhibition for quinolonyl DKA compounds was proposed.

3.1. Physicochemical characterization

3.1.1. Crystal structure analysis of 6-bromide derivative

Crystal structure determination of **2a** and the different intra and intermolecular interactions stabilizing crystal packing are represented in figure 3.1 and table 1, respectively. Quinolone compound **2a** cocrystallized with DMSO, both molecules being linked by hydrogen bonds between carboxylic acid group and DMSO oxygen O_{33a}. The DKA chain and the quinolinone ring of compound **2a** are nearly coplanar with torsion angle (T_1) C_4-C_3-C_{18}-O_{25} of 177°. The orientation of the diketo moiety with respect to the quinolinone ring is governed by intramolecular C_2-H_2---O_{25} and C_{19}-H_{19}---O_{26} hydrogen bonds. In this solid-state structure, the equilibrium between β-diketo and keto enol forms is displaced in favour of the keto-enol isomer, the hydrogens on C_{19} and O_{25} being clearly identified by Fourier difference. However, it is difficult to discriminate between the two potential keto-enol tautomers. Indeed, H_{25} is involved in a strong hydrogen bond with O_{24} and the O_{25}-H_{25} distance (1.06 Å) is greater than commonly observed for O-H bonds (0.82 Å). Furthermore, both carbonyl (C_{18}-O_{25} and C_{20}-O_{24}) and carbon-carbon (C_{18}-C_{19} and C_{19}-C_{20}) bond distances are similar and intermediate between standard single and double bonds, indicative of strong electronic delocalization within this keto-enol moiety.

In the crystal packing, π-π stacking interactions between quinolone rings (centroid-centroid distances of 3.6 Å) are observed and could influence the binding to the enzyme.

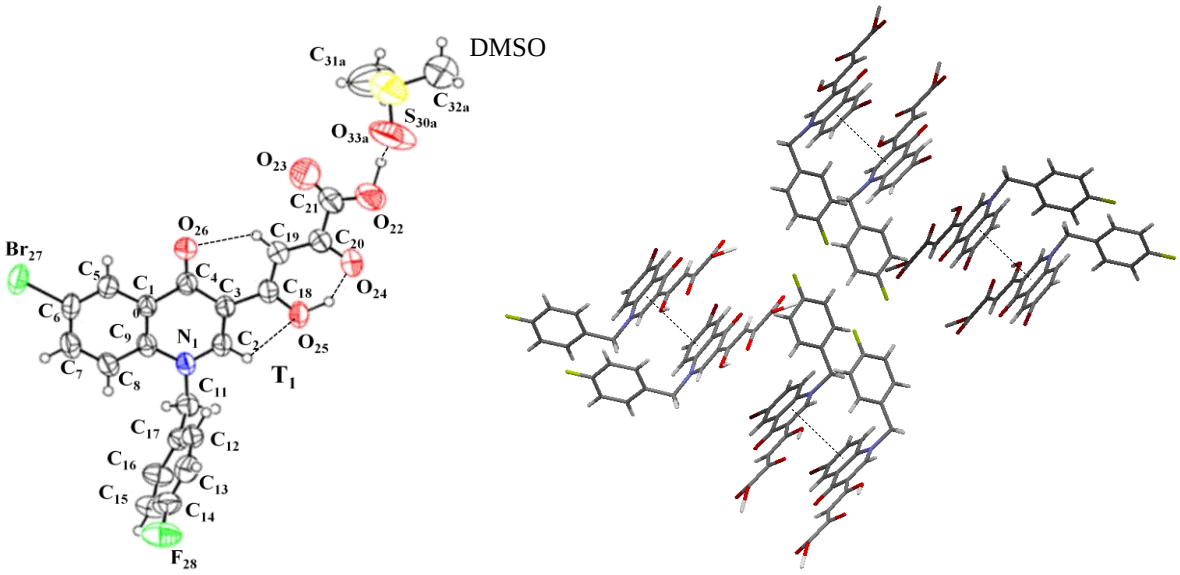

Figure 3.1. (Left) Crystal structure (ORTEP) of compound **2a** (cocrystallized with DMSO) showing the atom-numbering and hydrogen-bonding scheme. Displacement ellipsoids are drawn at the 30% level.[155] (Right) Crystal packing representation revealing π-π stacking interactions between quinolone ring.

Table 1. Intra and intermolecular interactions involved in crystal structure (symetry #1: 2-x,-y,1-z ; symetry #2: 1+x, y, z). H bonds between acceptors A and donors D-H are characterized by a distance 1 D-A, a distance 2 H…A and an angle D-H…A. π-π stacking interactions are characterized by a distance 1 between centroids.

interactions	partners	distance 1 (Å)	distance 2 (Å)	angle (°)
H bonds	O25-H…O24	2,467(6)	1,520	145
	O22-H…O33$^{\#1}$	2,519(10)	1,710	120
C-H…O interactions	C19-H…O26	2,912(7)	2,290	124
π-π stacking	Cycles I-II$^{\#2}$	3,659(4)	-	-

3.1.2. Solution-state conformation analysis

Solid-state XRD study allowed to identify a stable conformation of neutral compound **2a**. Nevertheless, under physiological conditions, the DKA chain is unprotonated.[143,156] Based on these considerations, the solution-state conformation of dianionic compound **2a** was investigated using UV-visible spectroscopy and theoretical calculation considering bulk solvent effects.[157]

First of all, geometries optimization and simulation of UV-visible absorption spectrum of neutral compound **2a** was investigated to validate the chosen theoretical approach. The most stable geometry obtained at PCM-PBE0/6-311G(d,p) level of theory can be straightforwardly compared to the experimental XRD data (Figure 3.2 left). We noted that the PBE0 and XRD orientation of the DKA side chain completely matched (the C_2-C_3-C_{18}-C_{19} torsion angle being close to 180° in both cases), as well as on the enol nature of this chain. The same agreement holds for the relative positions of the p-F-benzyle and central quinolone rings, with a twist angle of -51° by XRD and -55° with DFT. Moreover, theoretical electronic transition obtained at PCM-PBE0/6-311+G(2d,p) level of theory for the most stable conformation of neutral compound **2a** was in agreement with experiment, with two predicted absorption bands at 382 nm and 303 nm, close to the measured values (Figure 3.2 right). The first absorption (382 nm) corresponds to a HOMO to LUMO electronic transition, whereas the second peak (303 nm) presents an HOMO-2 to LUMO character with a smaller HOMO to LUMO + 1 contribution. The topologies of these frontier orbitals are sketched in Figure 3.3. The HOMO is mainly centered on the quinolone rings, the LUMO being located on the lateral chain. Therefore the first transition implies an electron transfer from the quinolone to the diketo side chain. For the second transition, the amplitude of the charge-transfer is obviously reduced. The chosen theoretical approach accurately restored experimental conformation of neutral compound **2a** and predicts in a satisfactory way the electronic transitions (λ_{max}), confirming the robustness of the PBE0 functional.

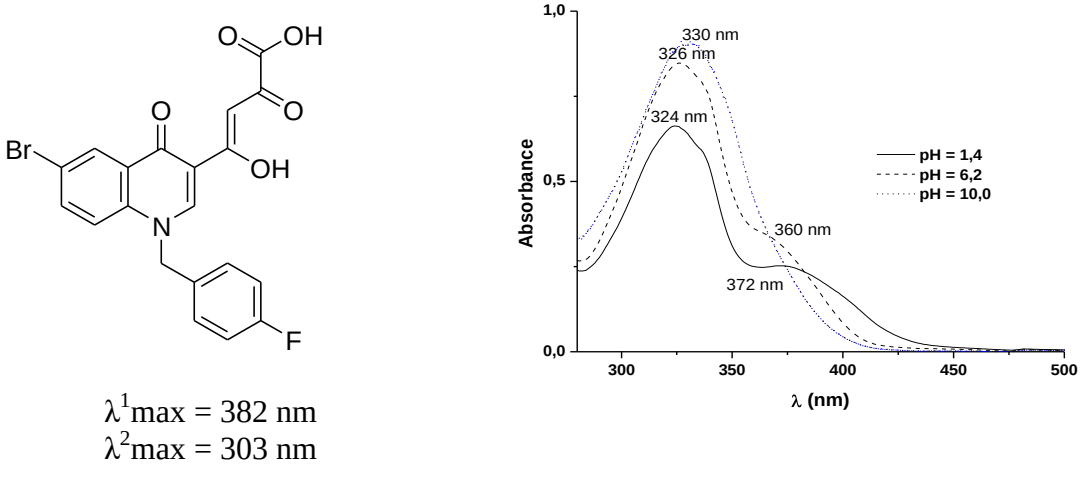

Figure 3.2. (Left) Most stable conformation and electronic transitions calculated for neutral compound **2a**. (Right) Experimental UV/Vis spectra recorded in a methanol/water mixture (80:20) under three typical pH, corresponding to the neutral (1,4), mono-anionic (6.2) and di-anionic (10.0) forms.

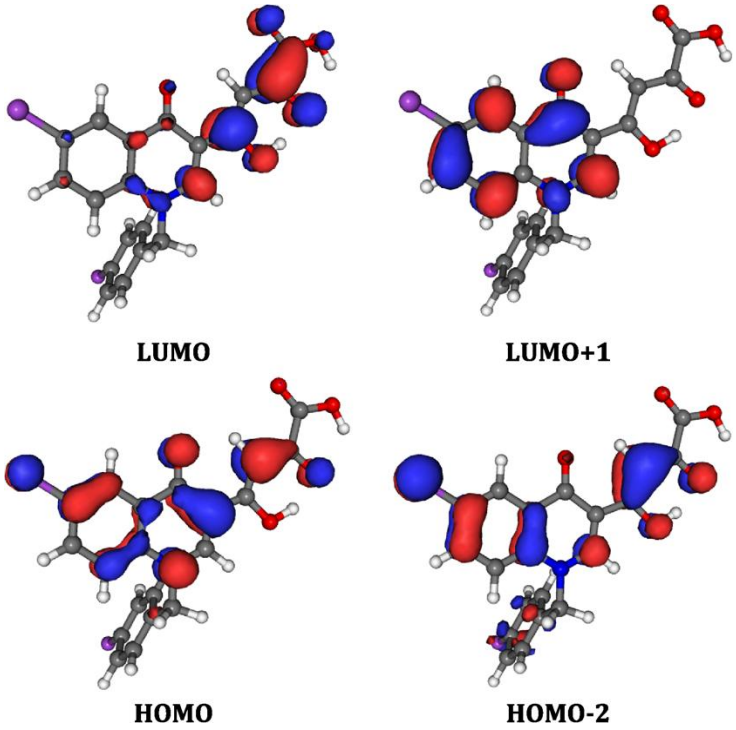

Figure 3.3. Frontier orbitals for neutral compound **2a** (contour threshold: 0.4 au).

Two stable conformations with a low energy difference (+ 0.44 kcal/mol) and a C_2-C_3-C_{18}-C_{19} torsion angle of -57° and 180° were identified for di-anionic compound **2a** (Figure 3.4). For both species, the DKA side chain was almost planar though the terminal carboxylate group undergoes a deviation from planarity of 10° or 15°. All C=O bond lengths of DKA were equal to 1.250 ± 0.006 Å indicating that the negative charges were delocalized on the side chain. This was confirmed by the partial atomic charge analysis that allowed to calculate a charge of -1.70 e (T_1 = -52°) and -1.75 e (T_1 = 180°) for the DKA moiety. The UV-visible spectra of dianionic species were obtained in aqueous solution (H_2O/MeOH (80/20)) at pH value higher than 7 (Figure 3.2 right). This spectrum showed a strong absorption at 330 nm. The simulated spectra with the 6-311+G(2d,p) basis set for the two most stable conformations were in agreement with experimental spectra, with one strong absorption band at 327 nm (T1 = -52°) and 353 nm (T1 = 180°) mainly due to π-π^* transitions corresponding to an electron transfer from the side chain to the quinolone moiety. The very weak difference of 3 nm observed between the electronic transition calculated for the stable conformation with T1 = -52° and the experimental value is probably partially originating in a error compensation (functional/solute-solvent hydrogen bonds), as it is known that the description of a di-anionic organic compounds remains difficult with TD-DFT.[158]

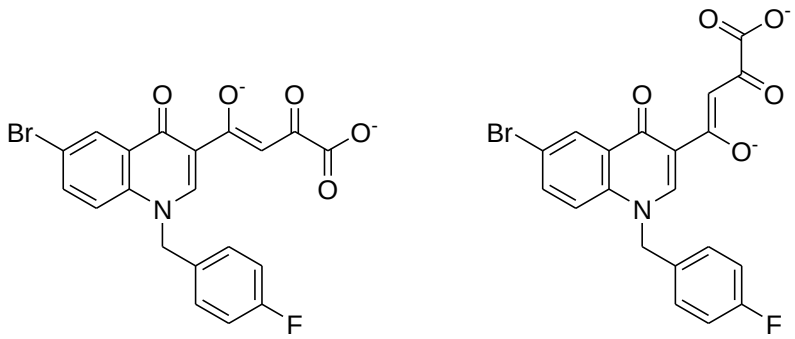

Figure 3.4. Most stable conformation and corresponding electronic transitions calculated for di-anionic compound **2a**.

3.1.3. Magnesium-chelating properties of DKA moiety

Due to the low available amount of quinolonyl DKA compounds and their poor solubility in aqueous solution, we decided to study the magnesium-chelating properties of DKA moiety in solution state using an aryl diketoacid (ADKA) model compound commercially available (Figure 3.5).

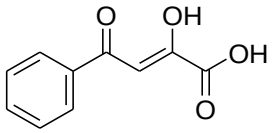

Figure 3.5. Structure of aryl diketoacid (ADKA) model compound.

IR spectra of di-anionic ADKA in Tris-buffered aqueous solution (pH > 7.4) containing $MgCl_2.6H_2O$ was recorded using attenuated total reflectance (ATR) spectroscopy (Figure 3.6). In this technique, the liquid sample is put on a crystal (ZnSe) of high refractive index. A beam of infrared light is passed through this one, resulting in multiple internal reflections which extend into the sample. Diketoacid functional groups directly involved in the interaction with Mg^{2+} ions were identified by observing the shift of carbonyl stretching vibrations. The IR spectrum for di-anionic ADKA (Figure 3.6a, left) showed four characteristics bands corresponding to the carbonyl groups of diketoacid moiety. The bands at 1590 and 1508 cm^{-1} were assigned to the symmetric and asymmetric carbonyl stretching vibration of ketoenolate group whereas the bands at 1555 and 1375 cm^{-1} were assigned to the symmetric and asymmetric stretch of carboxylate moiety.

Upon the addition of $MgCl_2.6H_2O$ to the di-anionic ADKA solution, all carbonyl stretching vibrations were shifted towards higher frequency (Figure 3.6b, left), indicating that both keto-enolate and carboxylate group of DKA side chain interacted with Mg^{2+} ions. Bathochromic shifts of the π-π^* transition that we observed by UV-visible analysis of ADKA and compound **2a** following the addition of increasing concentrations of magnesium ions in aqueous solutions (Figure 3.6 right) implied that complexation by Mg^{2+} increased the electronic density along DKA moiety. Although these data do not allow to obtain a quantitative determination of the complexation constant as well as the stoechiometry of the complex formed, it give a good indication of the interaction between DKA side chain and Mg^{2+} ions.

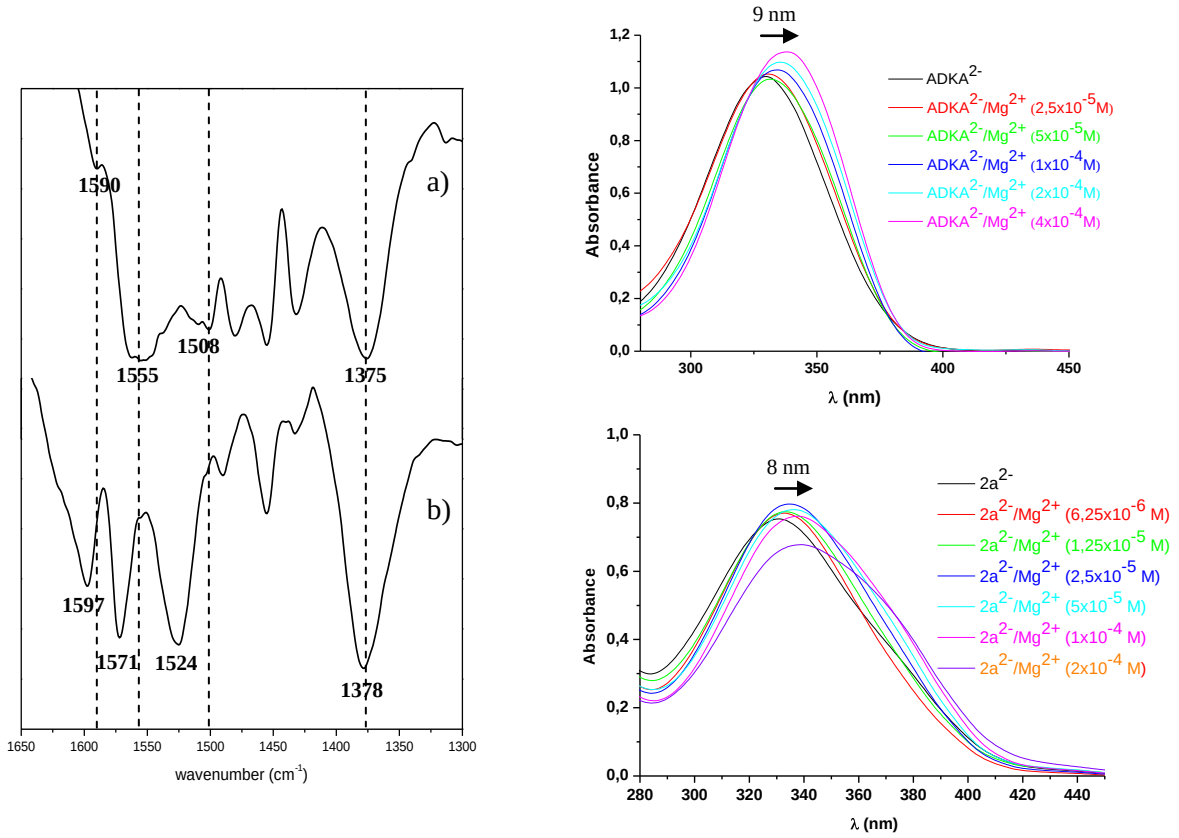

Figure 3.6. (Left) ATR spectra of a) 0.2 M di-anionic ADKA in aqueous buffer (Tris-HCl, pH 10.0) and b) in the presence of 0.4 M magnesium. (Right) UV-visible spectra of 5 x 10^{-5} M di-anionic ADKA in aqueous buffer (Tris-HCl, pH 10.0) (Top) and compound **2a** in MeOH/water buffer (Tris-HCl, pH 10.0) (Bottom) alone (black line) and in the presence of increasing concentrations of magnesium (color lines). The arrows indicate the batochromic shift upon addition of magnesium.

Based on these results, it was plausible to propose a two-metal chelating mode of DKA moiety in solution where both the magnesium binding sites are involved in the sequestration of metal ions. This coordination mode is in agreement with mass data and potentiometric measurement which suggested two magnesium ions octahedrally coordinated by the diketoacid moiety and other ligands (water molecules, another diketoacid chain, ...) (Figure 3.7).[143,159]

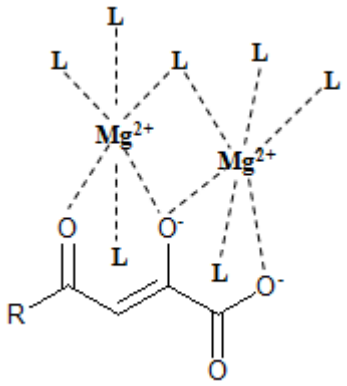

Figure 3.7. Structural hypothesis for the chelation mode of diketoacid moiety with Mg^{2+} ions. Ligands (water molecules, diketoacid moiety, ...) completing the octahedral geometry of magnesium ions are denoted as L.

3.2. Molecular modeling study

3.2.1. HIV-1 IN/DNA model building

Due to the lack of HIV-1 IN/DNA experimental structures, the building of a reliable model is essential for predicting docking of INSTIs. The polynucleotidyl transferase family comprises numerous DNA-binding enzymes involved in a wide range of processes such as transposition, viral DNA integration, replication and repair of DNA, homologous recombination and RNA-mediated gene silencing. Among these, Tn5 transposase and PFV IN showed remarkable mechanistic similarities with HIV-1 IN by catalyzing the same two-step metal-dependent process. While these two enzymes have low overall primary sequence identity with HIV-1 IN (~ 7 % for Tn5 transposase and ~ 20 % for PFV IN), structure-based sequence alignment (Discovery Studio software[160]) of the catalytic core domains (Figure 3.8) revealed a common RNaseH-like fold with highly conserved active site residues such as the DDE triad and lysine residues involved in Mg^{2+} sequestration and DNA binding, respectively. Moreover, the active-site loop of PFV IN (residues 211-220) directly involved in separating the viral DNA strands shares high sequence identity with the one of HIV-1 IN (residues 140-149). Based on these considerations, the available crystal structures of Tn5 transposase/DNA transposon and PFV IN/DNA complexes provided useful scaffold for modeling the engagement of DNA with the active site of HIV-1 IN.

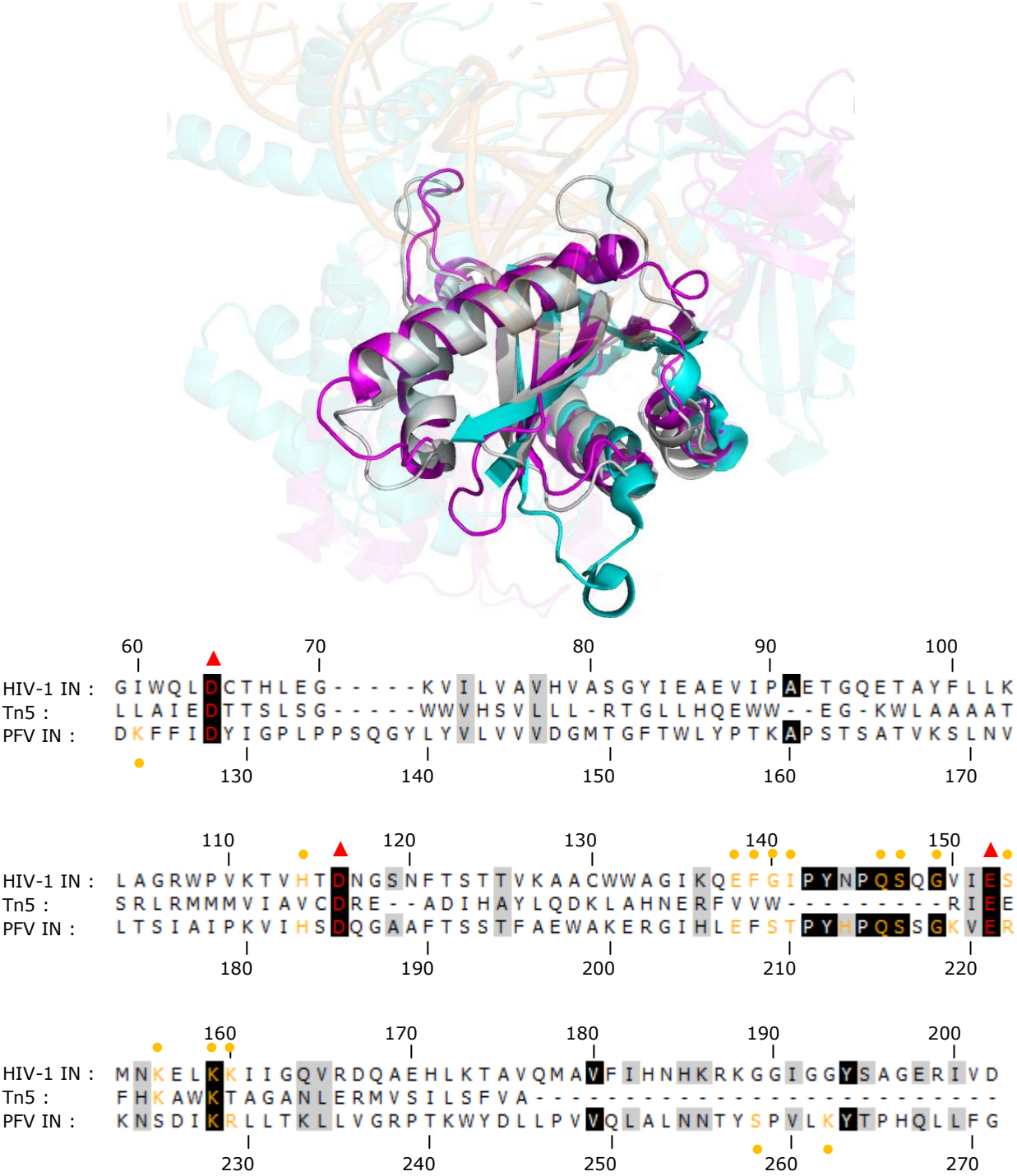

Figure 3.8. Structure-based alignment of Tn5 transposase and PFV IN with HIV-1 IN. The alignment was based on RnaseH fold of catalytic core domains and RMSD (3.224 Å and 2.178 Å for PFV IN and Tn5 transposase, respectively) calculated using C_α atoms. Secondary structure of proteins are shown as cartoon and color-coded: grey for HIV-1 IN, magenta for PFV IN and cyan for Tn5 transposase. Identical amino acid residues conserved across all three proteins are marked in black, while similar residues are marked in grey. DDE motifs which bind metal cations and residues interacting with DNA are marked by ▲ and ●, respectively.

Based on the recent crystal structure of PFV IN in complex with its cognate DNA and INSTIs, models of HIV-1 IN/DNA complex in its active and INSTI inhibited forms have been reported[161,162].

Nevertheless, these simulated structures did not consider the octahedral inner sphere coordination environments of the two active-site Mg^{2+} ions, in particular explicit water molecules which could be involved in the catalytic reaction mechanism. Interestingly, by superimposing the Cα atoms of the DDE active site residues of Tn5 transposase (PDB code 1MUS)[163], PFV IN (PDB code 3L2S)[112] and HIV-1 IN CCD (PDB code 1BL3C)[106], water molecules present in both Tn5 transposase and HIV-1 IN crystal structures occupy similar positions and complete the octahedral geometry of the two divalent metal ions from PFV crystal structure (Figure 3.9). The 5' phosphate group of Tn5 transposon superimposes with both bridging (w_4) and apical (w_1) water molecules from HIV-1 IN CCD. This superimposition reveals a plausible conformation of a scissile phosphodiester group from the target DNA interacting with the two divalent ions by displacing two water molecules. In this way, the scissile phosphodiester group might be properly positioned for the attack of the 3'-OH nucleophilic group of the viral DNA.

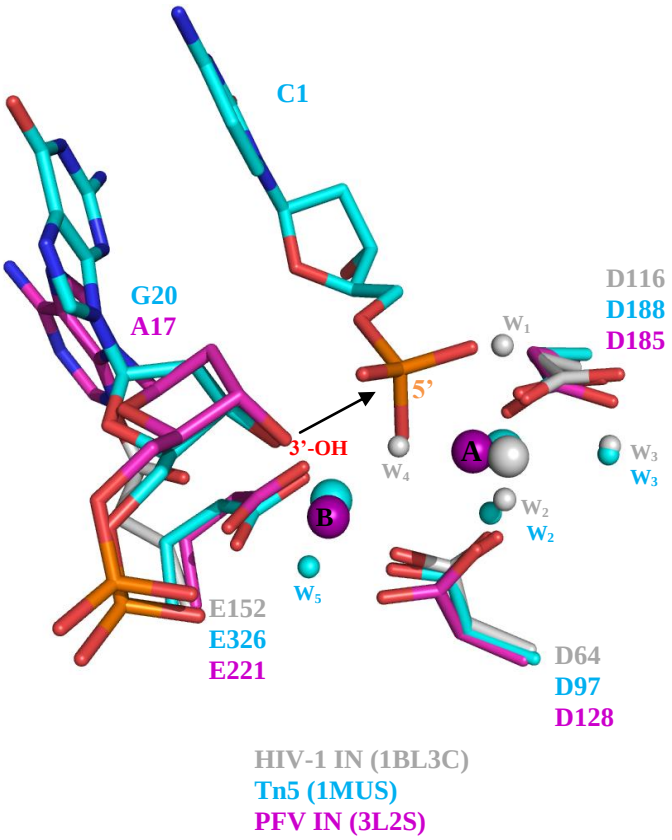

Figure 3.9. Superimposition of the active sites of HIV-1 IN, Tn5 transposase and PFV IN based on the positions of C-α atoms of the active-site DDE residues. Side chains of DDE-motif and terminal nucleotides are shown as sticks. Divalent metal ions (labeled A and B) and waters molecules (labeled w) are shown as spheres. The arrow indicates the 3'-OH end attacking the scissile phosphate of the target DNA mimicked by the 5'-phosphate end of Tn5 transposon.

These observations prompted us to build a model of the HIV-1 IN/DNA complex in its INSTI inhibited form by considering explicit water molecules (see material and methods for procedure details).[153] HIV-1 IN/DNA model building was initiated by overlaying the structures of HIV-1 IN CCD (1BL3C)[106], Tn5 transposome (1MUS)[163] and elvitegravir-bound PFV structure (3L2U)[112] with their Cα positions of active-site DDE residues. This step properly oriented PFV DNA substrate, metal ions and explicit water molecules within the active site of HIV-1 IN (Figure 3.10). This superimposition was followed by (a) the mutation of PFV DNA , (b) the modeling of two Mg^{2+} ions and the merging of water molecules, c) the reorientation of glutamate residues to interact with Mg^{2+} ion and (d) the construction of the active-site loop to obtain after minimization procedure a new model used as template to perform docking studies.

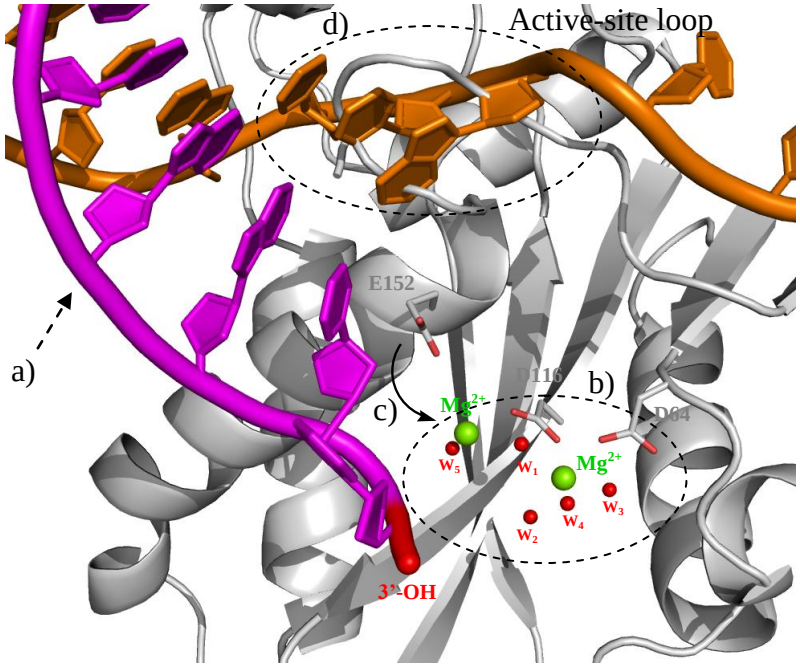

Figure 3.10. Schematic representation of the different steps followed in the building of HIV-1 IN/DNA model. The two Mg^{2+} ions and coordinated water molecules (w) are shown as green and red spheres, respectively. The nontransferred (orange) and reactive (magenta) DNA strand are shown as cartoon. Catalytic core domain is shown as grey cartoon.

3.2.2. Docking studies

3.2.2.1. Validation of docking method

Before studying the interaction between quinolone compounds and the modeled HIV-1 IN/DNA complex, docking software (Gold[164]) was validated to check if it allowed to correctly position a ligand in a target enzyme as observed in the crystal structure.

Because no experimental structure of HIV-1 IN in complex with DNA substrate and INSTI was reported, we simulated the interaction between PFV IN/DNA complex and INSTIs (raltegravir and elvitegravir) which crystal structures of ternary complexes are available in the Protein Data Bank. Docking results (figure 3.11) indicated that Gold procedure faithfully predicted the binding mode observed in crystallographic structures, with RMSD deviation between the predicted and observed atom positions of 0.98 and 2.03 Å for raltegravir and elvitegravir, respectively. This procedure was so used to predict the binding mode of quinolone compounds in the active site of modeled enzyme.

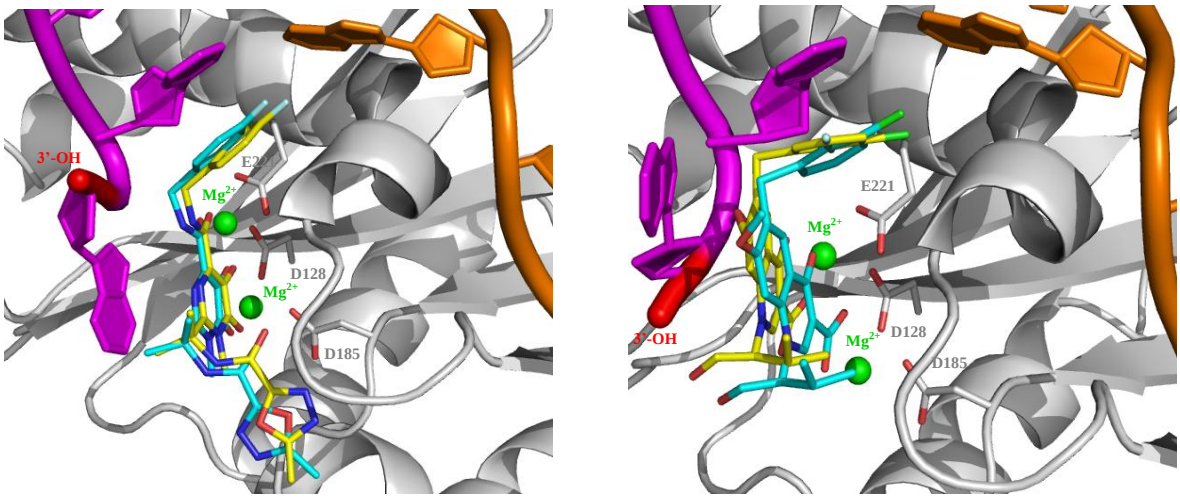

Figure 3.11. Comparaison between poses of raltegravir (left) and elvitegravir (right) within the active site of PFV IN/DNA complex obtained by docking (yellow) and crystallography (cyan).

3.2.2.2. Docking of quinolonyl DKA compounds within HIV-1 IN/DNA model

Docking of the best DKA quinolone compounds (**2a**, **2b** and **2c**) in the newly built model was performed with the Gold Software.[164] All these compounds showed a similar interfacial binding mode in which the DKA moiety chelated the two Mg^{2+} ions (see docking result of **2a**, Figure 3.12). In this orientation, the w_1 (bridging) and w_4 (apical) coordinated water molecules were totally displaced by carboxylate and enolate oxygen atoms, respectively, whereas the keto oxygen atom replaces the 3'-OH extremity of viral DNA. As a result, the displaced 3'-adenosine terminal base (A17) was involved in a π-stacking interaction with the quinolone ring in such a way that bromine atom at C-6 pointed out to the solvent-exposed surface. The *p*-F-benzyl group fitted within a tight pocket formed by cytosine 16 (C16), guanine 4 (G4) and two catalytic loop residues P145 and Q146. The fluorobenzyl group made π-stacking interaction with C16 taking the space originally occupied by A17. These docking results are in agreement with the SARs observed.

Indeed, the chelation of the carboxylate group to Mg^{2+} ion could explain the stronger inhibitory potency of acidic compounds compared to ester compounds. Moreover, the orientation of the substituent at position 6 of the quinolone scaffold towards the solvent-exposed surface could also explain the unmodified potency of 6-substituted quinolone derivatives. The observed binding mode for DKA quinolone compounds suggests resistance profiles similar to raltegravir and elvitegravir. Both Q148H/R/K and N155H resistance pathways, implying a energetic penalty upon the binding of the inhibitor and the moving of the two magnesium ions which destabilises the complexation of the chelating moiety, are very susceptible to reduce inhibitory potency of DKA quinolone compounds. Due to the absence of interactions between quinolone compounds and Y143, the resistance pathway involving the mutation Y143R/C should not reduce the susceptibility of the inhibitors.

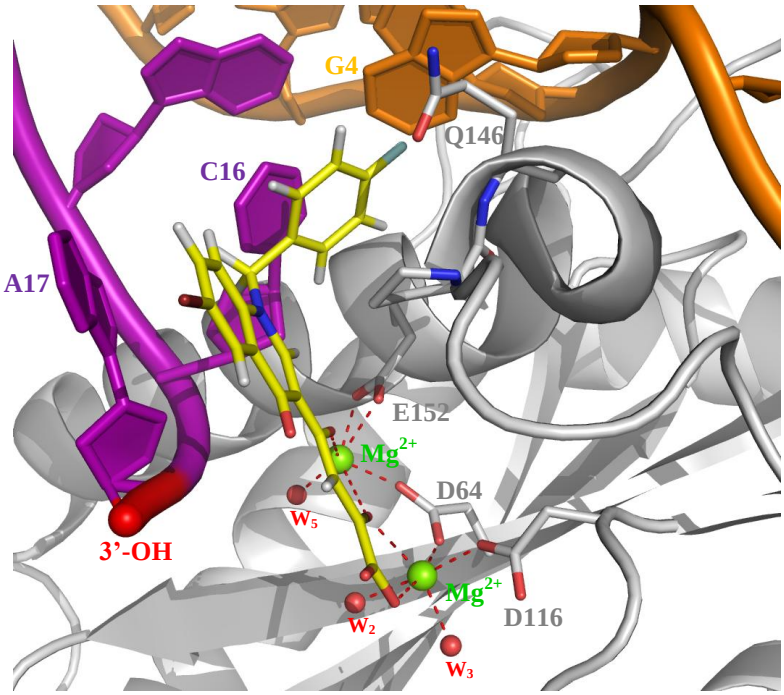

Figure 3.12. Docking result of compound **2a** (yellow) into the HIV-1 IN/DNA model. The two Mg^{2+} ions and coordinated water molecules (w) are shown as green and red spheres, respectively. The nontransferred (orange) and reactive (magenta) DNA strands are shown as cartoon. Catalytic core domain is shown as grey cartoon with main amino acids as sticks. Note that the two Mg^{2+} ions are octahedrally coordinated by the DDE motif, water molecules and the diketoacid chain of the quinolone inhibitor.

These molecular modeling studies allow us to propose a mechanism of inhibition by DKA compounds (Figure 3.13).[153] After the processing of viral DNA, the active site of HIV-1 IN adopts an active conformation in which two Mg^{2+} ions are octahedrally coordinated by the DDE motif, the 3'-OH extremity and water molecules.

This active conformation facilitates the binding of a scissile phosphodiester group from target DNA which displaces bridging (w_1) and apical (w_4) water molecules from the active site, forming the ST complex. Once the inhibitor binds in the active site, the chelating moiety (DKA chain) interacts with the two Mg^{2+} ions by displacing the 3'-OH extremity and the two water molecules originally occupied by the phosphodiester group. The newly formed octahedral complex is then stabilized by the properly oriented hydrophobic benzyl moiety by replacing the 3' A17 displaced from the active site to form a tighter complex. In this way, the inhibitor prevents the formation of the ST complex rendering it catalytically inactive. This mechanism of action is in agreement with the two-step mechanism of binding of INSTIs proposed by Garvey *et al.*.[165]

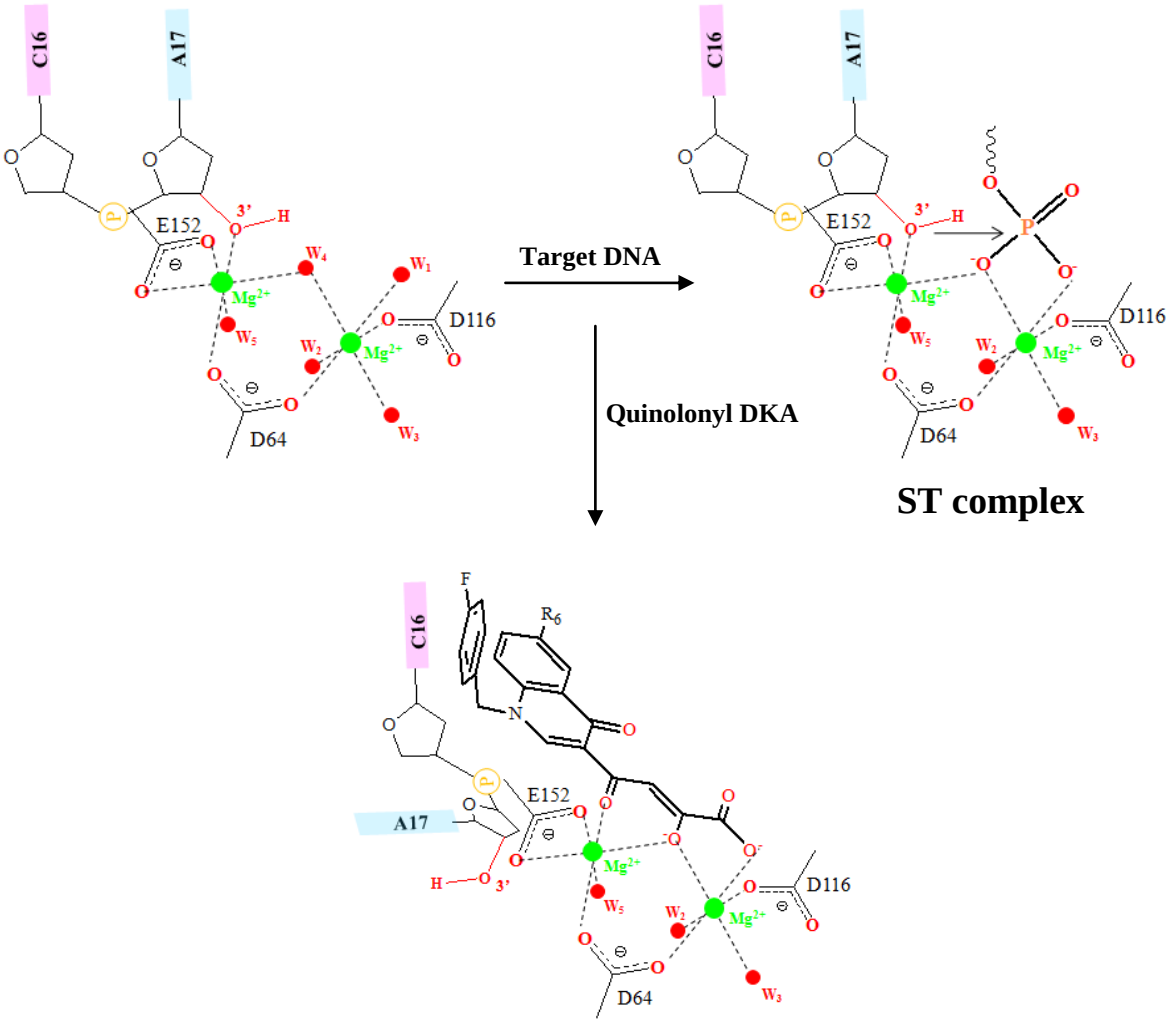

Figure 3.13. Mechanism of inhibition for quinolonyl DKA compounds.

3.3. Conclusion

In this third chapter of results, physicochemical and molecular modeling studies were investigated to elucidate the binding mode of quinolone compounds to HIV-1 IN/DNA complex. X-ray diffraction, UV-visible spectroscopy and theoretical calculations allowed to identify two most stable conformations of the diketoacid moiety. Spectroscopic characterization (ATR, UV-vis) of DKA derivative/Mg^{2+} complexes allowed to postulate a two-metal chelating mode by the DKA moiety. Docking studies performed on a newly build HIV-1 IN DNA model allowed to propose a mechanism of inhibition for quinolonyl DKA compounds in agreement with the biological activities we observed and biochemical study of HIV-1 IN inhibition kinetic.

Part IV
Conclusion and prospects

HIV-1 is the causal agent of AIDS. In the design of new antiviral agents, HIV-1 IN constitutes an attractive target because this enzyme plays a major role in the viral replication cycle by catalyzing the integration of viral DNA into the host cell DNA.

The objective of this work was to study the inhibition mechanism of HIV-1 IN by quinolone compounds with the aim to provide a detailed understanding of the mechanism of action of INSTIs.

In a first time, we explored the effect of chemical modifications at position 6 of the quinolone scaffold by synthesizing new compounds containing at C-6 bromine atom, acrylate or p-fluoro-benzyloxy groups and evaluating their antiviral and anti-integrase activities. The expression and purification of active wild-type HIV-1 IN allowed to evaluate IC_{50} values of the synthesized quinolone compounds. The results of *in vitro* assays showed that acid derivatives were more potent than their corresponding esters, with in each case a selectivity for the ST reaction. The introduction of both hydrophilic and hydrophobic substituents at C-6 did not modified potency against HIV-1 IN. Antiviral data, which were in agreement with enzymatic activity, showed that quinolone compounds inhibited viral replication in cells at non-cytotoxic concentrations.

Having in mind to crystallize enzyme-ligands complexes, HIV-1 IN CCD was expressed and purified. All purification attempts performed did not allow to obtain a sufficient amount of pure enzyme to perform cristallization. Giving the fact that HIV-1 IN CCD was previously crystallized without His_6-tag[106], thrombin cleavage of purified His-tagged enzyme collected after affinity chromatography should be performed. Thrombin as well as non-cleaved fraction of protein would be then separated from the cleaved protein by passing successively sample through benzamidine sepharose and Ni-NTA column. The cleaved HIV-1 IN CCD isolated could be finally purified using other purification techniques.

To predict the binding mode of quinolone compounds within the active site of HIV-1 IN, physicochemical studies were performed to identify stable conformations as input for docking studies. X-ray diffraction structure determination of compound **2a** revealed that the diketo acid chain was present under keto enol form and coplanar with the quinolone ring (Figure 1 left). Complementary theoretical calculations on the di-anionic form of compound **2a** considering solvent effects indicated the existence of two stable conformations in solution (ΔE = 0.44 kcal/mole), with one of these corresponding to the experimental structure obtained by XRD (Figure 1 right).

A solution-state study of the complexation of diketoacid model compound with Mg^{2+} ions using ATR and UV-visible spectroscopy allowed to propose a two-metal chelating mode by the DKA moiety where both magnesium binding sites of the chelating moiety are involved in the sequestration of metal ions.

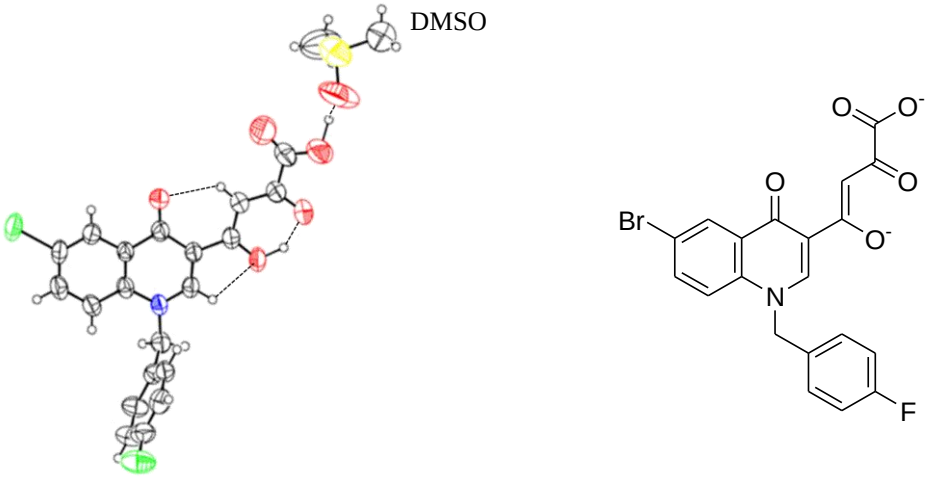

Figure 1. (Left) Crystal structure of compound **2a** with displacement ellipsoids at the 30% probability level. (Right) Stable conformation of di-anionic compound **2a** obtained using DFT calculations at PCM-PBE0/6-311G(d,p) level.

Based on these physicochemical studies, we have modeled the interaction between quinolone compounds and the DNA-bound form of HIV-1 IN. A structural analysis of the catalytic core domain of HIV-1 IN, Tn5 transposase and PFV IN led us to build a new HIV-1 IN/DNA model taking into account explicit water molecules to complete the octahedral geometry of the two active-site magnesium ions.

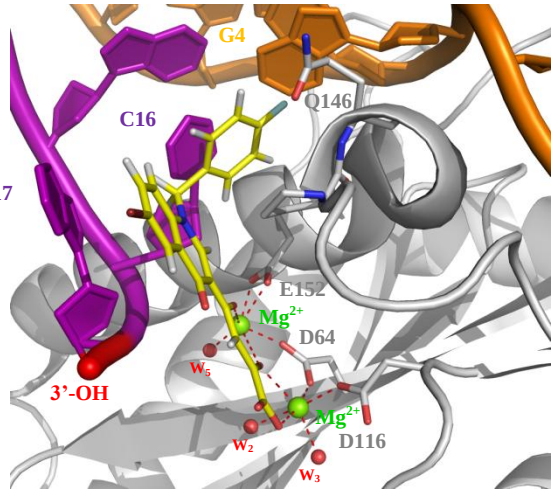

Figure 2. Docking result of compound **2a** into the HIV-1 IN/DNA model.

Our further docking studies including water molecules predicted an interfacial binding mode in agreement with the biological activities we observed in which the DKA moiety chelated the two Mg^{2+} ions by displacing two water molecules from the active site and replaced the 3'-OH extremity of viral DNA (Figure 2). The quinolone ring and p-F-benzyl group were involved in π-stacking interactions with terminal nucleotides in such a way that substituent at C-6 pointed out to the solvent-exposed surface.

Finally, molecular modeling studies led us to propose a mechanism of inhibition for quinolonyl DKA compounds highlighting a two-step binding reaction (Figure 3). In this mechanism, the inhibitor firstly form an octahedral complex by displacing 3'-OH extremity and water molecules originally occupied by the host DNA phosphodiester group. This complex is then tightened due to the replacement of the displaced 3' A17 by the hydrophobic benzyl moiety.

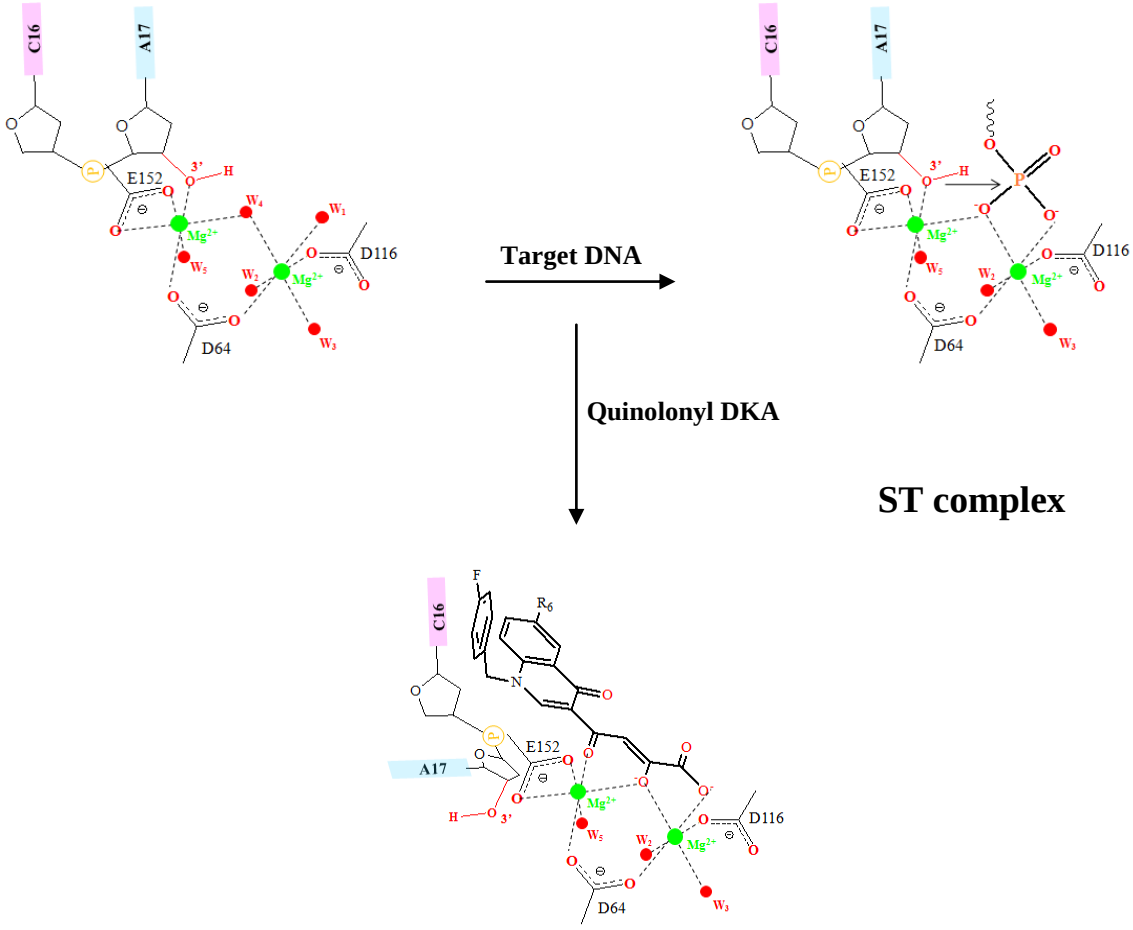

Figure 3. Mechanism of inhibition for quinolonyl DKA compounds.

This work provides new structural insights into the mechanism of action of INSTIs and opens interesting **perspectives** for rational design of new inhibitors.

Pharmacomodulations around the quinolone scaffold could be notably investigated to increase inhibitory potency and biodisponibility of the quinolonyl DKA derivatives (Figure 4). Benzyl group at N-1 involved in π-stacking interaction with DNA substrate could be substituted at various positions by halogen atoms (F, Cl) or replaced by DNA base analogs to obtain quinolone derivatives having higher affinity for the DNA-bound form of HIV-1 IN.

Giving the fact that substituents at C-6 of the quinolone scaffold do not interact with HIV-1 IN/DNA complex, hydrophilic aminoalkyl or hydroxyl groups could be introduced at C-6 to improve solubility of the compounds. The chemically unstable diketoacid moiety known to bind irreversibly plasma proteins could be replaced by a more stable chelating moiety. The replacement by a 4-oxo-3-hydroxyfuran-2(5H)-one moiety could improve pharmacokinetic profile as well as enforce coplanarity of the heteroatoms.

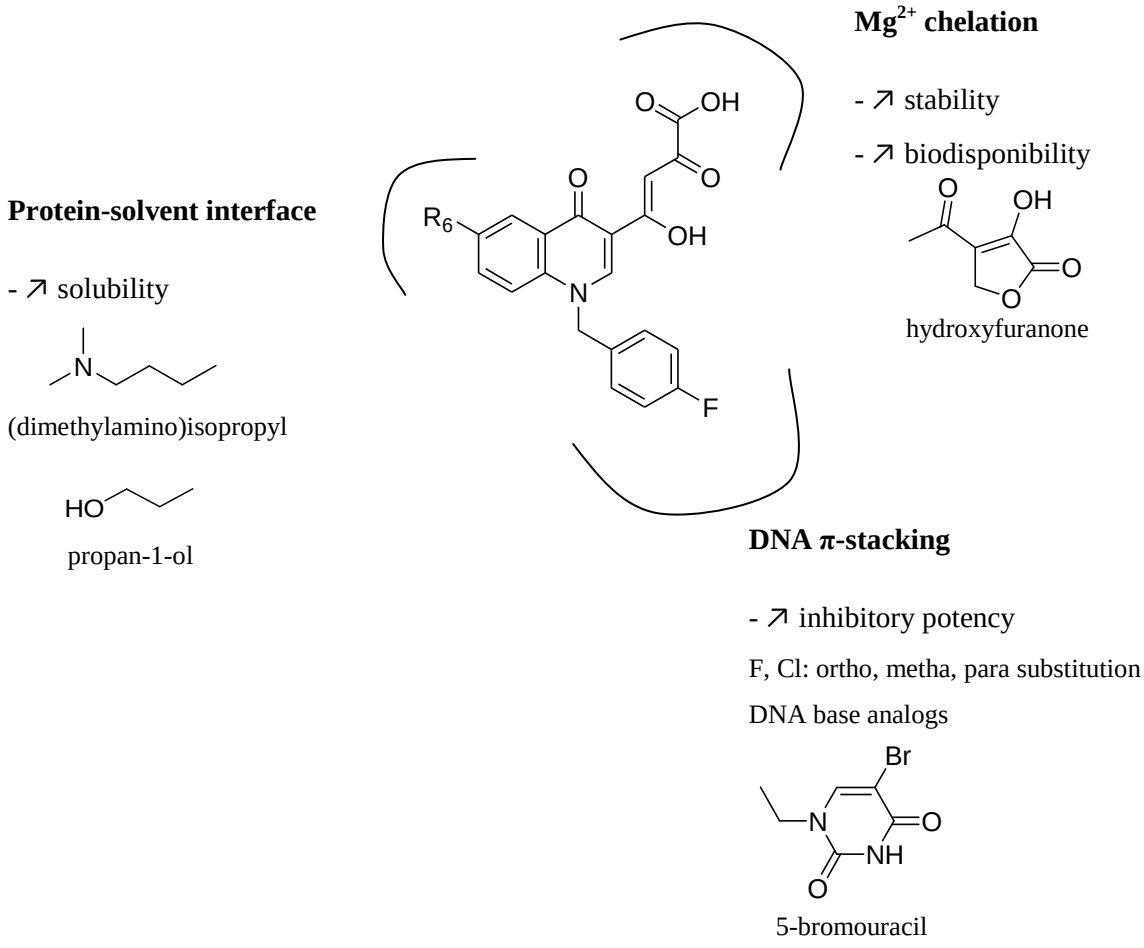

Figure 4. Propositon of pharmacomodulations at 1-, 3- and 6-position of the quinolone scaffold to increase inhibitory potency and biodisponibility of quinolonyl DKA compounds.

The newly build HIV-1 IN/DNA model could be used as a platform to develop new compounds with improved affinity and selectivity. *In silico* screening of large compounds libraries could be first performed to identify new promising structures. Another computational approach should be fragment-based *de novo* design in which a library of fragments are screened, positioned into the enzyme active site and finally linked together to generate a variety of new molecules. In parallel, the high-throughput colorimetric assay could be optimized to screen potential inhibitors identified.

Beside quinolonyl DKA compounds, we disposed of another series of quinolone compounds presenting at C-3 carboxylic moiety. The possibility to substitute at various positions around the quinolone scaffold makes it a privileged structure for obtaining new compounds able to act on another step of the viral replication cycle.

A possible line of research to envisage should be the inhibition of LEDGF/p75-IN interaction.[149-151] This new therapeutic approach could be interesting to overcome the appearance of viral strains resistant to current HIV-1 IN inhibitors. The recent crystal structure of 2-(quinolin-3-yl)acetic acid compound in complex with the LEDGF/p75-binding pocket located within HIV-1 IN CCD highlights the possibility to prevent the binding of host cell cofactor LEDGF/p75 to HIV-1 IN essential for host cell DNA targeting of HIV-1 IN during integration process.[149] In this complex (Figure 5 left), the inhibitor mimics the Ile365 and Asp366 dipeptide located in the LEDGF/p75 integrase binding domain loop by forming equivalent hydrogen bonds between carboxylate moiety and the main chain nitrogens of residues Glu170 and His171 and occupying the hydrophobic region formed by Leu102, Ala128 and Ala129. Interestingly, docking of unsubstituted quinolone compounds within the LEDGF/p75 binding pocket of HIV-1 IN CCD (Figure 5 right) showed that quinolone rings occupy the hydrophobic region pocket whereas diketoacid chain and carboxylate moiety form hydrogen bonds with E170 and H171 residues involved in the recognition process between IN and LEDGF/p75. These results suggest that these scaffolds could constitute a starting point toward the design of new inhibitors of LEDGF/p75-IN interaction. The crystallization of enzyme-ligand complexes would be useful in the optimization of lead compounds. For that purpose, further optimization of the purification of the HIV-1 IN CCD produced during our work could be investigated.

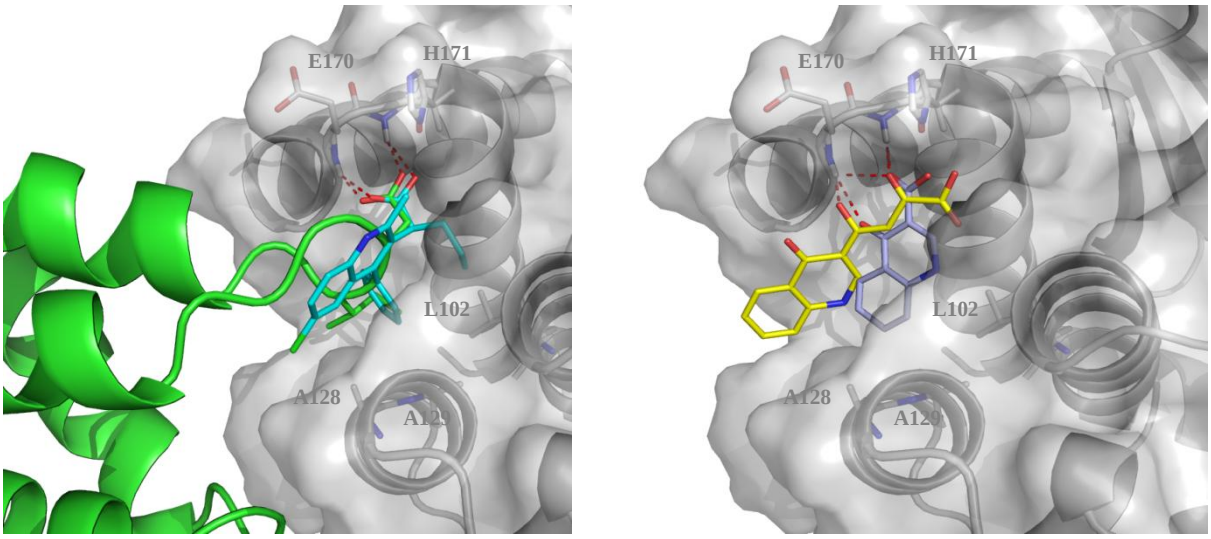

Figure 5. (Left) Cartoon representation of the integrase core dimer (grey) with the soaked 2-(quinolin-3-yl)acetic acid compound[149] (cyan stick) superimposed with the LEDGF/p75-IN complex structure (PDB code 2B4J)[114] revealing mimicry of the protein-protein interaction by the inhibitor. LEDGF/p75 protein is shown as green cartoon. (Right) Docking results of unsubstituted quinolonyl diketoacid (yellow stick) and 3-carboxylic acid quinolone (light blue stick) compound within the LEDGF/p75 binding pocket of the IN-core (PDB code 2B4J).[114]

Another interesting strategy would be the design of dual inhibitors of HIV-1 IN and RT enzyme.[166-168] This novel and attractive therapeutic way could alleviate the major issues occurring during combination therapy such as toxicity and quick emergence of drug resistance. RT enzyme catalyzes reverse transcription of viral RNA into viral DNA using RNA/DNA dependent polymerase and Rnase H activities. RT RnaseH domain and HIV-1 IN CCD share similar fold structures with the same DDE triad sequestering divalent metal ions absolutely required for catalytic activity. In this context, the simultaneous inhibition of HIV-1 IN and RT RnaseH activities by metal-chelating compounds appear an interesting approach to design dual inhibitors. Because quinolonyl DKA and 3-carboxylic quinolone compounds possess chelating moiety able to bind two divalent metal ions, these one could be considered as potential lead for the development of novel dual IN/RNaseH inhibitors.

Part V
Experimental section

1 Chemistry

All the reagents and solvents employed were used without further purification. ^{1}H NMR and and ^{13}C NMR spectra were recorded on a Jeol JNM EX-400 spectrometer. Chemical shifts (δ scale) are reported in parts per million (ppm) downfield from tetramethylsilane (TMS) used as an internal standard. Infrared (IR) spectra were recorded to the solid state on a Perkin-Elmer Spectrum 65. Melting points were determined with a TOTOLLI-BUCHI Melting Point B-545 apparatus. Analytical thin-layer chromatography (TLC) was done on Merck silica gel 60 F_{254} plates. Mass spectra were recorded on an 1100 series MSD Trap spectrometer equipped with an electron spray ionization (ESI) source.

Synthesis of 2-aminomethylene intermediates (3a,b). (i) General method. An equimolar mixture of ethylethoxymethyleneacetoacetate (4.6 g, 23 mmol) and appropriate substituted aniline (23 mmole) was stirred at 120°C for 10 min. After cooling, the formed precipitate was filtered and washed with *n*-hexane to obtain pure compound **3a**,**b** used in the next reaction without further purification.

(ii) 2-[[(4-bromophenyl)amino]methylene]-3-oxobutanoic acid ethyl ester (3a): White solid, yield: 62 %, mp: 102°C. ^{1}H NMR ($CDCl_3$, 400 MHz): δ 1.34 (t, 3H, CH_2CH_3), 1.41 (t, 3H, CH_2CH_3), 2.47 (s, 3H, CH_3), 2.54 (s, 3H, CH_3), 4.26 (q, 2H, CH_2CH_3), 4.31 (q, 2H, CH_2CH_3), 7.05 (d, 2H, J = 8.8 Hz, benzene H), 7.49 (d, 2H, J = 8.8 Hz, benzene H), 8.43 (d, 1H, J = 13.7 Hz, C=CH), 12.71 (d, 1H, J = 13.5 Hz, NH).

(iii) 2-[[(4-phenol)amino]methylene]-3-oxobutanoic acid ethyl ester (3b): Yellow solid, yield: 55 %, mp: 113°C. ^{1}H NMR (DMSO-d_6, 400 MHz): δ 1.22 (t, 3H, CH_2CH_3), 2.36 (s, 3H, CH_3), 2.54 (s, 3H, CH_3), 4.10 (q, 2H, CH_2CH_3), 6.76 (d, 2H, J= 8.8 Hz, benzene H), 7.18 (d, 2H, J = 8.8 Hz, benzene H), 8.29 (d, 1H, J= 13.7 Hz, C=CH), 9.54 (s, 1H, OH), 12.54 (d, 1H, J = 13.7 Hz, NH).

Synthesis of 3-Acetyl-4(1*H*)-quinolinones intermediates (4a,b). (i) General method. 4.2 g of appropriate intermediates **3a**,**b** (17 mmol) was added portionwise to 200 ml of boiling diphenyl ether previously heated at 250°C. The solution was kept at 250°C for 1h30. After cooling, the formed precipitate was collected. The crude product was purified by chromatography on silica gel column (EtOH/CH_2Cl_2 as eluant) to provide pure derivative **4a**,**b**.

(ii) 3-acetyl-6-bromo-4(1H)-quinolinone (4a): Brown solid, yield: 74 %, mp: > 250°C. ^{1}H NMR (DMSO-d_6, 400 MHz): δ 2.58 (s, 1H, CH_3), 7.57 (d, 1H, $J_{8,7}$ = 8.7 Hz, C_8-H

quinolinone), 7.84 (dd, 1H, $J_{7,5}$ = 2.6 Hz, $J_{7,8}$ = 8.7 Hz, C_7-H quinolinone), 8.26 (d, 1H, $J_{5,7}$ = 2.6 Hz, C_5-H quinolinone), 8.52 (s, 1H, C_2-H quinolinone).

(iii) 3-acetyl-6-hydroxy-4(1H)-quinolinone (4b): Brown solid, yield: 46 %, mp: > 250°C. ^{1}H NMR (DMSO-d_6, 400 MHz): δ 2.56 (s, 1H, CH_3), 7.15 (dd, 1H, $J_{7,5}$ = 2.6 Hz, $J_{7,8}$ = 8.7 Hz, C_7-H quinolinone), 7.46 (d, 1H, $J_{8,7}$ = 8.7 Hz, C_8-H quinolinone), 7.51 (d, 1H, $J_{5,7}$ = 2.6 Hz, C_5-H quinolinone), 8.37 (s, 1H, C_2-H quinolinone), 9.91 (bs, 1H, OH).

Synthesis of 3-Acetyl-1-(4-fluorophenyl)methyl-4(1*H*)-quinolinones (**5a,b**). **(i) General method.** 4-Fluorophenylmethyl bromide (1.7 g, 9 mmol) and anhydrous K_2CO_3 (1.3 g, 9 mmol) was added to a mixture of appropriate intermediates **4a,b** in dry DMF (30 ml). The resulting suspension was stirred at 100°C for 5 h. After the mixture was cooled, water (50 ml) was added and the precipitate was filtered, washed with petroleum ether and purified by chromatography on silica gel column (AcOEt/petroleum ether 4/6 and then AcOEt as eluant).

(ii) 3-acetyl-1-((4-fluorophenyl)methyl)-6-bromo-4(1H) quinolinone (5a): Brown solid, yield: 85 %, mp: 203°C. ^{1}H NMR ($CDCl_3$, 400 MHz): δ 2.80 (s, 3H, CH_3), 5.36 (s, 2H, CH_2), 7.05-7.12 (m, 4H, Ar-H), 7.2 (d, 1H, $J_{8,7}$ = 9.4 Hz, C_8-H quinolinone), 7.64 (dd, 1H, $J_{7,5}$ = 3 Hz, $J_{7,8}$ = 9.4 Hz, C_7-H quinolinone), 8.61 (s, 1H, C_2-H quinolinone), 8.65 (d, 1H, $J_{5,7}$= 3 Hz, C_5-H quinolinone).

(iii) 3-acetyl-1-((4-fluorophenyl)methyl)-6-(4-fluorobenzyloxy)-4(1H) quinolinone (5b): Yellow solid, yield: 73 %, mp: 219°C. ^{1}H NMR (DMSO-d_6, 400 MHz): δ 2.61 (s, 3H, CH_3), 5.16 (s, 2H, CH_2), 5.62 (s, 2H, CH_2), 7.1-7.3 (m, 6H, Ar-H), 7.35 (dd, 1H, $J_{7,5}$ = 3 Hz, $J_{7,8}$ = 9.4 Hz, C_7-H quinolinone), 7.44-7.52 (m, 2H, Ar-H), 7.61 (d, 1H, $J_{8,7}$ = 9.4 Hz, C_8-H quinolinone), 8.65 (d, 1H, $J_{5,7}$= 3 Hz, C_5-H quinolinone), 8.78 (s, 1H, C_2-H quinolinone).

Synthesis of (E)-ethyl [3-acetyl-1-(4-fluorophenyl)methyl-4(1H)-quinolinon-6-yl] acrylate (5c): 3-acetyl-6-bromo-1-((4-fluorophenyl)methyl)-4(*1H*)-quinolinone (**5a**) (0.450 g, 1.2 mmol) was added to a mixture of acrylic acid ethyl ester (0.202 g, 2.4 mmol), $Pd(OAc)_2$ (0.013 g, 0.06mmol), PPh_3 (0.061 g, 0.24 mmol) and NEt_3 (0.134 g, 1.2 mmol) in 3 ml of DMF. The reaction mixture was stirred under argon for 48 h at 80°C. The reaction was cooled to room temperature and extracted with ethyl acetate. The organic phases were washed four times with brine (10 ml) and dried with $MgSO_4$. Upon removal of the solvent, the residue obtained was purified by chromatography on silica gel column (ACOEt/petroleum ether 3/7 and then 1/1 as eluant) to afford pure derivative **5c**. Yellow solid, yield: 62 %, mp: 220°C. ^{1}H NMR ($CDCl_3$, 400 MHz): δ 1.33 (t, 3H, CH_2CH_3), 2.82 (s, 3H, CH_3), 4.26 (q, 2H, CH_3CH_2), 5.38 (s, 2H, CH_2), 6.51 (d, 1H, J_{trans}= 16 Hz, CH=CH), 7.02-7.18 (m, 4H, Ar-H), 7.32 (d, 1H, $J_{8,7}$ = 8.9 Hz,

C_8-H quinolinone), 7.71 (dd, 1H, $J_{7,5}$= 1 Hz, $J_{7,8}$= 8.9 Hz, C_7-H quinolinone), 7.73 (d, 1H, J_{trans}= 16 Hz, CH=CH), 8.59 (s, 1H, C_2-H quinolinone), 8.65 (d, 1H, $J_{5,7}$= 1 Hz, C_5-H quinolinone).

Synthesis of diketo esters derivatives (1a-c). (i) General method. Freshly prepared sodium ethoxide (0.272 g, 2 mmol) was added to a well stirred mixture of diethyl oxalate (0.584 g, 4 mmol) and appropriate acetyl derivative **5a-c** (2 mmol) in anhydrous THF (2 ml) under nitrogen atmosphere. The reaction mixture was stirred at room temperature for 20h. *n*-hexane (70 ml) was added and the formed precipitate was filtered, washed with *n*-hexane and stirred for 30 min in 1N HCl (70 ml). The solid was filtered off and washed with *n*-hexane. Residual water was removed by azeotropic distillation using acetonitrile to provide pure diketo esters **1a-c**.

(ii) Ethyl [6-bromo-1-(4-fluorophenylmethyl)-4(1H)-quinolinon-3-yl]-4-hydroxy-2-oxo-3-butenoate (1a): Yellow solid, yield: 83 %, mp: 105°C. IR υ_{max} (KBr/cm^{-1}): 1750 (C=O carboxylic ester), 1645 (C=O quinolinone), 1594 (C=O + C=C keto-enol). ^{1}H NMR ($CDCl_3$, 400 MHz): δ 1.42 (t, 3H, CH_3), 4.40 (q, 2H, $CH_3C\mathit{H}_2$), 5.40 (s, 2H, CH_2), 7.07-7.18 (m, 4H,Ar-H), 7.24 (d, 1H, $J_{8,7}$ = 8.9 HZ, C_8-H quinolinone), 7.66 (dd, 1H, $J_{7,5}$ = 3 Hz, $J_{7,8}$ = 8.9 Hz, C_7-H quinolinone), 8.08 (s, 1H, C_3-H butenoate), 8.66 (d, 1H, $J_{5,7}$ = 3 Hz, C_5-H quinolinone), 8.72 (s, 1H, C_2-H quinolinone). ^{13}C NMR (DMSO-d_6, 400 MHz): δ 14.81 (CH_3), 56.04 (N-CH_2), 62.82 (CH_2), 102.01 (CH), 114.87 (C), 116.24 (d, J = 22.0 Hz, 2C-ArH), 120.06 (CH), 121.6 (CH), 129.9 (d, J = 8.6 Hz, 2C-ArH), 130.81 (C), 132.04 (C), 136.51 (C), 138.12 (CH), 150.09 (C), 162.40 (C), 162,51 (d, J = 247.28 Hz, C-ArH), 162.74 (C), 169.58 (C), 174.02 (C), 188.01 (C). LC-MS: $(M+H)^+$ 474.2, 476.0

(iii) 4-[6-(4-fluorobenzyloxy)-1-(4-fluorophenyl)methyl-4(1H)-quinolinon-3-yl]-2-hydroxy-4-oxo-2-butenoic acid ethyl ester (1b): Yellow solid, yield: 82 %, mp: 160°C. IR υ_{max} (KBr/cm^{-1}): 1743 (C=O carboxylic ester), 1634 (C=O quinolinone), 1605 (C=O + C=C keto-enol). ^{1}H NMR (DMSO-d_6, 400 MHz): δ 1.28 (t, 3H, $CH_2\mathit{CH}_3$), 4.27 (q, 2H, CH_2CH_3), 5.17 (s, 2H, CH_2), 5.72 (s, 2H, CH_2), 7.09-7.34 (m, 6H, Ar-H), 7.39 (dd, 1H, $J_{7,5}$ = 3 Hz, $J_{7,8}$ = 9.4 Hz, C_7-H quinolinone), 7.43-7.53 (m, 2H, Ar-H), 7.66 (d, 1H, $J_{8,7}$ = 9.4 Hz, C_8-H quinolinone), 7.79 (d, 1H, $J_{5,7}$= 3 Hz, C_5-H quinolinone), 8.00 (s, 1H, C_3-H butenoate), 9.04 (s, 1H, C_2-H quinolinone). ^{13}C NMR ($CDCl_3$, 400 MHz): 14.26 (CH_3), 57.59 (N-CH_2), 62.42 (CH_2), 69.91 (O-CH_2), 102.47 (CH), 108.58 (CH), 114.27 (C), 115.72 (d, J = 22.0 Hz, 2C-ArH), 116.65 (d, J = 22.0 Hz, 2C-ArH), 118.71 (CH), 123.68 (CH), 128.12 (d, J = 8.6 Hz, 2C-ArH), 129.66 (d, J = 8.6 Hz, 2C-ArH), 130.55 (C), 131.90 (d, J = 2.8 Hz, C-ArH), 133.28 (C), 147.50 (CH), 156.77 (C), 162.62 (C), 162.73 (d, J = 247.28 Hz, C-ArH), 162.81 (d, J = 248.24 Hz, C-ArH), 169.21 (C), 174.83 (C), 188.09 (C). LC-MS: $(M+H)^+$ 520.0.

(iv) 4-[6-((E)-3-ethoxy-3-oxoprop-1-enyl)-1-(4-fluorophenyl)methyl-4(1H)-quinolinon-3-yl]-2-hydroxy-4-oxo-2-butenoic acid ethyl ester (1c): Yellow solid, yield: 79 %, mp: 146°C. IR υ_{max} (KBr/cm^{-1}): 1733 (C=O carboxylic ester), 1702 (C=O acrylic ester), 1644 (C=O quinolinone), 1600 (C=O + C=C keto-enol). ^{1}H NMR ($CDCl_3$, 400 MHz): δ 1.33 (t, 3H, $CH_2\mathit{CH_3}$), 1.41 (t, 3H, $CH_2\mathit{CH_3}$), 4.26 (q, 2H, $\mathit{CH_2}CH_3$), 4.40 (q, 2H, $\mathit{CH_2}CH_3$), 5.42 (s, 2H, CH_2), 6.52 (d, 1H, J_{trans}= 16 Hz, CH=CH), 7.04-7.20 (m, 4H, Ar-H), 7.36 (d, 1H, $J_{8,7}$ = 8.7 Hz, C_8-H quinolinone), 7.69-7.76 (m, 2H, CH=CH and C_7-H quinolinone), 8.11 (s, 1H, C_3-H butenoate), 8.67 (d, 1H, $J_{5,7}$= 2 Hz, C_5-H quinolinone), 8.72 (s, 1H, C_2-H quinolinone). ^{13}C NMR ($CDCl_3$, 400 MHz): 14.24 (CH_3), 14.37 (CH_3), 57.46 (N-CH_2), 60.87 (CH_2), 62.51 (CH_2), 102.51 (CH), 115.80 (C), 116.78 (d, J = 22.0 Hz, 2C-ArH), 117.54 (CH), 120.37 (CH), 127.93 (CH), 128.10 (d, J = 8.6 Hz, 2C-ArH), 129.29 (C), 129.39 (d, J = 2.8 Hz, C-ArH), 131.86 (C), 132.23 (CH), 139.62 (C), 142.36 (CH), 148.68 (CH), 162.45 (C), 162.90 (d, J = 249.20 Hz, C-ArH), 166.58 (C), 169.58 (C), 174.96 (C), 187.55 (C). LC-MS: $(M+H)^+$ 494.0.

Synthesis diketo acids derivatives (**2a-c**)**. (i) General method.** A mixture of the appropriate ester **1a-c** (1.3 mmol) and 1N NaOH (12 ml) in THF/methanol (1:1, 15 ml) was stirred at room temperature for 3h under nitrogen atmosphere, poured onto crushed ice and treated with 1N HCl to reach pH 2. The formed precipitate was filtered off and successively washed with water, ethanol and petroleum ether to give pure acids **2a-c**.

(ii) [6-bromo-1-(4-fluorophenylméthyl)-4(1H)-quinolinon-3-yl]-4-hydroxy-2-oxo-3-butenoïc acid (2a): Yellow solid, yield: 73 %, mp: 192°C. IR υ_{max} (KBr/cm^{-1}): 1708 (C=O carboxylic acid), 1638 (C=O quinolinone), 1595 (C=O + C=C keto-enol). ^{1}H NMR (DMSO-d_6, 400 MHz): δ 5.72 (s, 2H, CH_2), 7.15-7.18 (m, 2H, Ar-H), 7.29-7.31 (m, 2H, Ar-H), 7.65 (d, 1H, $J_{8,7}$ = 8.9 HZ, C_8-H quinolinone), 7.88 (dd, 1H, $J_{7,5}$ = 3 Hz, $J_{7,8}$ = 8.9 Hz, C_7-H quinolinone), 8.34 (s, 1H, butenoate C_3-H), 8.99 (d, 1H, $J_{5,7}$ = 3 Hz, C_5-H quinolinone), 9.09 (s, 1H, C_2-H quinolinone). ^{13}C NMR (DMSO-d_6, 400 MHz): δ 56.02 (N-CH_2), 102.04 (CH), 114.77 (C), 116.34 (d, J = 21.09 Hz, 2C-ArH), 119.26 (CH), 121.23 (CH), 129.28 (C), 129.41 (d, J = 7.67 Hz, 2C-ArH), 130.31 (C), 132.10 (C), 136.09 (C), 138.28 (CH), 150.09 (C), 162.24 (d, J = 247 Hz, C-ArH), 164.26 (C), 173.57 (C). LC-MS: $(M+H)^+$ 446.1, 448.0.

(iii) 4-[6-(4-fluorobenzyloxy)-1-(4-fluorophenyl)methyl-4(1H)-quinolinon-3-yl]-2-hydroxy-4-oxo-2-butenoic acid (2b): Yellow solid, yield: 79 %, mp: 194°C. IR υ_{max} (KBr/cm^{-1}): 1731 (C=O carboxylic acid), 1718 (C=O quinolinone), 1612 (C=O + C=C keto-enol). ^{1}H NMR (DMSO-d_6, 400 MHz): δ 5.17 (s, 2H, CH_2), 5.71 (s, 2H, CH_2), 7.09-7.34 (m, 6H, Ar-H), 7.39 (m, 1H, C_7-H quinolinone), 7.43-7.53 (m, 2H, Ar-H), 7.68 (d, 1H, $J_{8,7}$ = 9.4 Hz, C_8-H

quinolinone), 7.77 (d, 1H, $J_{5,7}$= 3 Hz, C_5-H quinolinone), 7.99 (s, 1H, C_3-H butenoate), 9.03 (s, 1H, C_2-H quinolinone). ^{13}C NMR (DMSO-d_6, 400 MHz): 56.13 (N-CH_2), 69.47 (O-CH_2), 102.10 (CH), 108.93 (CH), 113.35 (C), 115.86 (d, J = 22.0 Hz, 2C-ArH), 116.32 (d, J = 21.0 Hz, 2C-ArH), 120.64 (CH), 123.11 (CH), 129.39 (d, J = 7.6 Hz, 2C-ArH), 130.31 (C), 130.57 (d, J = 8.6 Hz, 2C-ArH), 132.35 (C), 133.30 (d, J = 1.9 Hz, C-ArH), 133.56 (C), 148.96 (CH), 156.61 (C), 162.22 (d, J = 244.41 Hz, C-ArH), 162.36 (d, J = 243.45 Hz, C-ArH), 164.22 (C), 174.33 (C). LC-MS: $(M+H)^+$ 492.0.

(iv) 4-[6-((E)-3-hydroxy-3-oxoprop-1-enyl)-1-(4-fluorophenyl)methyl-4(1H)-quinolinon-3-yl]-2-hydroxy-4-oxo-2-butenoic acid (2c): Yellow solid, yield: 70 %, mp: 163°C. IR υ_{max} (KBr/cm^{-1}): 1703 (C=O carboxylic acid), 1698 (C=O acrylic acid), 1636 (C=O quinolinone), 1599 (C=O + C=C keto-enol). ^{1}H NMR (DMSO-d_6, 400 MHz): δ 5.75 (s, 2H, CH_2), 6.58 (d, 1H, J_{trans}= 16 Hz, CH=CH), 7.05-7.42 (m, 4H, Ar-H), 7.61-7.78 (m, 2H, CH=CH and C_8-H quinolinone), 7.96 (s, 1H, C_3-H butenoate), 8.05 (m, 1H, C_7-H quinolinone), 8.43 (d, 1H, $J_{5,7}$= 2 Hz, C_5-H quinolinone), 9.08 (s, 1H, C_2-H quinolinone). ^{13}C NMR (DMSO-d_6, 400 MHz): 56.01 (N-CH_2), 102.17 (CH), 116.35 (d, J = 22.0 Hz, 2C-ArH), 119.46 (CH), 121.19 (CH), 127.61 (CH), 129.41 (d, J = 8.6 Hz, 2C-ArH), 132.06 (C), 132.28 (d, J = 1.9 Hz, C-ArH), 140.07 (C), 142.85 (CH), 150.01 (C), 150.42 (CH), 162.32 (d, J = 245.37 Hz, C-ArH), 162.85 (C), 164.19 (C), 167.87 (C), 174.65 (C). LC-MS: $(M+H)^+$ 438.0.

2 Biology

2.1. Enzyme production

Transformation of *E. coli* BL21(DE3)pLysS chemically competent cells. Plasmids encoding recombinant enzymes were introduced into cells in a heat shock step (10 sec at 42°C). Then the bacteria were grown up in a small culture (200 µl LB medium for 1 h at 37°c). The bacteria were spread on an LB-agar plate containing ampicilline and incubated overnight at 37°C to allow growing of single bacteria colonies which contained the antibiotic resistance gene. Three single colonies were in turn amplified overnight at 37°C in a 5 mL pre-culture (LB medium) containing ampicilline (100 µg/ml).

Expression. (i) General method. Preculture was reseeded and further growned in the same LB/ampicilline medium at 37 °C. Once optical density (OD) was reached, fusion protein expression was induced in bacterial culture by the addition of 1 mM IPTG. Cultures were incubated for 3 h at 37 °C, after which cells were centrifuged at 4°C (30 min at 4000 rpm).

The cell pellet was resuspended in ice-cold buffer and lysed. After centrifugation at 4°C (40 min at 10 000 rpm), the supernatant obtained was finally filtered (0.45 µm).

(ii) His-tagged wild-type HIV-1 IN: IPTG induction was performed at OD 1.0. Cell pellet was resuspended in 25 ml buffer A containing 20 mM Tris-HCl (pH 8), 1 M NaCl, 4 mM β-mercaptoethanol and lysed by French Press (1200 bars).

(iii) His-tagged HIV-1 IN CCD (F185K): IPTG induction was performed at OD 0.7. Cell pellet was resuspended in 10 ml buffer A containing 25 mM HEPES (pH 7.5), 0.5 M NaCl, 2 mM β-mercaptoethanol, 5 mM Imidazole and lysed by sonication (10 cycles of 30 seconds "ON" and 30 seconds "OFF").

Western blot. Proteins separated by SDS/PAGE were electrotransferred to Hybond-C extra nitrocellulose membrane (Amersham) in PBS buffer (Phosphate Buffered Saline) for 1h at constant voltage (80 volts). The membrane was then incubated overnight at 4°C in TBST buffer (Tris Buffered Saline, 0.1 % Tween 20) containing 1 % milk (TBSTM). Anti-integrase antibodies diluted to 1:1000 in TBSTM were added and incubated for 2 h at room temperature under agitation. Anti-rabbit secondary antibodies (horseradish peroxidase conjugated) diluted to 1:3000 in TBSTM were added and incubated for 1 h at room temperature under agitation. Between each step, the membrane was extensively washed (three times) with TBST. Finally, antibodies revelation was performed with ECL plus Western blotting *detection system* (GE Healthcare).

2.2. Enzyme purification

His-tagged wild-type HIV-1 IN. Ni-NTA agarose beads (Pharmacia) was preequilibrated with buffer A and incubated overnight at 4°C with the supernatant of crude *E. coli*. The beads were washed three times with 45 ml of buffer A and 45 ml of buffer A with 80 mM imidazole. His-tagged IN was then eluted with buffer A supplemented with 1M imidazole and 50 µM $ZnSO_4$ to favour the folding structure of zinc-finger. Finally, a dialysis was performed overnight at 4°C against 20 mM TrisHCl (pH 8), 1 M NaCl, 4 mM β-mercaptoethanol, and 10% (v/v) glycerol. Fractions were aliquoted and rapidly frozen at -80 °C.

His-tagged HIV-1 IN CCD (F185 K). (i) Nickel affinity chromatography: Ni-NTA sepharose (GE Healthcare) column was preequilibrated with buffer A and loaded with the supernatant of crude *E. coli* at a flow rate of 1 ml/min. Washing buffer A containing 60 mM imidazole was applied at a flow rate of 3 ml/min and linear imidazole gradient (from 60 mM to 1 M) was applied at a flow rate of 1ml/min over a total volume of 100 ml.

(ii) Size exclusion chromatography: Protein sample obtained from affinity chromatography was dialyzed overnight at 4°C against 25 mM HEPES (pH 7.5), 0.5 M NaCl, 1 mM DTT, 1 mM EDTA and 10% (v/v) glycerol. Superdex 75 column (GE Healthcare) was preequilibrated with elution buffer containing 25 mM HEPES (pH 7.5), 0.5 M NaCl, 1mM DTT and 1 mM EDTA. 100 µl of protein sample was injected onto the column. Elution buffer was then applied at a flow rate of 1 ml/min to elute proteins.

(iii) Ion exchange chromatography. (A) Anion exchange chromatography: Protein sample obtained from affinity chromatography was dialyzed overnight at 4°C against buffer A containing 25 mM CHES (pH 9.5), 0.25 M NaCl, 1 mM DTT, 1 mM EDTA and 10 % (v/v) glycerol. MonoQ column (GE Healthcare) was preequilibrated with buffer A and loaded with protein sample at a flow rate of 0.5 ml/min. Linear gradient of NaCl from 25 mM to 1 M was applied at a flow rate of 1 ml/min over a total volume of 100 ml. **(B) Cation exchange chromatography:** Protein sample obtained from affinity chromatography was dialyzed overnight at 4°C against buffer A containing 20 mM NaH_2PO_4 (pH 6), 0.25 M NaCl, 1 M urea, 1 mM DTT, 1 mM EDTA and 10 % (v/v) glycerol. SP column (GE Healthcare) was preequilibrated with buffer A and loaded with protein sample at a flow rate of 0.5 ml/min. Linear gradient of NaCl from 25 mM to 1 M was applied at a flow rate of 1 ml/min over a total volume of 100 ml.

2.3. His-tag cleavage

Thrombin (50 NIH unit) was added to 1 mg of His-tagged HIV-1 IN CCD and the solution incubated for 20, 40 and 60 min at 28°C. Cleaved enzyme was applied at a flow rate of 0.5 ml/min to a column of Ni-NTA sepharose resin (GE Healthcare) equilibrated with buffer A containing 25 mM HEPES (pH 7.5), 0.5 M NaCl, 2 mM β-mercaptoethanol, 5 mM Imidazole. Two washing steps were performed with buffer A containing 20 and 60 mM imidazole. Finally, a linear imidazole gradient (from 60 to 1M imidazole) was applied at a flow rate of 1 ml/min.

2.4. Biological assays

Radioactive gel-based assays. His-tagged wild-type HIV-1 IN or His-tagged HIV-1 IN CCD (F185 K) were incubated with 12.5 nM of the 5'-end ^{32}P-labeled oligonucleotide substrate in a reaction buffer (20 mM HEPES $pH_{7.5}$, 1mM DTT, 10 mM $MgCl_2$, 10% dimethyl sulfoxyde) 1 h at 37°C. For His-tagged HIV-1 IN CCD (F185 K), $MgCl_2$ was replaced by $MnCl_2$ in reaction buffer.

Oligonucleotides were precipitated in a precipitation buffer (3M sodium acetate pH 7, 10 mg/ml glycogen, Tris (10 mM)-EDTA (1mM) buffer pH 7.5), extracted with phenol/chloroform and washed with ethanol. The oligonucleotides were resuspended in 10 µl of 10 mM formamide/EDTA, denatured and separated by electrophoresis on a polyacrylamide/urea gel (16 % acrylamide, 7 M urea). Gels were dried, exposed in a PhosphorImager cassette, analyzed using a Storm mode imager (Amersham Biosciences) and quantified using ImageQuant. The IC_{50} values were determined from a curve (drug concentration versus percent inhibition) fitted on experimental data (Prism software) to obtain the concentration that produced 50 % inhibition.

Colorimetric assay. His-tagged wild-type HIV-1 was incubated with 30 nM biotinylated oligonucleotide substrate, 100 nM digoxigenin-labeled oligonucleotide target in a reaction buffer (20 mM HEPES pH 6.8, 1 mM DTT, 10 mM $MgCl_2$, 10% dimethyl sulfoxyde) 2 h at 37°C. The reaction was stopped by adding 60 µl of solution containing 20 mM Tris-HCl, 400 mM NaCl, 10 mM EDTA and 0.1 mg/ml salmon sperm DNA. The reaction products were transferred into 96-well streptavidin-coated plate first incubated for 1 h with PBSTM buffer (Phosphate Buffered Saline containing 0.05 % tween 20 and 1 % milk) and washed three times with PBST buffer for 5 minutes. The reaction mixture was incubated for 1h at room temperature under low agitation and the wells were washed with a washing buffer (30 mM NaOH, 200 mM NaCl and 1 mM EDTA) for 5 minutes. 100 µl diluted anti-digoxigenin antibodies (1:2000) were added to the wells and incubated at 37°C for 3h30. The wells were washed five times with PBST buffer containing 0.1 % HSA (human serum albumin) and 200 µl ABTS were added to give green solution quantified using a microplate reader at 405 nm.

Cell-based assays. (i) Cells and viruses: The following reagents were obtained through the AIDS Research and Reference Reagent Program, Division of AIDS, NIAID, NIH: TZM-bl from Dr. John C. Kappes, Dr. Xiaoyun Wu and Tranzyme Inc. TZM-bl cells were grown at 37°C, 5% CO_2 in DMEM medium (Invitrogen) supplemented with 5% (v/v) heat-inactivated bovine serum, 50 U of penicilin/ml and 50 µg of streptomycin/ml (Invitrogen). Exponentially growing cells were trypsinised, centrifuged and split twice weekly. The HIV strain used in this study is HIV-1 NL4-3 derived from the infectious molecular clone pNL4-3. HIV-1 stocks were stored as cell-free supernatants at -80°C.

(ii) Antiviral activity: Antiviral activity of the compounds was evaluated using the TZM-bl cell line.[38] This TZM-bl cell line uses a Tat protein-induced transactivation of the HIV-1 LTR promoter driving the expression of the β-galactosidase gene. In brief, exponentially growing cells were plated at 5000 cells/well in flat-bottom 96-well microtiter plates.

After a 48 h incubation, the medium was removed and replaced by 100 µl of medium containing the quinolinone derivatives at concentrations ranging from 0.00128 to 4 µM. Four hours after drug treatment, cells were infected with equal amount of cell-free virus (NL4-3 strain), corresponding to 100 ng of HIV p24 antigen. Forty-eight hours post-infection, the medium was removed and cells were lysed in PBS containing 0.1% NP-40 and 5 mM $MgCl_2$. β-galactosidase activity was measured using chlorophenol red β-D-galactopyranoside (Roche) assays. The 50% effective concentration (EC_{50}) was calculated from each dose response curve using Prism software.

(iii) Cytotoxicity: Flat bottom 96-well plates were filled with 50 µl of complete medium containing 5000 TZM-bl cells. Two hours later, 50 µl of medium containing an appropriate dilution of the test compounds (from 100 to 0.032 µM) was added. Cells and compounds were incubated at 37°C in growth medium for 3 days. Cell viability was determined by a colorimetric assay based on the cleavage of the tetrazolium salt WST-1 (Roche) by mitochondrial dehydrogenases in viable cells. Absorbance of converted dye was measured in an ELISA plate reader at the wavelength of 570 nm. The cytotoxicity of the compounds was calculated as the reduction percentage of viable cells observed in the drug-free control cell culture. The drug concentration required to reduce cell viability by 50% was named CC_{50}.

3 Physicochemistry

3.1. X-ray crystallography

Crystals of compound **2** were obtained by slow evaporation of an acetone/DMSO solution at 4°C. X-ray intensities were collected on a graphite-monochromated CAD-4 Enraf-Nonius diffractometer with Cu Kα radiation (λ = 1.54178Å) using θ-2θ scan technique. The structure was solved using PLATON.[155] Non-hydrogen atoms were refined anisotropically while hydrogen atoms were calculated geometrically (except H25 and H22 found by Fourier difference and fixed at this position). The discrepancy index R is equal to 6,6%. Structure coordinates have been deposited in the Cambridge structural database (CCDC730039).

Formula		C22 H19 BR F N O6 S	
Formula Weight		524.35	
Crystal System		Monoclinic	
Space group		P21/c	(No. 14)
a, b, c [Angstrom]	5.105(3)	26.98(1)	16.093(5)
alpha, beta, gamma	90	97.705(8)	90
V [Ang**3]		2196.5(17)	

Z	4
D(calc) [g/cm**3]	1.586
Mu(CuKa) [/mm]	3.871
F(000)	1064
Crystal Size [mm]	0.01 x 0.07 x 0.13
Data Collection	
Temperature (K)	293
Radiation [Angstrom]	CuKa 1.54178
Theta Min-Max	3.2, 75.0
Dataset	-6: 0 ; 0: 33 ; -19: 20
Tot., Uniq. Data, R(int)	5047, 4535, 0.023
Observed data [I > 2.0 sigma(I)]	2743
Refinement	
Nref, Npar	4535, 291
R, wR2, S	0.0659, 0.2036, 1.03
Max. and Av. Shift/Error	0.04, 0.00
Min. and Max. Resd. Dens. [e/Ang^3]	-0.74, 0.75

3.2. Solution-state study

Experiment. (i) UV-visible absorption: UV-visible spectra were recorded on an UVIKON 930 UV spectrophotometer at room temperature. All measurements were carried out with a final concentration of compounds of 5 x 10^{-5} M. Compound **2** was solubilized in methanol/water mixture (80:20) and ADKA in water solution. The pH was adjusted by adding non-absorbing buffer solutions to a final concentration of 0.1 M. Citrate and tris(hydroxy-methyl)amino methane (Tris) buffers were used at pH 1.4 and 10.0, respectively. An aqueous solution of magnesium chloride hexahydrate ($MgCl_2.6H_2O$) at 1x10^{-4} M was prepared and added to compounds in equal volume.

(ii) Attenuated total reflectance: ATR spectra were recored on a Perkin-Elmer Spectrum 65 by connecting horizontal ATR (HATR) units using ZnSe crystal. ADKA was solubilized in aqueous solution buffered with 0.1 M Tris at pH 10 at a final concentration of 0.2 M. An aqueous solution of magnesium chloride hexahydrate ($MgCl_2.6H_2O$) at 0.4 M was prepared and added to the compound in equal volume.

Theory. To investigate the structure and UV-visible spectroscopic properties of DKA derivative, we respectively selected DFT and time-dependent DFT (TD-DFT), combined to the PBE0 global hybrid, that includes 25% of exact exchange.[169,170]

We have followed a well-described and robust three-step strategy[171]: (1) the optimization of the ground-state structure; (2) the analytic determination of the vibrational spectrum to confirm the absence of imaginary frequencies; (3) the evaluation of the low-lying electronic excited-states. For all calculations, the self-consistent field convergence criteria have been tightened to, at least, 10^{-8} a.u. All the computations have been performed with the GAUSSIAN 03 suite of programs[172], using default parameters and thresholds. The ground-state structures have been optimised with the 6-311G(d,p) basis set. The vibrational frequencies have been evaluated by the analytical determination of the Hessian matrix using the same level of theory whereas, for each molecule the first 15 vertical singlet excited-states have been computed by TD-PBE0. These UV/Vis spectra simulations have been performed with the doubly-polarised 6-311+G(2d,p) basis set. The partial atomic charges have been computed with the Merz-Kollman approximation (so-called ESP charges) with the same methodology as the one used for TD-DFT. In the following, the relative energies reported are Gibbs free energies (G) computed with the PCM-PBE0/6-311G(d,p) method, corrected by the total (internal) energies computed at the PCM-PBE0/6-311+G(2d,p) level of approximation. The bulk solvent effects are evaluated at each stage by means of the Conducting Polarisable Continuum Model (C-PCM)[173], which divides the model into a solute part (QDKA) lying inside a cavity surrounded by the solvent continuum. As we target biological applications, water has been selected as medium. To build the cavity, we have used the UAKS radii especially optimised for the PBE0 functional. The TD-DFT calculations have been performed using the non-equilibrium procedure designed for the study of absorption processes[174].

3.3. Molecular modeling

Model building. The HIV-1 IN/DNA model in its INSTI-inhibited form was initiated by overlaying the structures of HIV-1 IN CCD (1BL3C), Tn5 transposome (1MUS) and elvitegravir-bound PFV structure (3L2U) with their Cα positions of active-site residues Asp64, Asp116, and Glu152 (DDE motif). Bases of the 19-mer PFV DNA properly oriented into the HIV-1 IN CCD were mutated in order to correspond to the HIV-1 DNA sequence. Two Mg^{2+} ions were then modeled into the HIV-1 active site based on the two Mn^{2+} ions coordinates from PFV structure and glutamate 152 residue (E152) was reoriented to interact with Mg^{2+} ions. Coordinated water molecules present in both HIV-1 IN CCD and Tn5 transposome crystal structure were then merged into the HIV-1 model to complete the octahedral geometry of the two Mg^{2+} ions.

The slightly resolved active site loop (residues 141-148) was removed and replaced by the equivalent PFV IN loop (residues 210-217), after which residues were mutated to correspond to the HIV-1 IN sequence. To remove bad intramolecular contacts without altering the architecture of the binding site, the resulting model was energy-minimized by 500 steps of steepest descent using CHARMm force field and Generalized Born (GB) model as solvation treatment implemented in Discovery Studio 2.5.[160] Coordinates of model are available upon request to the authors.

Docking. Docking of quinolone compounds into the HIV-1 IN/DNA model was carried out using GOLD (version 1.3.1) Software.[164] All compounds were modelled by considering the stable conformation previously identified by experimental and theoretical studies. The binding region was defined as a 15 Å radius sphere centered on Mg^{2+} ions chelated by E152. An octahedral geometry was imposed on the two Mg^{2+} ions whereas explicit water molecules were allowed to switch on and off and to rotate around their three principal axes. For the 30 genetic algorithm (GA) runs performed, a total of 100 000 genetic operations were carried out on five islands, each containing 100 individuals. The niche size was set to 2, and the value for the selection pressure was set to 1.1. Genetic operator weights for crossover, mutation, and migration were set to 95, 95 and 10, respectively. The scoring function used to rank the docking was Goldscore. Among the 30 poses generated for each compound, the best-docked was principally based on ligand binding position. The parameter used for identifying the best ligand binding position was the two-metal chelating mode of DKA chain with Mg^{2+} ions. IN/DNA/ligand complex obtained by docking studies were minimized using steepest descent method (10 kcal. mol^{-1}. $Å^{-1}$ convergence) followed by conjugate gradient minimization (0.0001 kcal. mol^{-1}. $Å^{-1}$ convergence) imposing the coplanarity of the diketoacid moiety. All complexes were minimized using CHARMm force field and GB model as solvation treatment implemented in Discovery Studio 2.5.[160]

Part VI
Bibliography

(1) Kaposi's sarcoma and Pneumocystis pneumonia among homosexual men--New York City and California. *MMWR Morb Mortal Wkly Rep* **1981,** *30*, 305-308.

(2) Hymes, K. B.; Cheung, T.; Greene, J. B.; Prose, N. S.; Marcus, A.; Ballard, H.; William, D. C.; Laubenstein, L. J. Kaposi's sarcoma in homosexual men-a report of eight cases. *Lancet* **1981,** *2*, 598-600.

(3) Barre-Sinoussi, F.; Chermann, J. C.; Rey, F.; Nugeyre, M. T.; Chamaret, S.; Gruest, J.; Dauguet, C.; Axler-Blin, C.; Vezinet-Brun, F.; Rouzioux, C.; Rozenbaum, W.; Montagnier, L. Isolation of a T-lymphotropic retrovirus from a patient at risk for acquired immune deficiency syndrome (AIDS). *Science* **1983,** *220*, 868-871.

(4) Gallo, R. C.; Sarin, P. S.; Gelmann, E. P.; Robert-Guroff, M.; Richardson, E.; Kalyanaraman, V. S.; Mann, D.; Sidhu, G. D.; Stahl, R. E.; Zolla-Pazner, S.; Leibowitch, J.; Popovic, M. Isolation of human T-cell leukemia virus in acquired immune deficiency syndrome (AIDS). *Science* **1983,** *220*, 865-867.

(5) Clavel, F.; Brun-Vezinet, F.; Guetard, D.; Chamaret, S.; Laurent, A.; Rouzioux, C.; Rey, M.; Katlama, C.; Rey, F.; Champelinaud, J. L.; Nina, J. S.; Mansinho, K.; Santos-Ferreira, M.-O.; Klatzmann, D.; Montagnier, L. [LAV type II: a second retrovirus associated with AIDS in West Africa]. *C R Acad Sci III* **1986,** *302*, 485-488.

(6) Clavel, F.; Guetard, D.; Brun-Vezinet, F.; Chamaret, S.; Rey, M. A.; Santos-Ferreira, M. O.; Laurent, A. G.; Dauguet, C.; Katlama, C.; Rouzioux, C.; Klatzmann, D.; Champalimaud, J. L.; Montagnier, L. Isolation of a new human retrovirus from West African patients with AIDS. *Science* **1986,** *233*, 343-346.

(7) Sharp, P. M.; Hahn, B. H. The evolution of HIV-1 and the origin of AIDS. *Philos Trans R Soc Lond B Biol Sci* **2010,** *365*, 2487-2494.

(8) Mitsuya, H.; Weinhold, K. J.; Furman, P. A.; St Clair, M. H.; Lehrman, S. N.; Gallo, R. C.; Bolognesi, D.; Barry, D. W.; Broder, S. 3'-Azido-3'-deoxythymidine (BW A509U): an antiviral agent that inhibits the infectivity and cytopathic effect of human T-lymphotropic virus type III/lymphadenopathy-associated virus in vitro. *Proc. Natl. Acad. Sci. USA* **1985,** *82*, 7096-7100.

(9) Folkers, G. ACTG 175: new insights into treating patients with intermediate-stage HIV disease. *NIAID AIDS Agenda* **1995**, 4-5.

(10) King, E. AZT delta study: major European/Australian study finds combinations better than AZT alone. *AIDS Treat News* **1995**, 3-4.

(11) Palella, F. J., Jr.; Delaney, K. M.; Moorman, A. C.; Loveless, M. O.; Fuhrer, J.; Satten, G. A.; Aschman, D. J.; Holmberg, S. D. Declining morbidity and mortality among patients with advanced human immunodeficiency virus infection. HIV Outpatient Study Investigators. *N Engl J Med* **1998,** *338*, 853-860.

(12) ONUSIDA 2010 Global report. **2010**.

(13) Fauci, A.S; Desrosiers, R.C. Pathogenesis of HIV and SIV. Retroviruses.**1997**, 587-636 in Coffin, J.M., Hugues, S.H. et Varmus, H.E. (editeurs). Cold Spring Harbor Laboratory Press, Cold Spring Harbor, New York.

(14) Frankel, A. D.; Young, J. A. HIV-1: fifteen proteins and an RNA. *Annu Rev Biochem* **1998,** *67*, 1-25.

(15) Furtado, M. R.; Callaway, D. S.; Phair, J. P.; Kunstman, K. J.; Stanton, J. L.; Macken, C. A.; Perelson, A. S.; Wolinsky, S. M. Persistence of HIV-1 transcription in peripheral-blood mononuclear cells in patients receiving potent antiretroviral therapy. *N Engl J Med* **1999,** *340*, 1614-1622.

(16) Berger, E. A.; Murphy, P. M.; Farber, J. M. Chemokine receptors as HIV-1 coreceptors: roles in viral entry, tropism, and disease. *Annu Rev Immunol* **1999,** *17*, 657-700.

(17) Gallo, S. A.; Finnegan, C. M.; Viard, M.; Raviv, Y.; Dimitrov, A.; Rawat, S. S.; Puri, A.; Durell, S.; Blumenthal, R. The HIV Env-mediated fusion reaction. *Biochim Biophys Acta* **2003,** *1614*, 36-50.

(18) Arhel, N. Revisiting HIV-1 uncoating. *Retrovirology* **2010,** *7*, 96.

(19) Bukrinsky, M. A hard way to the nucleus. *Mol Med* **2004,** *10*, 1-5.

(20) Marin, M.; Rose, K. M.; Kozak, S. L.; Kabat, D. HIV-1 Vif protein binds the editing enzyme APOBEC3G and induces its degradation. *Nat Med* **2003,** *9*, 1398-1403.

(21) Sheehy, A. M.; Gaddis, N. C.; Malim, M. H. The antiretroviral enzyme APOBEC3G is degraded by the proteasome in response to HIV-1 Vif. *Nat Med* **2003,** *9*, 1404-1407.

(22) McDonald, D.; Vodicka, M. A.; Lucero, G.; Svitkina, T. M.; Borisy, G. G.; Emerman, M.; Hope, T. J. Visualization of the intracellular behavior of HIV in living cells. *J Cell Biol* **2002,** *159*, 441-452.

(23) Arhel, N. J.; Souquere-Besse, S.; Munier, S.; Souque, P.; Guadagnini, S.; Rutherford, S.; Prevost, M. C.; Allen, T. D.; Charneau, P. HIV-1 DNA Flap formation promotes uncoating of the pre-integration complex at the nuclear pore. *Embo J* **2007,** *26*, 3025-3037.

(24) Ganser-Pornillos, B. K.; Chandrasekaran, V.; Pornillos, O.; Sodroski, J. G.; Sundquist, W. I.; Yeager, M. Hexagonal assembly of a restricting TRIM5alpha protein. *Proc Natl Acad Sci U S A* **2011,** *108*, 534-539.

(25) Cherepanov, P.; Maertens, G.; Proost, P.; Devreese, B.; Van Beeumen, J.; Engelborghs, Y.; De Clercq, E.; Debyser, Z. HIV-1 integrase forms stable tetramers and associates with LEDGF/p75 protein in human cells. *J Biol Chem* **2003,** *278*, 372-381.

(26) Sokolskaja, E.; Berthoux, L.; Luban, J. Cyclophilin A and TRIM5alpha independently regulate human immunodeficiency virus type 1 infectivity in human cells. *J Virol* **2006,** *80*, 2855-2862.

(27) Miller, M. D.; Farnet, C. M.; Bushman, F. D. Human immunodeficiency virus type 1 preintegration complexes: studies of organization and composition. *J Virol* **1997,** *71*, 5382-5390.

(28) Woodward, C. L.; Chow, S. A. The nuclear pore complex: A new dynamic in HIV-1 replication. *Nucleus* **2010,** *1*, 18-22.

(29) Kogan, M.; Rappaport, J. HIV-1 accessory protein Vpr: relevance in the pathogenesis of HIV and potential for therapeutic intervention. *Retrovirology* **2011,** *8*, 25.

(30) Woodward, C. L.; Prakobwanakit, S.; Mosessian, S.; Chow, S. A. Integrase interacts with nucleoporin NUP153 to mediate the nuclear import of human immunodeficiency virus type 1. *J Virol* **2009,** *83*, 6522-6533.

(31) Cherepanov, P.; Maertens, G.; Proost, P.; Devreese, B.; Van Beeumen, J.; Engelborghs, Y.; De Clercq, E.; Debyser, Z. HIV-1 integrase forms stable tetramers and associates with LEDGF/p75 protein in human cells. *J Biol Chem* **2003,** *278*, 372-381.

(32) Karn, J. Tackling Tat. *J Mol Biol* **1999,** *293*, 235-254.

(33) Joseph, A. M.; Ladha, J. S.; Mojamdar, M.; Mitra, D. Human immunodeficiency virus-1 Nef protein interacts with Tat and enhances HIV-1 gene expression. *FEBS Lett* **2003,** *548*, 37-42.

(34) Pollard, V. W.; Malim, M. H. The HIV-1 Rev protein. *Annu Rev Microbiol* **1998,** *52*, 491-532.

(35) Bieniasz, P. D. The cell biology of HIV-1 virion genesis. *Cell Host Microbe* **2009,** *5*, 550-558.

(36) Dube, M.; Paquay, C.; Roy, B. B.; Bego, M.; Mercier, J.; Cohen, E. A. HIV-1 Vpu antagonizes BST-2 by interfering mainly with the trafficking of newly synthesized BST-2 to the cell surface. *Traffic* **2011**.

(37) Wild, C.; Greenwell, T.; Matthews, T. A synthetic peptide from HIV-1 gp41 is a potent inhibitor of virus-mediated cell-cell fusion. *AIDS Res Hum Retroviruses* **1993,** *9*, 1051-1053.

(38) Wei, X.; Decker, J. M.; Liu, H.; Zhang, Z.; Arani, R. B.; Kilby, J. M.; Saag, M. S.; Wu, X.; Shaw, G. M.; Kappes, J. C. Emergence of resistant human immunodeficiency virus type 1 in patients receiving fusion inhibitor (T-20) monotherapy. *Antimicrob Agents Chemother* **2002,** *46*, 1896-1905.

(39) Dwyer, J. J.; Wilson, K. L.; Davison, D. K.; Freel, S. A.; Seedorff, J. E.; Wring, S. A.; Tvermoes, N. A.; Matthews, T. J.; Greenberg, M. L.; Delmedico, M. K. Design of helical, oligomeric HIV-1 fusion inhibitor peptides with potent activity against enfuvirtide-resistant virus. *Proc Natl Acad Sci U S A* **2007,** *104*, 12772-12777.

(40) He, Y.; Cheng, J.; Lu, H.; Li, J.; Hu, J.; Qi, Z.; Liu, Z.; Jiang, S.; Dai, Q. Potent HIV fusion inhibitors against Enfuvirtide-resistant HIV-1 strains. *Proc Natl Acad Sci U S A* **2008,** *105*, 16332-16337.

(41) Ernst, J. T.; Kutzki, O.; Debnath, A. K.; Jiang, S.; Lu, H.; Hamilton, A. D. Design of a protein surface antagonist based on alpha-helix mimicry: inhibition of gp41 assembly and viral fusion. *Angew Chem Int Ed Engl* **2002,** *41*, 278-281.

(42) Dorr, P.; Westby, M.; Dobbs, S.; Griffin, P.; Irvine, B.; Macartney, M.; Mori, J.; Rickett, G.; Smith-Burchnell, C.; Napier, C.; Webster, R.; Armour, D.; Price, D.; Stammen, B.; Wood, A.; Perros, M. Maraviroc (UK-427,857), a potent, orally bioavailable, and selective small-molecule inhibitor of chemokine receptor CCR5 with broad-spectrum anti-human immunodeficiency virus type 1 activity. *Antimicrob Agents Chemother* **2005,** *49*, 4721-4732.

(43) Lieberman-Blum, S. S.; Fung, H. B.; Bandres, J. C. Maraviroc: a CCR5-receptor antagonist for the treatment of HIV-1 infection. *Clin Ther* **2008,** *30*, 1228-1250.

(44) Strizki, J. M.; Tremblay, C.; Xu, S.; Wojcik, L.; Wagner, N.; Gonsiorek, W.; Hipkin, R. W.; Chou, C. C.; Pugliese-Sivo, C.; Xiao, Y.; Tagat, J. R.; Cox, K.; Priestley, T.; Sorota, S.; Huang, W.; Hirsch, M.; Reyes, G. R.; Baroudy, B. M. Discovery and characterization of vicriviroc (SCH 417690), a CCR5 antagonist with potent activity against human immunodeficiency virus type 1. *Antimicrob Agents Chemother* **2005,** *49*, 4911-4919.

(45) Stupple, P. A.; Batchelor, D. V.; Corless, M.; Dorr, P. K.; Ellis, D.; Fenwick, D. R.; Galan, S. R.; Jones, R. M.; Mason, H. J.; Middleton, D. S.; Perros, M.; Perruccio, F.; Platts, M. Y.; Pryde, D. C.; Rodrigues, D.; Smith, N. N.; Stephenson, P. T.; Webster, R.; Westby, M.; Wood, A. An Imidazopiperidine Series of CCR5 Antagonists for the Treatment of HIV: The Discovery of N-{(1S)-1-(3-Fluorophenyl)-3-[(3-endo)-3-(5-isobutyryl-2-methyl-4,5,6,7-te trahydro-1H-imidazo[4,5-c]pyridin-1-yl)-8-azabicyclo[3.2.1]oct-8-yl]propyl }acetamide (PF-232798). *J Med Chem* **2011**.

(46) Takashima, K.; Miyake, H.; Kanzaki, N.; Tagawa, Y.; Wang, X.; Sugihara, Y.; Iizawa, Y.; Baba, M. Highly potent inhibition of human immunodeficiency virus type 1 replication by TAK-220, an orally bioavailable small-molecule CCR5 antagonist. *Antimicrob Agents Chemother* **2005,** *49*, 3474-3482.

(47) Idemyor, V. Human immunodeficiency virus (HIV) entry inhibitors (CCR5 specific blockers) in development: are they the next novel therapies? *HIV Clin Trials* **2005,** *6*, 272-277.

(48) Cihlar, T.; Ray, A. S. Nucleoside and nucleotide HIV reverse transcriptase inhibitors: 25 years after zidovudine. *Antiviral Res* **2010,** *85*, 39-58.

(49) Brinkman, K.; ter Hofstede, H. J.; Burger, D. M.; Smeitink, J. A.; Koopmans, P. P. Adverse effects of reverse transcriptase inhibitors: mitochondrial toxicity as common pathway. *Aids* **1998,** *12*, 1735-1744.

(50) Goldschmidt, V.; Marquet, R. Primer unblocking by HIV-1 reverse transcriptase and resistance to nucleoside RT inhibitors (NRTIs). *Int J Biochem Cell Biol* **2004,** *36*, 1687-1705.

(51) Van Rompay, A. R.; Johansson, M.; Karlsson, A. Phosphorylation of nucleosides and nucleoside analogs by mammalian nucleoside monophosphate kinases. *Pharmacol Ther* **2000,** *87*, 189-198.

(52) Gallant, J. E.; Deresinski, S. Tenofovir disoproxil fumarate. *Clin Infect Dis* **2003,** *37*, 944-950.

(53) Mackman, R. L.; Ray, A. S.; Hui, H. C.; Zhang, L.; Birkus, G.; Boojamra, C. G.; Desai, M. C.; Douglas, J. L.; Gao, Y.; Grant, D.; Laflamme, G.; Lin, K. Y.; Markevitch, D. Y.; Mishra, R.; McDermott, M.; Pakdaman, R.; Petrakovsky, O. V.; Vela, J. E.; Cihlar, T. Discovery of GS-9131: Design, synthesis and optimization of amidate prodrugs of the novel nucleoside phosphonate HIV reverse transcriptase (RT) inhibitor GS-9148. *Bioorg Med Chem* **2010,** *18*, 3606-3617.

(54) Bacheler, L. T. Resistance to non-nucleoside inhibitors of HIV-1 reverse transcriptase. *Drug Resist Updat* **1999,** *2*, 56-67.

(55) de Bethune, M. P. Non-nucleoside reverse transcriptase inhibitors (NNRTIs), their discovery, development, and use in the treatment of HIV-1 infection: a review of the last 20 years (1989-2009). *Antiviral Res* **2010,** *85*, 75-90.

(56) Johnson, L. B.; Saravolatz, L. D. Etravirine, a next-generation nonnucleoside reverse-transcriptase inhibitor. *Clin Infect Dis* **2009,** *48*, 1123-1128.

(57) Summa, V.; Petrocchi, A.; Bonelli, F.; Crescenzi, B.; Donghi, M.; Ferrara, M.; Fiore, F.; Gardelli, C.; Gonzalez Paz, O.; Hazuda, D. J.; Jones, P.; Kinzel, O.; Laufer, R.; Monteagudo, E.; Muraglia, E.; Nizi, E.; Orvieto, F.; Pace, P.; Pescatore, G.; Scarpelli, R.; Stillmock, K.; Witmer, M. V.; Rowley, M. Discovery of raltegravir, a potent, selective orally bioavailable HIV-integrase inhibitor for the treatment of HIV-AIDS infection. *J Med Chem* **2008,** *51*, 5843-5855.

(58) Kassahun, K.; McIntosh, I.; Cui, D.; Hreniuk, D.; Merschman, S.; Lasseter, K.; Azrolan, N.; Iwamoto, M.; Wagner, J. A.; Wenning, L. A. Metabolism and disposition in humans of raltegravir (MK-0518), an anti-AIDS drug targeting the human immunodeficiency virus 1 integrase enzyme. *Drug Metab Dispos* **2007,** *35*, 1657-1663.

(59) Grinsztejn, B.; Nguyen, B. Y.; Katlama, C.; Gatell, J. M.; Lazzarin, A.; Vittecoq, D.; Gonzalez, C. J.; Chen, J.; Harvey, C. M.; Isaacs, R. D. Safety and efficacy of the HIV-1 integrase inhibitor raltegravir (MK-0518) in treatment-experienced patients with multidrug-resistant virus: a phase II randomised controlled trial. *Lancet* **2007,** *369*, 1261-1269.

(60) Steigbigel, R. T.; Cooper, D. A.; Kumar, P. N.; Eron, J. E.; Schechter, M.; Markowitz, M.; Loutfy, M. R.; Lennox, J. L.; Gatell, J. M.; Rockstroh, J. K.; Katlama, C.; Yeni, P.; Lazzarin, A.; Clotet, B.; Zhao, J.; Chen, J.; Ryan, D. M.; Rhodes, R. R.; Killar, J. A.; Gilde, L. R.; Strohmaier, K. M.; Meibohm, A. R.; Miller, M. D.; Hazuda, D. J.; Nessly, M. L.; DiNubile, M. J.; Isaacs, R. D.; Nguyen, B. Y.; Teppler, H. Raltegravir with optimized background therapy for resistant HIV-1 infection. *N Engl J Med* **2008,** *359*, 339-354.

(61) Hazuda, D.; Iwamoto, M.; Wenning, L. Emerging pharmacology: inhibitors of human immunodeficiency virus integration. *Annu Rev Pharmacol Toxicol* **2009,** *49*, 377-394.

(62) Cooper, D. A.; Steigbigel, R. T.; Gatell, J. M.; Rockstroh, J. K.; Katlama, C.; Yeni, P.; Lazzarin, A.; Clotet, B.; Kumar, P. N.; Eron, J. E.; Schechter, M.; Markowitz, M.; Loutfy, M. R.; Lennox, J. L.; Zhao, J.; Chen, J.; Ryan, D. M.; Rhodes, R. R.; Killar, J. A.; Gilde, L. R.; Strohmaier, K. M.; Meibohm, A. R.; Miller, M. D.; Hazuda, D. J.; Nessly, M. L.; DiNubile, M. J.; Isaacs, R. D.; Teppler, H.; Nguyen, B. Y. Subgroup and resistance analyses of raltegravir for resistant HIV-1 infection. *N Engl J Med* **2008,** *359*, 355-365.

(63) Hu, Z.; Kuritzkes, D. R. Effect of raltegravir resistance mutations in HIV-1 integrase on viral fitness. *J Acquir Immune Defic Syndr* **2010,** *55*, 148-155.

(64) Sato, M.; Kawakami, H.; Motomura, T.; Aramaki, H.; Matsuda, T.; Yamashita, M.; Ito, Y.; Matsuzaki, Y.; Yamataka, K.; Ikeda, S.; Shinkai, H. Quinolone carboxylic acids as a novel monoketo acid class of human immunodeficiency virus type 1 integrase inhibitors. *J Med Chem* **2009,** *52*, 4869-4882.

(65) Sato, M.; Motomura, T.; Aramaki, H.; Matsuda, T.; Yamashita, M.; Ito, Y.; Kawakami, H.; Matsuzaki, Y.; Watanabe, W.; Yamataka, K.; Ikeda, S.; Kodama, E.; Matsuoka, M.; Shinkai, H. Novel HIV-1 integrase inhibitors derived from quinolone antibiotics. *J Med Chem* **2006,** *49*, 1506-1508.

(66) Zolopa, A. R.; Berger, D. S.; Lampiris, H.; Zhong, L.; Chuck, S. L.; Enejosa, J. V.; Kearney, B. P.; Cheng, A. K. Activity of elvitegravir, a once-daily integrase inhibitor, against resistant HIV Type 1: results of a phase 2, randomized, controlled, dose-ranging clinical trial. *J Infect Dis* **2010,** *201*, 814-822.

(67) Goethals, O.; Clayton, R.; Van Ginderen, M.; Vereycken, I.; Wagemans, E.; Geluykens, P.; Dockx, K.; Strijbos, R.; Smits, V.; Vos, A.; Meersseman, G.; Jochmans, D.; Vermeire, K.; Schols, D.; Hallenberger, S.; Hertogs, K. Resistance mutations in human immunodeficiency virus type 1 integrase selected with elvitegravir confer reduced susceptibility to a wide range of integrase inhibitors. *J Virol* **2008,** *82*, 10366-10374.

(68) Vandekerckhove, L. GSK-1349572, a novel integrase inhibitor for the treatment of HIV infection. *Curr Opin Investig Drugs* **2010,** *11*, 203-212.

(69) Wensing, A. M.; van Maarseveen, N. M.; Nijhuis, M. Fifteen years of HIV Protease Inhibitors: raising the barrier to resistance. *Antiviral Res* **2010,** *85*, 59-74.

(70) Youle, M. Overview of boosted protease inhibitors in treatment-experienced HIV-infected patients. *J Antimicrob Chemother* **2007,** *60*, 1195-1205.

(71) Temesgen, Z.; Cainelli, F.; Vento, S. Tipranavir. *Drugs Today (Barc)* **2005,** *41*, 711-720.

(72) Tsibris, A. M.; Hirsch, M. S. Antiretroviral therapy in the clinic. *J Virol* **2010,** *84*, 5458-5464.

(73) Gallant, J. E.; DeJesus, E.; Arribas, J. R.; Pozniak, A. L.; Gazzard, B.; Campo, R. E.; Lu, B.; McColl, D.; Chuck, S.; Enejosa, J.; Toole, J. J.; Cheng, A. K. Tenofovir DF, emtricitabine, and efavirenz vs. zidovudine, lamivudine, and efavirenz for HIV. *N Engl J Med* **2006,** *354*, 251-260.

(74) Pozniak, A. L.; Gallant, J. E.; DeJesus, E.; Arribas, J. R.; Gazzard, B.; Campo, R. E.; Chen, S. S.; McColl, D.; Enejosa, J.; Toole, J. J.; Cheng, A. K. Tenofovir disoproxil fumarate, emtricitabine, and efavirenz versus fixed-dose zidovudine/lamivudine and efavirenz in antiretroviral-naive patients: virologic, immunologic, and morphologic changes--a 96-week analysis. *J Acquir Immune Defic Syndr* **2006,** *43*, 535-540.

(75) Sax, P. E.; Tierney, C.; Collier, A. C.; Fischl, M. A.; Mollan, K.; Peeples, L.; Godfrey, C.; Jahed, N. C.; Myers, L.; Katzenstein, D.; Farajallah, A.; Rooney, J. F.; Ha, B.; Woodward, W. C.; Koletar, S. L.; Johnson, V. A.; Geiseler, P. J.; Daar, E. S. Abacavir-lamivudine versus tenofovir-emtricitabine for initial HIV-1 therapy. *N Engl J Med* **2009,** *361*, 2230-2240.

(76) Killingley, B.; Pozniak, A. The first once-daily single-tablet regimen for the treatment of HIV-infected patients. *Drugs Today (Barc)* **2007,** *43*, 427-442.

(77) Clark, E.; Santiago, F.; Deng, L.; Chong, S.; de La Fuente, C.; Wang, L.; Fu, P.; Stein, D.; Denny, T.; Lanka, V.; Mozafari, F.; Okamoto, T.; Kashanchi, F. Loss of G(1)/S checkpoint in human immunodeficiency virus type 1-infected cells is associated with a lack of cyclin-dependent kinase inhibitor p21/Waf1. *J Virol* **2000,** *74*, 5040-5052.

(78) Le Tourneau, C.; Faivre, S.; Laurence, V.; Delbaldo, C.; Vera, K.; Girre, V.; Chiao, J.; Armour, S.; Frame, S.; Green, S. R.; Gianella-Borradori, A.; Dieras, V.; Raymond, E. Phase I evaluation of seliciclib (R-roscovitine), a novel oral cyclin-dependent kinase inhibitor, in patients with advanced malignancies. *Eur J Cancer* **2010,** *46*, 3243-3250.

(79) Wang, D.; de la Fuente, C.; Deng, L.; Wang, L.; Zilberman, I.; Eadie, C.; Healey, M.; Stein, D.; Denny, T.; Harrison, L. E.; Meijer, L.; Kashanchi, F. Inhibition of human immunodeficiency virus type 1 transcription by chemical cyclin-dependent kinase inhibitors. *J Virol* **2001,** *75*, 7266-7279.

(80) Van Aerschot, A. Oligonucleotides as antivirals: Dream or realistic perspective? *Antiviral Research* **2006,** *71*, 307-316.

(81) Matzen, K.; Elzaouk, L.; Matskevich, A. A.; Nitzsche, A.; Heinrich, J.; Moelling, K. RNase H-mediated retrovirus destruction in vivo triggered by oligodeoxynucleotides. *Nat Biotechnol* **2007,** *25*, 669-674.

(82) Haasnoot, J.; Westerhout, E. M.; Berkhout, B. RNA interference against viruses: strike and counterstrike. *Nat Biotechnol* **2007,** *25*, 1435-1443.

(83) Bruno, C. J.; Jacobson, J. M. Ibalizumab: an anti-CD4 monoclonal antibody for the treatment of HIV-1 infection. *J Antimicrob Chemother* **2010,** *65*, 1839-1841.

(84) Kuritzkes, D. R.; Jacobson, J.; Powderly, W. G.; Godofsky, E.; DeJesus, E.; Haas, F.; Reimann, K. A.; Larson, J. L.; Yarbough, P. O.; Curt, V.; Shanahan, W. R., Jr. Antiretroviral activity of the anti-CD4 monoclonal antibody TNX-355 in patients infected with HIV type 1. *J Infect Dis* **2004,** *189*, 286-291.

(85) Zhang, X. Q.; Sorensen, M.; Fung, M.; Schooley, R. T. Synergistic in vitro antiretroviral activity of a humanized monoclonal anti-CD4 antibody (TNX-355) and enfuvirtide (T-20). *Antimicrob Agents Chemother* **2006,** *50*, 2231-2233.

(86) Duerr, A.; Wasserheit, J. N.; Corey, L. HIV vaccines: new frontiers in vaccine development. *Clin Infect Dis* **2006,** *43*, 500-511.

(87) Rerks-Ngarm, S.; Pitisuttithum, P.; Nitayaphan, S.; Kaewkungwal, J.; Chiu, J.; Paris, R.; Premsri, N.; Namwat, C.; de Souza, M.; Adams, E.; Benenson, M.; Gurunathan, S.; Tartaglia, J.; McNeil, J. G.; Francis, D. P.; Stablein, D.; Birx, D. L.; Chunsuttiwat, S.; Khamboonruang, C.; Thongcharoen, P.; Robb, M. L.; Michael, N. L.; Kunasol, P.; Kim, J. H. Vaccination with ALVAC and AIDSVAX to prevent HIV-1 infection in Thailand. *N Engl J Med* **2009,** *361*, 2209-2220.

(88) Delelis, O.; Carayon, K.; Saib, A.; Deprez, E.; Mouscadet, J. F. Integrase and integration: biochemical activities of HIV-1 integrase. *Retrovirology* **2008,** *5*, 114.

(89) Nowotny, M. Retroviral integrase superfamily: the structural perspective. *EMBO Rep* **2009,** *10*, 144-151.

(90) Yoder, K. E.; Bushman, F. D. Repair of gaps in retroviral DNA integration intermediates. *J Virol* **2000,** *74*, 11191-11200.

(91) Chow, S. A.; Vincent, K. A.; Ellison, V.; Brown, P. O. Reversal of integration and DNA splicing mediated by integrase of human immunodeficiency virus. *Science* **1992,** *255*, 723-726.

(92) Leh, H.; Brodin, P.; Bischerour, J.; Deprez, E.; Tauc, P.; Brochon, J. C.; LeCam, E.; Coulaud, D.; Auclair, C.; Mouscadet, J. F. Determinants of Mg2+-dependent activities of recombinant human immunodeficiency virus type 1 integrase. *Biochemistry* **2000,** *39*, 9285-9294.

(93) Van Maele, B.; Busschots, K.; Vandekerckhove, L.; Christ, F.; Debyser, Z. Cellular co-factors of HIV-1 integration. *Trends Biochem Sci* **2006,** *31*, 98-105.

(94) Engelman, A.; Craigie, R. Efficient magnesium-dependent human immunodeficiency virus type 1 integrase activity. *J Virol* **1995,** *69*, 5908-5911.

(95) Esposito, D.; Craigie, R. Sequence specificity of viral end DNA binding by HIV-1 integrase reveals critical regions for protein-DNA interaction. *Embo J* **1998,** *17*, 5832-5843.

(96) Gerton, J. L.; Herschlag, D.; Brown, P. O. Stereospecificity of reactions catalyzed by HIV-1 integrase. *J Biol Chem* **1999,** *274*, 33480-33487.

(97) Kennedy, A. K.; Haniford, D. B.; Mizuuchi, K. Single active site catalysis of the successive phosphoryl transfer steps by DNA transposases: insights from phosphorothioate stereoselectivity. *Cell* **2000,** *101*, 295-305.

(98) Krakowiak, A.; Owczarek, A.; Koziolkiewicz, M.; Stec, W. J. Stereochemical course of Escherichia coli RNase H. *Chembiochem* **2002,** *3*, 1242-1250.

(99) Nowotny, M.; Gaidamakov, S. A.; Crouch, R. J.; Yang, W. Crystal structures of RNase H bound to an RNA/DNA hybrid: substrate specificity and metal-dependent catalysis. *Cell* **2005,** *121*, 1005-1016.

(100) Nowotny, M.; Yang, W. Stepwise analyses of metal ions in RNase H catalysis from substrate destabilization to product release. *Embo J* **2006,** *25*, 1924-1933.

(101) Maertens, G. N.; Hare, S.; Cherepanov, P. The mechanism of retroviral integration from X-ray structures of its key intermediates. *Nature* **2010,** *468*, 326-329.

(102) Cai, M.; Zheng, R.; Caffrey, M.; Craigie, R.; Clore, G. M.; Gronenborn, A. M. Solution structure of the N-terminal zinc binding domain of HIV-1 integrase. *Nat Struct Biol* **1997,** *4*, 567-577.

(103) Lodi, P. J.; Ernst, J. A.; Kuszewski, J.; Hickman, A. B.; Engelman, A.; Craigie, R.; Clore, G. M.; Gronenborn, A. M. Solution structure of the DNA binding domain of HIV-1 integrase. *Biochemistry* **1995,** *34*, 9826-9833.

(104) Dyda, F.; Hickman, A. B.; Jenkins, T. M.; Engelman, A.; Craigie, R.; Davies, D. R. Crystal structure of the catalytic domain of HIV-1 integrase: similarity to other polynucleotidyl transferases. *Science* **1994,** *266*, 1981-1986.

(105) Goldgur, Y.; Dyda, F.; Hickman, A. B.; Jenkins, T. M.; Craigie, R.; Davies, D. R. Three new structures of the core domain of HIV-1 integrase: an active site that binds magnesium. *Proc Natl Acad Sci U S A* **1998,** *95*, 9150-9154.

(106) Maignan, S.; Guilloteau, J. P.; Zhou-Liu, Q.; Clement-Mella, C.; Mikol, V. Crystal structures of the catalytic domain of HIV-1 integrase free and complexed with its metal cofactor: high level of similarity of the active site with other viral integrases. *J Mol Biol* **1998,** *282*, 359-368.

(107) Greenwald, J.; Le, V.; Butler, S. L.; Bushman, F. D.; Choe, S. The mobility of an HIV-1 integrase active site loop is correlated with catalytic activity. *Biochemistry* **1999,** *38*, 8892-8898.

(108) Wang, J. Y.; Ling, H.; Yang, W.; Craigie, R. Structure of a two-domain fragment of HIV-1 integrase: implications for domain organization in the intact protein. *Embo J* **2001,** *20*, 7333-7343.

(109) Chen, J. C.; Krucinski, J.; Miercke, L. J.; Finer-Moore, J. S.; Tang, A. H.; Leavitt, A. D.; Stroud, R. M. Crystal structure of the HIV-1 integrase catalytic core and C-terminal domains: a model for viral DNA binding. *Proc Natl Acad Sci U S A* **2000,** *97*, 8233-8238.

(110) Faure, A.; Calmels, C.; Desjobert, C.; Castroviejo, M.; Caumont-Sarcos, A.; Tarrago-Litvak, L.; Litvak, S.; Parissi, V. HIV-1 integrase crosslinked oligomers are active in vitro. *Nucleic Acids Res* **2005,** *33*, 977-986.

(111) Guiot, E.; Carayon, K.; Delelis, O.; Simon, F.; Tauc, P.; Zubin, E.; Gottikh, M.; Mouscadet, J. F.; Brochon, J. C.; Deprez, E. Relationship between the oligomeric status of HIV-1 integrase on DNA and enzymatic activity. *J Biol Chem* **2006,** *281*, 22707-22719.

(112) Hare, S.; Gupta, S. S.; Valkov, E.; Engelman, A.; Cherepanov, P. Retroviral intasome assembly and inhibition of DNA strand transfer. *Nature* **2010,** *464*, 232-236.

(113) Michel, F.; Crucifix, C.; Granger, F.; Eiler, S.; Mouscadet, J. F.; Korolev, S.; Agapkina, J.; Ziganshin, R.; Gottikh, M.; Nazabal, A.; Emiliani, S.; Benarous, R.; Moras, D.; Schultz, P.; Ruff, M. Structural basis for HIV-1 DNA integration in the human genome, role of the LEDGF/P75 cofactor. *Embo J* **2009,** *28*, 980-991.

(114) Cherepanov, P.; Ambrosio, A. L.; Rahman, S.; Ellenberger, T.; Engelman, A. Structural basis for the recognition between HIV-1 integrase and transcriptional coactivator p75. *Proc Natl Acad Sci U S A* **2005,** *102*, 17308-17313.

(115) Mouscadet, J. F.; Desmaele, D. Chemistry and structure-activity relationship of the styrylquinoline-type HIV integrase inhibitors. *Molecules* **2010,** *15*, 3048-3078.

(116) Pannecouque, C.; Pluymers, W.; Van Maele, B.; Tetz, V.; Cherepanov, P.; De Clercq, E.; Witvrouw, M.; Debyser, Z. New class of HIV integrase inhibitors that block viral replication in cell culture. *Curr Biol* **2002,** *12*, 1169-1177.

(117) Hombrouck, A.; Hantson, A.; van Remoortel, B.; Michiels, M.; Vercammen, J.; Rhodes, D.; Tetz, V.; Engelborghs, Y.; Christ, F.; Debyser, Z.; Witvrouw, M. Selection of human immunodeficiency virus type 1 resistance against the pyranodipyrimidine V-165 points to a multimodal mechanism of action. *J Antimicrob Chemother* **2007,** *59*, 1084-1095.

(118) Mousnier, A.; Leh, H.; Mouscadet, J. F.; Dargemont, C. Nuclear import of HIV-1 integrase is inhibited in vitro by styrylquinoline derivatives. *Mol Pharmacol* **2004,** *66*, 783-788.

(119) Du, L.; Zhao, Y. X.; Yang, L. M.; Zheng, Y. T.; Tang, Y.; Shen, X.; Jiang, H. L. Symmetrical 1-pyrrolidineacetamide showing anti-HIV activity through a new binding site on HIV-1 integrase. *Acta Pharmacol Sin* **2008,** *29*, 1261-1267.

(120) Ivanov, A. A.; Strel'tsov, S. A.; Prikazchikova, T. A.; Gottikh, M. B.; Zhuze, A. L. [Synthesis and properties of a symmetric dimeric bisbenzimidazole, a DNA-specific ligand]. *Bioorg Khim* **2008,** *34*, 285-288.

(121) Hazuda, D. J.; Felock, P.; Witmer, M.; Wolfe, A.; Stillmock, K.; Grobler, J. A.; Espeseth, A.; Gabryelski, L.; Schleif, W.; Blau, C.; Miller, M. D. Inhibitors of strand transfer that prevent integration and inhibit HIV-1 replication in cells. *Science* **2000,** *287*, 646-650.

(122) Goldgur, Y.; Craigie, R.; Cohen, G. H.; Fujiwara, T.; Yoshinaga, T.; Fujishita, T.; Sugimoto, H.; Endo, T.; Murai, H.; Davies, D. R. Structure of the HIV-1 integrase catalytic domain complexed with an inhibitor: a platform for antiviral drug design. *Proc Natl Acad Sci U S A* **1999,** *96*, 13040-13043.

(123) Billich, A. S-1360 Shionogi-GlaxoSmithKline. *Curr Opin Investig Drugs* **2003,** *4*, 206-209.

(124) Rosemond, M. J.; St John-Williams, L.; Yamaguchi, T.; Fujishita, T.; Walsh, J. S. Enzymology of a carbonyl reduction clearance pathway for the HIV integrase inhibitor, S-1360: role of human liver cytosolic aldo-keto reductases. *Chem Biol Interact* **2004,** *147*, 129-139.

(125) Barreca, M. L.; Ferro, S.; Rao, A.; De Luca, L.; Zappala, M.; Monforte, A. M.; Debyser, Z.; Witvrouw, M.; Chimirri, A. Pharmacophore-based design of HIV-1 integrase strand-transfer inhibitors. *J Med Chem* **2005,** *48*, 7084-7088.

(126) Zhuang, L.; Wai, J. S.; Embrey, M. W.; Fisher, T. E.; Egbertson, M. S.; Payne, L. S.; Guare, J. P., Jr.; Vacca, J. P.; Hazuda, D. J.; Felock, P. J.; Wolfe, A. L.; Stillmock, K. A.; Witmer, M. V.; Moyer, G.; Schleif, W. A.; Gabryelski, L. J.; Leonard, Y. M.; Lynch, J. J., Jr.; Michelson, S. R.; Young, S. D. Design and synthesis of 8-hydroxy-[1,6]naphthyridines as novel inhibitors of HIV-1 integrase in vitro and in infected cells. *J Med Chem* **2003,** *46*, 453-456.

(127) Hazuda, D. J.; Anthony, N. J.; Gomez, R. P.; Jolly, S. M.; Wai, J. S.; Zhuang, L.; Fisher, T. E.; Embrey, M.; Guare, J. P., Jr.; Egbertson, M. S.; Vacca, J. P.; Huff, J. R.; Felock, P. J.; Witmer, M. V.; Stillmock, K. A.; Danovich, R.; Grobler, J.; Miller, M. D.; Espeseth, A. S.; Jin, L.; Chen, I. W.; Lin, J. H.; Kassahun, K.; Ellis, J. D.; Wong, B. K.; Xu, W.; Pearson, P. G.; Schleif, W. A.; Cortese, R.; Emini, E.; Summa, V.; Holloway, M. K.; Young, S. D. A naphthyridine carboxamide provides evidence for discordant resistance between mechanistically identical inhibitors of HIV-1 integrase. *Proc Natl Acad Sci U S A* **2004,** *101*, 11233-11238.

(128) Egbertson, M.; Langford, H. M.; Melamed, J. Y.; Wai, J. S.; Han, W.; Perlow, D. S.; Zhuang, L.; Embrey, M.; Young, S. D. Preparation of N-(substituted benzyl)-8-hydroxy-1,6-naphthyridine-7-carboxamides useful as HIV integrase inhibitors for treatment of HIV infection/AIDS. . *PCT Int. Appl.* **2003**.

(129) Boros, E. E.; Edwards, C. E.; Foster, S. A.; Fuji, M.; Fujiwara, T.; Garvey, E. P.; Golden, P. L.; Hazen, R. J.; Jeffrey, J. L.; Johns, B. A.; Kawasuji, T.; Kiyama, R.; Koble, C. S.; Kurose, N.; Miller, W. H.; Mote, A. L.; Murai, H.; Sato, A.; Thompson, J. B.; Woodward, M. C.; Yoshinaga, T. Synthesis and antiviral activity of 7-benzyl-4-hydroxy-1,5-naphthyridin-2(1H)-one HIV integrase inhibitors. *J Med Chem* **2009,** *52*, 2754-2761.

(130) Garvey, E. P.; Johns, B. A.; Gartland, M. J.; Foster, S. A.; Miller, W. H.; Ferris, R. G.; Hazen, R. J.; Underwood, M. R.; Boros, E. E.; Thompson, J. B.; Weatherhead, J. G.; Koble, C. S.; Allen, S. H.; Schaller, L. T.; Sherrill, R. G.; Yoshinaga, T.; Kobayashi, M.; Wakasa-Morimoto, C.; Miki, S.; Nakahara, K.; Noshi, T.; Sato, A.; Fujiwara, T. The naphthyridinone GSK364735 is a novel, potent human immunodeficiency virus type 1 integrase inhibitor and antiretroviral. *Antimicrob Agents Chemother* **2008,** *52*, 901-908.

(131) Reddy, Y. S.; Min, S. S.; Borland, J.; Song, I.; Lin, J.; Palleja, S.; Symonds, W. T. Safety and pharmacokinetics of GSK364735, a human immunodeficiency virus type 1 integrase inhibitor, following single and repeated administration in healthy adult subjects. *Antimicrob Agents Chemother* **2007,** *51*, 4284-4289.

(132) Pace, P.; Di Francesco, M. E.; Gardelli, C.; Harper, S.; Muraglia, E.; Nizi, E.; Orvieto, F.; Petrocchi, A.; Poma, M.; Rowley, M.; Scarpelli, R.; Laufer, R.; Gonzalez Paz, O.; Monteagudo, E.; Bonelli, F.; Hazuda, D.; Stillmock, K. A.; Summa, V. Dihydroxypyrimidine-4-carboxamides as novel potent and selective HIV integrase inhibitors. *J Med Chem* **2007,** *50*, 2225-2239.

(133) Summa, V.; Petrocchi, A.; Matassa, V. G.; Gardelli, C.; Muraglia, E.; Rowley, M.; Paz, O. G.; Laufer, R.; Monteagudo, E.; Pace, P. 4,5-dihydroxypyrimidine carboxamides and N-alkyl-5-hydroxypyrimidinone carboxamides are potent, selective HIV integrase inhibitors with good pharmacokinetic profiles in preclinical species. *J Med Chem* **2006,** *49*, 6646-6649.

(134) Summa, V.; Petrocchi, A.; Matassa, V. G.; Taliani, M.; Laufer, R.; De Francesco, R.; Altamura, S.; Pace, P. HCV NS5b RNA-dependent RNA polymerase inhibitors: from alpha,gamma-diketoacids to 4,5-dihydroxypyrimidine- or 3-methyl-5-hydroxypyrimidinonecarboxylic acids. Design and synthesis. *J Med Chem* **2004,** *47*, 5336-5339.

(135) Wiscount, C. M.; Williams, P. D.; Tran, L. O.; Embrey, M. W.; Fisher, T. E.; Sherman, V.; Homnick, C. F.; Donnette Staas, D.; Lyle, T. A.; Wai, J. S.; Vacca, J. P.; Wang, Z.; Felock, P. J.; Stillmock, K. A.; Witmer, M. V.; Miller, M. D.; Hazuda, D. J.; Day, A. M.; Gabryelski, L. J.; Ecto, L. T.; Schleif, W. A.; DiStefano, D. J.; Kochansky, C. J.; Anari, M. R. 10-Hydroxy-7,8-dihydropyrazino[1',2':1,5]pyrrolo[2,3-d]pyridazine-1,9(2H,6 H)-diones: potent, orally bioavailable HIV-1 integrase strand-transfer inhibitors with activity against integrase mutants. *Bioorg Med Chem Lett* **2008,** *18*, 4581-4583.

(136) Vacca, J. W. J.; Fisher, T.; Embrey, M.; Hazuda, D.; Miller, M.; Felock, P.; Witmer, M.; Gabryelski, L.; Lyle, T. Discovery of MK-2048 - subtle changes confer unique resistance properties to a series of tricyclic hydroxypyrrole integrase strand transfer inhibitors. 4th IAS Conference. Sydney, Australia **2007**.

(137) Jin, H.; Cai, R. Z.; Schacherer, L.; Jabri, S.; Tsiang, M.; Fardis, M.; Chen, X.; Chen, J. M.; Kim, C. U. Design, synthesis, and SAR studies of novel and highly active tri-cyclic HIV integrase inhibitors. *Bioorg Med Chem Lett* **2006,** *16*, 3989-3992.

(138) Jin, H.; Wright, M.; Pastor, R.; Mish, M.; Metobo, S.; Jabri, S.; Lansdown, R.; Cai, R.; Pyun, P.; Tsiang, M.; Chen, X.; Kim, C. U. Tricyclic HIV integrase inhibitors: potent and orally bioavailable C5-aza analogs. *Bioorg Med Chem Lett* **2008,** *18*, 1388-1391.

(139) Jones, G. S.; Yu, F.; Zeynalzadegan, A.; Hesselgesser, J.; Chen, X.; Chen, J.; Jin, H.; Kim, C. U.; Wright, M.; Geleziunas, R.; Tsiang, M. Preclinical evaluation of GS-9160, a novel inhibitor of human immunodeficiency virus type 1 integrase. *Antimicrob. Agents Chemother.* **2009,** *53*, 1194-1203.

(140) Klibanov, O. M. Elvitegravir, an oral HIV integrase inhibitor, for the potential treatment of HIV infection. *Curr Opin Investig Drugs* **2009,** *10*, 190-200.

(141) Di Santo, R.; Costi, R.; Roux, A.; Artico, M.; Lavecchia, A.; Marinelli, L.; Novellino, E.; Palmisano, L.; Andreotti, M.; Amici, R.; Galluzzo, C. M.; Nencioni, L.; Palamara, A. T.; Pommier, Y.; Marchand, C. Novel bifunctional quinolonyl diketo acid derivatives as HIV-1 integrase inhibitors: design, synthesis, biological activities, and mechanism of action. *J Med Chem* **2006,** *49*, 1939-1945.

(142) Di Santo, R.; Costi, R.; Roux, A.; Miele, G.; Crucitti, G. C.; Iacovo, A.; Rosi, F.; Lavecchia, A.; Marinelli, L.; Di Giovanni, C.; Novellino, E.; Palmisano, L.; Andreotti, M.; Amici, R.; Galluzzo, C. M.; Nencioni, L.; Palamara, A. T.; Pommier, Y.; Marchand, C. Novel quinolinonyl diketo acid derivatives as HIV-1 integrase inhibitors: design, synthesis, and biological activities. *J Med Chem* **2008,** *51*, 4744-4750.

(143) Bacchi, A.; Biemmi, M.; Carcelli, M.; Carta, F.; Compari, C.; Fisicaro, E.; Rogolino, D.; Sechi, M.; Sippel, M.; Sotriffer, C. A.; Sanchez, T. W.; Neamati, N. From ligand to complexes. Part 2. Remarks on human immunodeficiency virus type 1 integrase inhibition by beta-diketo acid metal complexes. *J Med Chem* **2008,** *51*, 7253-7264.

(144) Espeseth, A. S.; Felock, P.; Wolfe, A.; Witmer, M.; Grobler, J.; Anthony, N.; Egbertson, M.; Melamed, J. Y.; Young, S.; Hamill, T.; Cole, J. L.; Hazuda, D. J. HIV-1 integrase inhibitors that compete with the target DNA substrate define a unique strand transfer conformation for integrase. *Proc Natl Acad Sci U S A* **2000,** *97*, 11244-11249.

(145) Langley, D. R.; Samanta, H. K.; Lin, Z.; Walker, M. A.; Krystal, M. R.; Dicker, I. B. The terminal (catalytic) adenosine of the HIV LTR controls the kinetics of binding and dissociation of HIV integrase strand transfer inhibitors. *Biochemistry* **2008,** *47*, 13481-13488.

(146) Hare, S.; Vos, A. M.; Clayton, R. F.; Thuring, J. W.; Cummings, M. D.; Cherepanov, P. Molecular mechanisms of retroviral integrase inhibition and the evolution of viral resistance. *Proc Natl Acad Sci U S A* **2010,** *107*, 20057-20062.

(147) Llano, M.; Saenz, D. T.; Meehan, A.; Wongthida, P.; Peretz, M.; Walker, W. H.; Teo, W.; Poeschla, E. M. An essential role for LEDGF/p75 in HIV integration. *Science* **2006,** *314*, 461-464.

(148) Hayouka, Z.; Rosenbluh, J.; Levin, A.; Loya, S.; Lebendiker, M.; Veprintsev, D.; Kotler, M.; Hizi, A.; Loyter, A.; Friedler, A. Inhibiting HIV-1 integrase by shifting its oligomerization equilibrium. *Proc Natl Acad Sci U S A* **2007,** *104*, 8316-8321.

(149) Christ, F.; Voet, A.; Marchand, A.; Nicolet, S.; Desimmie, B. A.; Marchand, D.; Bardiot, D.; Van der Veken, N. J.; Van Remoortel, B.; Strelkov, S. V.; De Maeyer, M.; Chaltin, P.; Debyser, Z. Rational design of small-molecule inhibitors of the LEDGF/p75-integrase interaction and HIV replication. *Nat Chem Biol* **2010,** *6*, 442-448.

(150) De Luca, L.; Ferro, S.; Gitto, R.; Barreca, M. L.; Agnello, S.; Christ, F.; Debyser, Z.; Chimirri, A. Small molecules targeting the interaction between HIV-1 integrase and LEDGF/p75 cofactor. *Bioorg Med Chem* **2010,** *18*, 7515-7521.

(151) Du, L.; Zhao, Y.; Chen, J.; Yang, L.; Zheng, Y.; Tang, Y.; Shen, X.; Jiang, H. D77, one benzoic acid derivative, functions as a novel anti-HIV-1 inhibitor targeting the interaction between integrase and cellular LEDGF/p75. *Biochem Biophys Res Commun* **2008,** *375*, 139-144.

(152) Vandurm, P.; Cauvin, C.; Guiguen, A.; Georges, B.; Le Van, K.; Martinelli, V.; Cardona, C.; Mbemba, G.; Mouscadet, J. F.; Hevesi, L.; Van Lint, C.; Wouters, J. Structural and theoretical studies of [6-bromo-1-(4-fluorophenylmethyl)-4(1H)-quinolinon-3-yl)]-4-hydroxy-2-oxo- 3-butenoic acid as HIV-1 integrase inhibitor. *Bioorg Med Chem Lett* **2009,** *19*, 4806-4809.

(153) Vandurm, P.; Guiguen, A.; Cauvin, C.; Georges, B.; Le Van, K.; Michaux, C.; Cardona, C.; Mbemba, G.; Mouscadet, J. F.; Laszlo, H.; Van Lint, C.; Wouters, J. Synthesis, biological evaluation and molecular modeling studies of quinolonyl diketo acid derivatives: New structural insight into the HIV-1 integrase inhibition. *Eur J Med Chem* **2010,** *46*, 1749-1756.

(154) Jenkins, T. M.; Hickman, A. B.; Dyda, F.; Ghirlando, R.; Davies, D. R.; Craigie, R. Catalytic domain of human immunodeficiency virus type 1 integrase: identification of a soluble mutant by systematic replacement of hydrophobic residues. *Proc Natl Acad Sci U S A* **1995,** *92*, 6057-6061.

(155) Spek, A. L. PLATON: A Multipurpose Crystallographic Tool, **2001**, University of Utrecht; Utrecht, The Netherlands.

(156) Sechi, M.; Bacchi, A.; Carcelli, M.; Compari, C.; Duce, E.; Fisicaro, E.; Rogolino, D.; Gates, P.; Derudas, M.; Al-Mawsawi, L. Q.; Neamati, N. From ligand to complexes: inhibition of human immunodeficiency virus type 1 integrase by beta-diketo acid metal complexes. *J Med Chem* **2006,** *49*, 4248-4260.

(157) Vandurm, P.; Cauvin, C.; Wouters, J.; Perpete, E. A.; Jacquemin, D. Electronic transitions of neutral and anionic quinolinone HIV-1 integrase inhibitor: Joint theory/experiment investigation. *Chemical Physics Letters* **2009,** *478*, 243-248.

(158) Casanovas, J.; Jacquemin, D.; Perpète, E.A.; Aleman, C. Fluorescein isothiocyanate: Molecular characterization by theoretical calculations. *Chem Phys.* **2008**, *354*, 155-161.

(159) Maurin, C.; Bailly, F.; Buisine, E.; Vezin, H.; Mbemba, G.; Mouscadet, J. F.; Cotelle, P. Spectroscopic studies of diketoacids-metal interactions. A probing tool for the pharmacophoric intermetallic distance in the HIV-1 integrase active site. *J Med Chem* **2004,** *47*, 5583-5586.

(160) Accelrys Software Inc., *Discovery Studio Modeling Environment, Release 2.5* , San Diego: Accelrys Software Inc., **2007**.

(161) Krishnan, L.; Li, X.; Naraharisetty, H. L.; Hare, S.; Cherepanov, P.; Engelman, A. Structure-based modeling of the functional HIV-1 intasome and its inhibition. *Proc Natl Acad Sci U S A* **2010,** *107*, 15910-15915.

(162) Tang, J.; Maddali, K.; Pommier, Y.; Sham, Y. Y.; Wang, Z. Scaffold rearrangement of dihydroxypyrimidine inhibitors of HIV integrase: Docking model revisited. *Bioorg Med Chem Lett* **2010,** *20*, 3275-3279.

(163) Steiniger-White, M.; Rayment, I.; Reznikoff, W. S. Structure/function insights into Tn5 transposition. *Curr Opin Struct Biol* **2004,** *14*, 50-57.

(164) Jones, G.; Willett, P.; Glen, R. C.; Leach, A. R.; Taylor, R. Development and validation of a genetic algorithm for flexible docking. *J Mol Biol* **1997,** *267*, 727-748.

(165) Garvey, E. P.; Schwartz, B.; Gartland, M. J.; Lang, S.; Halsey, W.; Sathe, G.; Carter, H. L., 3rd; Weaver, K. L. Potent inhibitors of HIV-1 integrase display a two-step, slow-binding inhibition mechanism which is absent in a drug-resistant T66I/M154I mutant. *Biochemistry* **2009,** *48*, 1644-1653.

(166) Billamboz, M.; Bailly, F.; Barreca, M. L.; De Luca, L.; Mouscadet, J. F.; Calmels, C.; Andreola, M. L.; Witvrouw, M.; Christ, F.; Debyser, Z.; Cotelle, P. Design, synthesis, and biological evaluation of a series of 2-hydroxyisoquinoline-1,3(2H,4H)-diones as dual inhibitors of human immunodeficiency virus type 1 integrase and the reverse transcriptase RNase H domain. *J Med Chem* **2008,** *51*, 7717-7730.

(167) Billamboz, M.; Bailly, F.; Lion, C.; Calmels, C.; Andreola, M. L.; Witvrouw, M.; Christ, F.; Debyser, Z.; De Luca, L.; Chimirri, A.; Cotelle, P. 2-hydroxyisoquinoline-1,3(2H,4H)-diones as inhibitors of HIV-1 integrase and reverse transcriptase RNase H domain: influence of the alkylation of position 4. *Eur J Med Chem 46*, 535-546.

(168) Billamboz, M.; Bailly, F.; Lion, C.; Touati, N.; Vezin, H.; Calmels, C.; Andreola, M. L.; Christ, F.; Debyser, Z.; Cotelle, P. Magnesium Chelating 2-Hydroxyisoquinoline-1,3(2H,4H)-diones, as Inhibitors of HIV-1 Integrase and/or the HIV-1 Reverse Transcriptase Ribonuclease H Domain: Discovery of a Novel Selective Inhibitor of the Ribonuclease H Function. *J Med Chem* **2010,** *54*, 1812-1824.

(169) Adamo, C.; Barone, V. Toward reliable density functional methods without adjustable parameters: The PBE0 model. *J. Chem. Phys.* **1999**, *110*, 6158 - 6170.

(170) Ernzerhof, M.; Scuseria, G. E. Assessment of the Perdew-Burke-Ernzerhof exchange-correlation functional. *J. Chem. Phys.*, **1999**, *110*, 5029-5036.

(171) Jacquemin, D.; Perpete, E. A.; Ciofini, I.; Adamo, C. Accurate simulation of optical properties in dyes. *Acc Chem Res* **2009,** *42*, 326-334.

(172) Frisch, M. J.; Trucks, G. W.; Schlegel, H. B.; Scuseria, G. E.; Robb, M. A.; Cheeseman, J. R.; Montgomery, Jr., J. A.; Vreven, T.; Kudin, K. N.; Burant, J. C.; et al. GAUSSIAN 03, Gaussian, Wallingford CT, **2004**.

(173) Tomasi, J.; Mennucci, B.; Cammi, R. Quantum mechanical continuum solvation models. *Chem Rev* **2005,** *105*, 2999-3093.

(174) Cossi, M.; Barone, V. Time-dependent density functional theory for molecules in liquid solutions. *Journal of Chemical Physics* **2001,** *115*, 4708-4717.